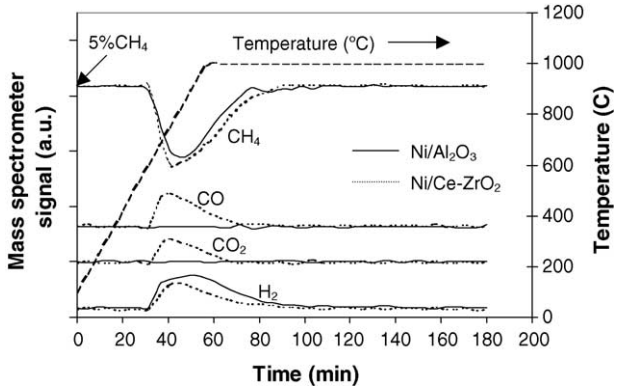

Fig. 4. Temperature-programmed methane adsorption (TPMA) of Ni/Ce–ZrO_2 (5 kPa CH_4).

CH_4 ratio to reduce the carbon formation. According to the table, the minimum requirement of inlet H_2O/CH_4 ratio to avoid the carbon formation for Ni/Al_2O_3 is 3.0.

3.4. Intrinsic reaction kinetic studies

3.4.1. Effects of temperature and methane

The inlet methane partial pressure was varied from 1 to 4 kPa, while the inlet steam was kept constant at 9 kPa. The operating temperature range was 650–850 °C. At steady state, the main products from this reaction were H_2 and CO with a small amount of CO_2, indicating a small contribution from the water–gas shift reaction, Eq. (2), and the reverse methanation (Eq. (3)). Fig. 6 showed the influences of temperature on the $CO/(CO + CO_2)$ production selectivity for both Ni/Ce–ZrO_2 and Ni/Al_2O_3. This selectivity increased with increasing operating temperature. At the same temperature, this selectivity for Ni/Al_2O_3 was observed to be higher than that over Ni/Ce–ZrO_2, which is due to the lower reactivity toward the water–gas shift reaction of Ni/Al_2O_3. The water–gas shift reaction (WGS) for each support was tested in order to ensure the influence of this reaction by using TPRx in CO/H_2O/He gas mixture (5 kPa CO, and 10 kPa H_2O). Fig. 7 shows the activities of

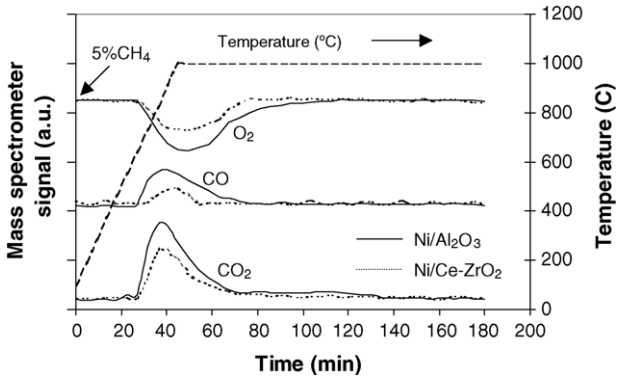

Fig. 5. Temperature-programmed oxidation (TPO) of Ni/Ce–ZrO_2 (10 kPa O_2).

Table 3
The dependence of inlet H_2O/CH_4 ratio on the amount of carbon formation remaining on the catalyst surface (calculated from CO and CO_2 yields during TPO)

H_2O/CH_4 ratio	Total carbon formation (monolayers)	
	Ni/Ce–ZrO_2	Ni/Al_2O_3
0	1.29[a] (1.31)[b]	2.35 (2.34)
0.2	0.47 (0.45)	2.26 (2.28)
0.4	0.39 (0.39)	1.97 (1.99)
0.6	0.21 (0.24)	1.66 (1.61)
0.8	0.11 (0.09)	1.33 (1.30)
1.0	~0 (0.005)	0.79 (0.81)
2.0	~0 (~0)	0.30 (0.27)
3.0	~0 (~0)	~0 (0.01)

[a] Calculated using CO and CO_2 yields from temperature-programmed oxidation (TPO) with 10% oxygen.
[b] Calculated from the balance of carbon in the system.

both supports toward this reaction. Clearly, the activity toward this reaction over Ce–ZrO_2 was significantly higher than that over Al_2O_3 at the same operating conditions.

Fig. 8 illustrates the influence of the inlet methane partial pressure on the turnover frequencies (N) for methane steam reforming over Ni/Ce–ZrO_2 at different operating temperatures. Turnover frequencies were calculated from the methane conversion following the given equation by assuming that all surface sites accessible by nitrogen adsorption (area per molecule 16.2×10^{-20} m^2 [40]) were active:

$$N = \frac{rN_A A_{N_2}}{m_c S} \tag{9}$$

Here r is the moles CH_4 per unit time, N_A the Avogadro's number, A_{N_2} the area occupied by an adsorbed nitrogen molecule (16.2×10^{-20} m^2), m_c the weight of catalyst used (50 mg), and S is the specific surface area of the catalyst (18 m^2 g^{-1}). The activities of each catalyst increased with increasing inlet methane partial pressure as well as operating temperature. Fig. 9 shows an Arrhenius-type plot for methane steam reforming over Ni/Ce–ZrO_2 with various

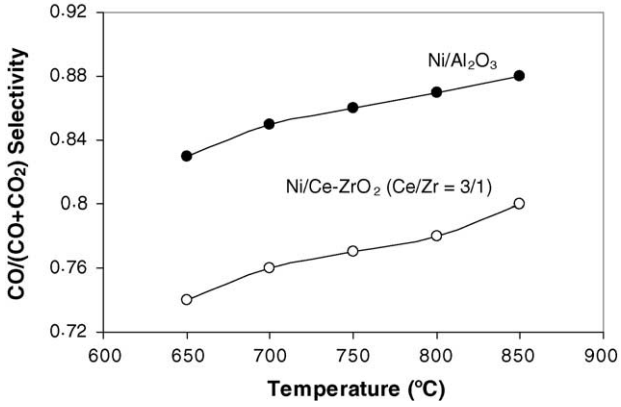

Fig. 6. Influence of temperature on $CO/(CO + CO_2)$ selectivity from methane steam reforming over Ni/Ce–ZrO_2 and Ni/Al_2O_3 (3 kPa CH_4, 9 kPa H_2O).

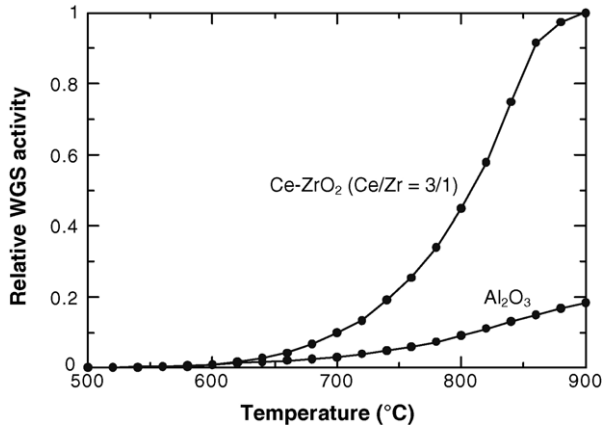

Fig. 7. The activities of Ce–ZrO_2 and Al_2O_3 toward the water-gas shift reaction using TPRx in CO/H_2O/He gas mixture (5 kPa CO, and 10 kPa H_2O).

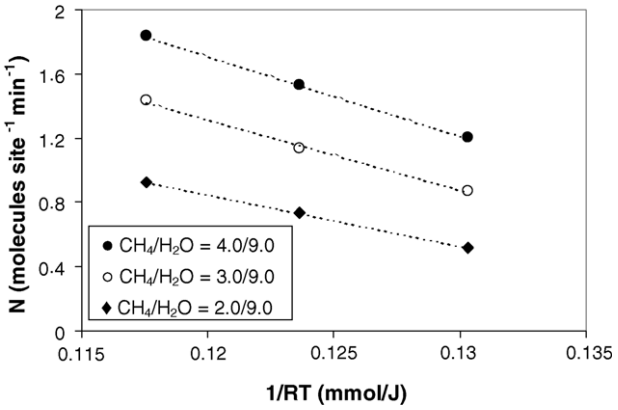

Fig. 9. Arrhenius plot of turnover frequencies (N) for methane steam reforming over Ni/Ce–ZrO_2 (Ce/Zr = 3/1) with different inlet methane/steam ratios.

methane/steam ratios over the temperature range of 650–750 °C. The corresponding activation energy observed for this catalyst is 142 ± 15 kJ mol^{-1}, slightly depending on the gas composition. The composition-dependence of activation energies from the Arrhenius plots has often been observed. The literature values, reviewed by Pointon [41] and Dicks et al. [39], were reported to be 35–287 and 154–253 kJ mol^{-1}, respectively.

The reaction orders in methane for both catalysts were observed to be 1.0 in all conditions. These values (n) were obtained experimentally by plotting $\ln(N)$ versus $\ln P_{CH_4}$ according to the equation below:

$$\ln(N) = \ln(k) + n(\ln P_{CH_4}) \quad (10)$$

The reaction order in methane seemed to be independent of the operating temperature in the range of conditions studied. By varying inlet steam partial pressure (9, 12, and 15 kPa) and adding hydrogen (1, 3, and 5 kPa), we found that the reaction order in methane was also independent of both components in this range of conditions.

3.4.2. Effect of hydrogen

Several inlet hydrogen concentrations (1–18 kPa) were added to the methane/steam in order to investigate the influence of this component on the steam reforming rate. Firstly, the inlet hydrogen partial pressure was varied from 0 to 5 kPa, while the inlet methane and steam partial pressure were kept constant at 3 and 9 kPa, respectively. In this range of conditions, hydrogen promoted the methane conversion as shown in Fig. 10. The reaction orders in hydrogen for Ni/Ce–ZrO_2 at this range of conditions studied were observed to be positive values between 0.18 and 0.20, while the reaction order in hydrogen for Ni/Al_2O_3 was in the range of 0.28–0.34. These values seemed to be independent of the inlet methane partial pressure and the operating temperature. However, they depended on the inlet steam partial pressure. The reaction order in hydrogen became slightly higher with increasing inlet steam partial pressure. This result is in good agreement with Dicks et al. [39] Fig. 11 showed the influences of hydrogen on the CO/(CO + CO_2) production selectivity. This selectivity increased with increasing inlet hydrogen partial pressure due to the promotion of the reverse water–gas shift reaction.

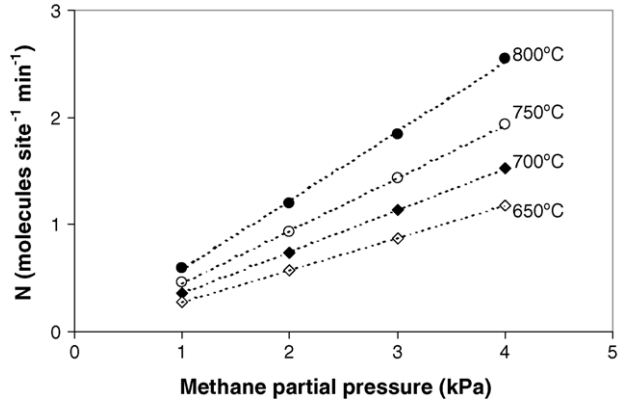

Fig. 8. Effect of methane partial pressure on the turnover frequencies (N) for steam reforming over Ni/Ce–ZrO_2 (Ce/Zr = 3/1) at different temperatures (9 kPa inlet H_2O).

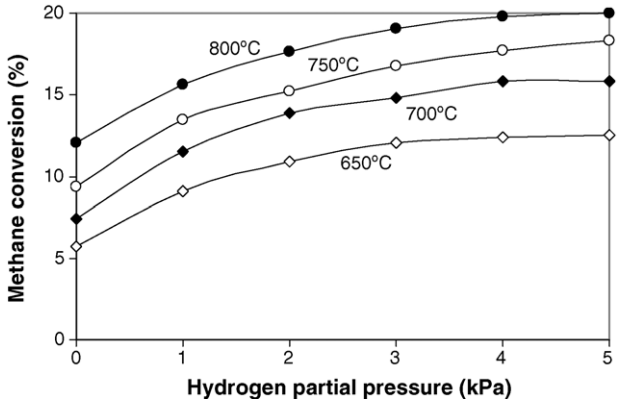

Fig. 10. Effect of hydrogen partial pressure on steam reforming rate over Ni/Ce–ZrO_2 (Ce/Zr = 3/1) at different temperatures (3 kPa CH_4, 9 kPa H_2O).

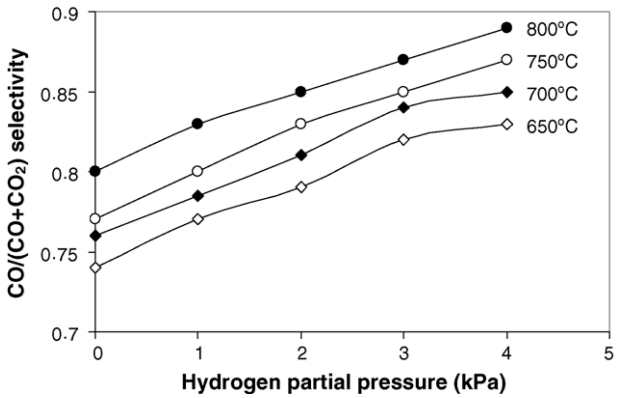

Fig. 11. Influence of hydrogen addition on CO/(CO + CO_2) selectivity from methane steam reforming over Ni/Ce–ZrO_2 at different temperatures (3 kPa CH_4, 9 kPa H_2O).

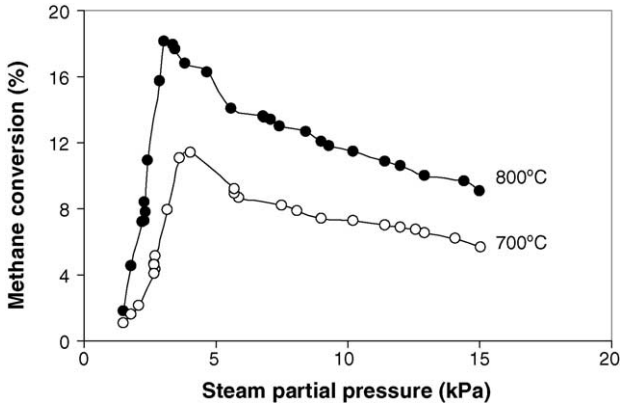

Fig. 13. Effect of steam partial pressure on steam reforming rate over Ni/Ce–ZrO_2 (Ce/Zr = 3/1) at 700 and 800 °C (3 kPa CH_4).

The steam reforming rates at higher inlet hydrogen partial pressures were then measured. The experiments yielded a non-linear positive hydrogen trend. When the inlet hydrogen partial pressure was greater than 8 kPa, the hydrogen influence on the steam reforming rate became much less pronounced. Moreover, the decrease in methane conversion was observed when the inlet hydrogen partial pressure was greater than 10 kPa (Fig. 12). Clearly, the negative effect of hydrogen for Ni/Ce–ZrO_2 was observed to be much stronger than that over Ni/Al_2O_3.

3.4.3. Effect of steam

In order to investigate the effect of inlet H_2O/CH_4 ratio on the steam reforming rate, this ratio was varied from 0.5 to 5.0 by changing the inlet steam partial pressure from 1.5 to 15 kPa. Two temperature levels of 700 and 800 °C were considered. As shown in Fig. 13, the dependence of steam on the rate of reforming is non-monotonic. The steam reforming rate increased with increasing inlet H_2O/CH_4 ratio until this ratio reached approximately 1.0–2.0. Then, steam presented a negative effect on the reforming rate at higher inlet H_2O/CH_4 ratio values. At the inlet H_2O partial pressure of 5–15 kPa, the reaction order related to steam decreased from −0.40 to −0.31 and −0.25 when the inlet hydrogen partial pressure increased from 0 to 1 and 2 kPa, respectively. This could be due to the decrease in the catalyst's oxidized state caused by a small addition of inlet hydrogen.

Unlike the effect of hydrogen, the reaction order in steam for the methane steam reforming over Ni/Al_2O_3 was close to that over Ni/Ce–ZrO_2 at the same operating conditions, indicating the same influence of steam on both Al_2O_3 and Ce–ZrO_2. This result was supported by the works of Laosiripojana [42], who reported the independence of inlet steam partial pressure on the methane steam reforming rate over ceria-based materials. Fig. 14 shows the influences of steam on the CO/(CO + CO_2) production selectivity. This selectivity decreased with increasing inlet steam partial pressure due to the promotion of the water–gas shift reaction in the forward direction. Table 4 presents the summary of observed reaction orders in each component (CH_4, H_2O, and H_2) for both Ni/Ce–ZrO_2 and Ni/Al_2O_3 at different temperatures and inlet compositions.

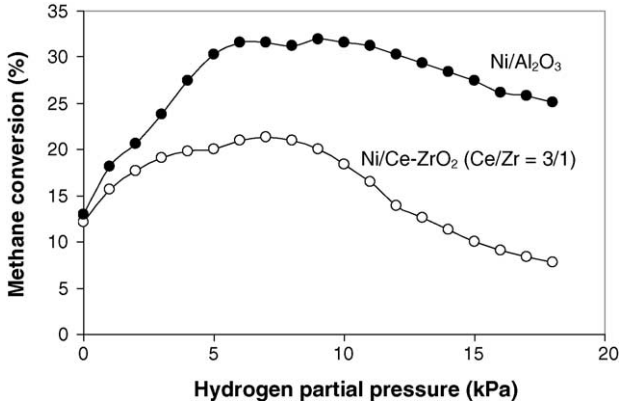

Fig. 12. Effect of hydrogen partial pressure on steam reforming rate over Ni/Ce–ZrO_2 (Ce/Zr = 3/1) and Ni/Al_2O_3 at high presence of hydrogen (0–18 kPa) at 800 °C.

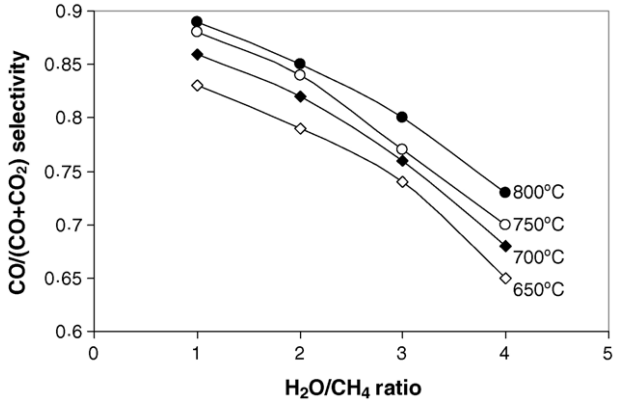

Fig. 14. Influence of inlet steam/methane ratio on CO/(CO + CO_2) selectivity from methane steam reforming over Ni/Ce–ZrO_2 at different temperatures (3 kPa CH_4).

Table 4
Reaction orders for the components of interest (CH_4, H_2O, and H_2) from methane steam reforming over Ni/Ce–ZrO_2 (Ce/Zr = 3/1) and Ni/Al_2O_3 at different operating conditions

Components of interest	Temperature (°C)	Other inlet compositions	Reaction order for components of interest	
			Ni/Ce–ZrO_2 (Ce/Zr = 3/1)	Ni/Al_2O_3
Methane (1–4 kPa)	650–800	9 kPaH_2O/0 kPaH_2	1.0 ± 0.04	1.0 ± 0.01
		12 kPa H_2O/0 kPa H_2	1.0 ± 0.05	1.0 ± 0.01
		15 kPaH_2O/0 kPa H_2	1.0 ± 0.02	1.0 ± 0.02
		9 kPaH_2O/1 kPa H_2	1.0 ± 0.02	1.0 ± 0.01
		9 kPa H_2O/3 kPa H_2	1.0 ± 0.01	1.0 ± 0.03
		9 kPaH_2O/5 kPa H_2	1.0 ± 0.03	1.0 ± 0.01
Hydrogen (1–4 kPa)	650	9 kPa H_2O/3 kPa CH_4	0.18	0.31
	700	9 kPa H_2O/3 kPa CH_4	0.20	0.28
	750	9 kPaH_2O/3 kPa CH_4	0.18	0.34
	800	9 kPa H_2O/3 kPa CH_4	0.19	0.33
	700	9 kPaH_2O/1 kPa CH_4	0.18	0.29
	700	9 kPa H_2O/5 kPa CH_4	0.20	0.32
	700	12 kPa H_2O/3 kPa CH_4	0.25	0.39
	700	15 kPa H_2O/3 kPa CH_4	0.28	0.42
Hydrogen (12–18 kPa)	650	9 kPaH_2 O/3 kPa CH_4	−0.31	−0.15
	700	9 kPa H_2O/3 kPa CH_4	−0.30	−0.16
	800	9 kPa H_2O/3 kPaCH_4	−0.34	−0.15
Steam (5–15 kPa)	650	0 kPa H_2/3 kPaCH_4	−0.39	−0.37
	700	0 kPa H_2/3 kPa CH_4	−0.40	−0.39
	750	0 kPa H_2/3 kPa CH_4	−0.38	−0.41
	800	0 kPaH_2/3 kPaCH_4	−0.42	−0.40
	700	1 kPa H_2/3 kPaCH_4	−0.31	−0.31
	700	2 kPaH_2/3 kPaCH_4	−0.25	−0.24
	700	3 kPa H_2/3 kPa CH_4	−0.22	−0.19

3.4.4. *Effect of oxygen*

As described earlier, autothermal reforming seems to be a promising reaction in order to produce hydrogen in the near future, as it is currently the most economical process. Methane steam reforming in the presence of oxygen or the autothermal reforming was then carried out by adding different oxygen partial pressures into the feed gas at several operating temperatures. The inlet methane and steam partial pressures were kept constant at 3 and 9 kPa, respectively, while the inlet oxygen partial pressure was varied from 0 to 4 kPa. At steady state, the methane steam reforming rate increased with increasing the inlet oxygen partial pressure as shown in Fig. 15. However, the CO/(CO + CO_2) production selectivity strongly decreased with increasing oxygen concentration due to the CO oxidation by O_2, as shown in Fig. 16. Hydrogen production also decreased with increasing oxygen concentration as shown in Fig. 17, which could be due to the inhibition of steam adsorption on the catalyst surface active sites by this component and also due to the combustion of H_2 production by inlet O_2.

4. Discussion

The steam reforming of methane over synthesized Ni/Ce–ZrO_2 was compared to conventional Ni/Al_2O_3 in the conditions where the influences of mass and heat transfer limitations could be considered negligible. Improvement of methane steam reforming performance in term of stability toward the deactivation by carbon deposition was achieved for Ni/Ce–ZrO_2. Compared to conventional Ni/Al_2O_3, Ni on Ce–ZrO_2 support provided higher resistance toward carbon formation and required significantly lower inlet H_2O/CH_4 ratio to prevent the formation of carbon species. These improvements are mainly related to the high redox property of Ce–ZrO_2 support.

Regarding the well known methane steam reforming mechanism over conventional Ni catalyst proposed by Dicks et al. [39], methane only adsorbs on the active surface site of Ni (*) and forms CH_x-*n. Simultaneously, the adsorption of

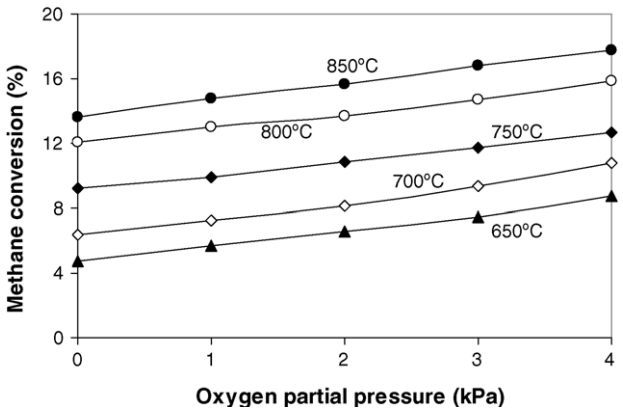

Fig. 15. Effect of oxygen partial pressure on steam reforming rate over Ni/Ce–ZrO_2 (Ce/Zr = 3/1) at different temperatures (3 kPa CH_4, 9 kPa H_2O).

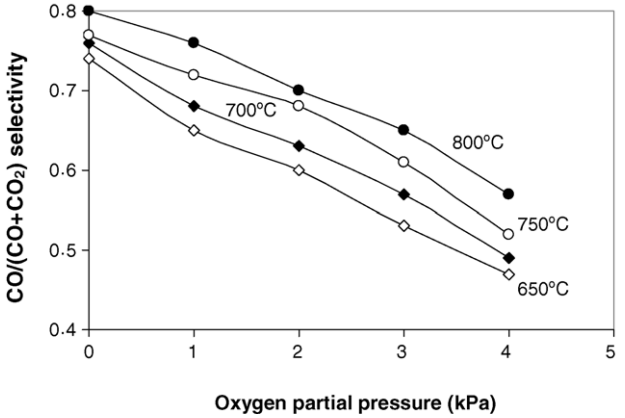

Fig. 16. Influence of oxygen addition on CO/(CO + CO_2) selectivity from methane steam reforming over Ni/Ce–ZrO_2 at different temperatures (3 kPa CH_4, 9 kPa H_2O).

inlet steam also takes place on the surface sites of Ni catalyst, forming O-*. These elements, O-* and CH_x-*n, eventually react with each other, producing CO and H_2, and the active surface site of Ni (*) also recovers as illustrated below:

$$CH_4 + n^* \rightarrow CH_x\text{-}*n + (4-x)/2H_2 \quad (11)$$

$$H_2O + * \Leftrightarrow O\text{-}* + H_2 \quad (12)$$

$$CH_x\text{-}*n + O\text{-}* \rightarrow CO + (x/2)H_2 + (n+1)^* \quad (13)$$

For the steam reforming of methane over Ni/Ce–ZrO_2, in addition to the reactions on Ni surface, the redox reaction between inlet CH_4 and the lattice oxygen (O_x) on Ce–ZrO_2 surface also takes place, producing H_2 and CO (Eq. (5)). Moreover, the reduced Ce–ZrO_2 can react with inlet H_2O to produce more H_2 and to recover O_x [42]. The proposed mechanism for these redox reactions, involving the reactions between methane and/or an intermediate surface hydrocarbon species with the lattice oxygen (O_x) on Ce–ZrO_2 surface and the recovery of O_x by steam, is presented

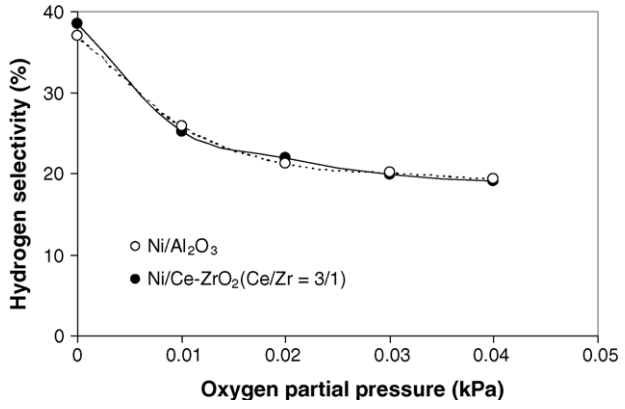

Fig. 17. Effect of oxygen on hydrogen selectivity (%) from methane steam reforming over Ni/Ce–ZrO_2 at 800 °C (3 kPa CH_4, 9 kPa H_2O).

schematically below:

$$CH_4 + 2S \Leftrightarrow CH_3\text{–}S + H\text{–}S \quad (14)$$

$$CH_3\text{–}S + S \Leftrightarrow CH_2\text{–}S + H\text{–}S \quad (15)$$

$$CH_2\text{–}S + S \Leftrightarrow CH\text{–}S + H\text{–}S \quad (16)$$

$$CH\text{–}S + S \Leftrightarrow C\text{–}S + H\text{–}S \quad (17)$$

$$C\text{–}S + O_x \Leftrightarrow CO + O_{x-1} + S \quad (18)$$

$$CO + O_x \Leftrightarrow CO_2 + O_{x-1} \quad (19)$$

$$2H\text{–}S \Leftrightarrow H_2 + 2S \quad (20)$$

$$H_2O + O_{x-1} \Leftrightarrow O_x + H_2 \quad (21)$$

The surface site (S) can be either a unique site, or it can also be considered to be the same site as the catalyst-oxidised site (O_x) [42]. It has been reported [43] that the controlling step of these redox reactions is the reaction of methane on the Ce–ZrO_2 surface; in addition, the lattice oxygen is replenished by a significant rapid surface reaction of the reduced state Ce–ZrO_2 with H_2O.

According to the possible formation of carbon species on the surface of catalyst during the steam reforming process, the following reactions are theoretically the most probable reactions that could lead to carbon formation:

$$2CO = CO_2 + C \quad (22)$$

$$CH_4 = 2H_2 + C \quad (23)$$

$$CO + H_2 = H_2O + C \quad (24)$$

$$CO_2 + 2H_2 = 2H_2O + C \quad (25)$$

C is the carbonaceous deposits. Reactions (24) and (25) are favorable at low temperature, while reaction (22) is thermodynamically unfavored [44]. At such a high temperature, the Boudard reaction (Eq. (22)) and the decomposition of methane (Eq. (23)) are the major pathways for carbon formation, as they show the largest change in Gibbs energy [45]. According to the range of temperature in this study, carbon formation would be formed via the decomposition of methane and Boudard reactions, especially at low inlet H_2O/CH_4 ratio. In the present work, we also observed a high amount of carbon formation on the surface of Ni/Al_2O_3 after exposure in methane steam reforming condition with the inlet H_2O/CH_4 ratio less than 3.0. By applying Ce–ZrO_2 as support, the formation of carbon species via Eqs. (22) and (23) could be inhibited by the redox reactions of methane and carbon monoxide (produced during the steam reforming process) with the lattice oxygen (O_x) at Ce–ZrO_2 surface (Eqs. (14)–(19)) forming hydrogen and carbon dioxide, which is thermodynamically unfavored to form carbon species in this range of conditions. Therefore, significant lower amounts of carbon deposition were consequently observed for Ni/Ce–ZrO_2 even at low inlet H_2O/CH_4 ratios. In addition, the reaction between the lattice oxygen (O_x) at

Ce–ZrO_2 surface with the adsorbed methane on Ni surface (CH_x-*n) and the rapid recovery of the lattice oxygen by the simultaneous supply of oxygen from H_2O also result in the higher resistance toward carbon formation and less inlet H_2O/CH_4 requirement for Ni/Ce–ZrO_2:

$$CH_x\text{-}*n + O_x \rightarrow CO + (x/2)H_2 + n^* + O_{x-1} \quad (26)$$

Many previous researchers have reported the excellent resistance toward carbon formation from methane cracking at high temperature for ceria-based materials including CeO_2 [27], Gd-doped CeO_2 [27], Nb-CeO_2 [46], and CeO_2-ZrO_2 [42]. One of them [42] also proposed that the addition of a small amount of H_2O to the inlet feed can eliminate all carbon species on the surface of CeO_2. The previous reports therefore agree well with the results in this work.

Regarding the kinetic studies over Ni/Ce–ZrO_2 in the present work, similar to the general metal catalysts as reported by previous researchers, the reaction orders in methane were observed to be approximately 1.0 in all conditions. The experiments yielded a non-linear positive hydrogen trend over this catalyst (Fig. 12). The positive effect at the low hydrogen appearance could be due to the reduction of oxidized state on the surface active site of nickel ($H_2 + O\text{-}* \Leftrightarrow H_2O + *$), while the inhibitory effect at high hydrogen partial pressure could be due to the promotion of the methanation, the reverse water–gas shift reactions and the reverse methane steam reforming [4-6]. In addition, the occupying of hydrogen atoms on some active sites of nickel particles ($H_2 + 2^* \Leftrightarrow 2H\text{-}*$) could also lead to the decrease in methane conversion, as explained by Xu and Froment [4–6].

Clearly, the negative effect of hydrogen for Ni/Ce–ZrO_2 was observed to be much stronger than that over Ni/Al_2O_3. This is due to the reduction of lattice oxygen (O_x) by hydrogen via the reverse of Eq. (21) ($O_x + H_2 \Leftrightarrow H_2O + O_{x-1}$) and consequently inhibits the reaction of the lattice oxygen (O_x) with the surface hydrocarbon species (both C–S and CH_x-n) in Eqs. (18) and (26) (C–S + $O_x \Leftrightarrow$ CO + O_{x-1} + S and CH_x-*n + $O_x \rightarrow$ CO + (x/2)H_2 + n^* + O_{x-1}). This explanation is in good agreement with the previous studies [42,43,46] which studied kinetics parameters for the methane steam reforming on ceria-based materials and reported the negative effect of hydrogen on methane conversion over these materials due to the change of Ce^{4+} to Ce^{3+}.

The dependence of steam on the rate of reforming is non-monotonic due to adsorption competition between CH_4 and H_2O on the catalyst active sites. Previous works [4,5] also reported the same results and explanation on Ni/ZrO_2. Furthermore, the study of autothermal reforming over this catalyst found that methane steam reforming rate increased with increasing the inlet oxygen partial pressure. However, the CO/(CO + CO_2) production selectivity and hydrogen production rates strongly decreased with increasing oxygen partial pressure. This is due to the inhibition of steam adsorption on the catalyst surface active sites and the oxidation of hydrogen by oxygen in the feed.

5. Conclusion

Methane steam reforming over Ni catalyst supported on Ce–ZrO_2 was studied at 650–900 °C in the conditions where the influence of mass transfer limitations could be considered negligible. At 900 °C, Ni/Ce–ZrO_2 with Ce/Zr ratio of 3/1 showed the best performance in term of activity and stability. The resistance toward carbon formation over this catalyst was higher than that over conventional Ni/Al_2O_3 at the same operating conditions regarding its high redox property; however, slight deactivation due to the sintering was observed over Ni/Ce–ZrO_2 at these high temperature conditions.

Similar to the conventional Ni/Al_2O_3, the reaction order in methane for Ni/Ce–ZrO_2 was always observed to be 1.0. The dependence of steam on the rate was non-monotonic, and the addition of oxygen promoted the rate but reduced CO and H_2 production selectivity. At high hydrogen appearance, Ni/Ce–ZrO_2 showed a stronger negative impact of hydrogen compared to Ni/Al_2O_3, due to the possible reduction of Ce–ZrO_2. This strong negative effect of hydrogen would be a major concern in applying Ni/Ce–ZrO_2 industrially. Although Ni/Ce–ZrO_2 is a good reforming catalyst in term of the high resistance toward the carbon formation, methane conversion could be significantly reduced at high hydrogen appearance, and the removal of hydrogen during the reforming process might be required.

Acknowledgements

The financial support from The Thailand Research Fund (TRF) throughout this project is gratefully acknowledged. The first author would like to acknowledge Professor David Chadwick from the Department of Chemical Engineering and Chemical Technology, Imperial College London, for his valuable suggestions.

References

[1] K. Otsuka, T. Ushiyama, I. Yamanaka, Chem. Lett. (1993) 1517.
[2] K. Otsuka, M. Hatano, A. Morikawa, J. Catal. 79 (1983) 493.
[3] K. Otsuka, M. Hatano, A. Morikawa, Inorg. Chim. Acta 109 (1985) 193.
[4] J. Xu, PhD Thesis, Laboratorium Voor Petrochemische Techniek, Rijkuniversiteit, Gent, Belgium, 1986.
[5] J. Xu, G.F. Froment, AIChE 35 (1989) 88.
[6] J. Xu, G.F. Froment, AIChE 35 (1989) 97.
[7] S.S.E.H. Elnashaie, A.M. Adris, A.S. Al-Ubaid, M.A. Soliman, Chem. Eng. Sci. 45 (1990) 491.
[8] S.S.E.H. Elnashaie, S.S. Elshishini, Modeling, Simulation and Optimization of Industrial Fixed Bed Catalytic Reactors, Gordon and Breach Science Publishers, UK, 1993.
[9] L.V. Mattos, E. Rodino, D.E. Resasco, F.B. Possos, F.B. Noronha, Fuel Proc. Technol. 83 (2003) 147.
[10] H.S. Roh, K.W. Jun, S.E. Park, Appl. Catal. A 251 (2003) 275.
[11] J.R. Rostrup-Nielsen, J.-H. Bak-Hansen, J. Catal. 144 (1993) 38.
[12] X. Wang, R.J. Gorte, Appl. Catal. A 224 (2002) 209.

[13] H.S. Roh, K.W. Jun, W.S. Dong, J.S. Chang, S.E. Park, Y.I. Joe, J. Mol. Catal. A 181 (2002) 137.
[14] Q. Miao, G. Xiong, S. Sheng, W. Cui, L. Xu, X. Guo, Appl. Catal. A 154 (1987) 17.
[15] A.A. Lemonidou, M.A. Goula, I.A. Vasalos, Catal. Today 46 (1987) 175.
[16] W.S. Dong, H.S. Roh, K.W. Jun, S.E. Park, Y.S. Oh, Appl. Catal. A 226 (2002) 63.
[17] M. Mamak, N. Coombs, G. Ozin, Adv. Mater. 12 (2000) 198.
[18] M. Mamak, N. Coombs, G. Ozin, J. Am. Chem. Soc. 122 (2000) 8932.
[19] M. Mamak, N. Coombs, G.A. Ozin, Chem. Mater. 13 (2001) 3564.
[20] P. Bera, S. Mitra, S. Sampath, M.S. Hegde, Chem. Commun. (2001) 927.
[21] A. Martinez-Arias, J.M. Coronado, R. Cataluna, J.C. Conesa, J.C. Soria, J. Phys. Chem. B 102 (1998) 4357.
[22] D. Skarmoutsos, F. Tietz, P. Nikolopoulos, Fuel Cells 1 (2001) 243.
[23] T. Takeguchi, S.N. Furukawa, M. Inoue, J. Catal. 202 (2001) 14.
[24] J. Sfeir, P.A. Philippe, P. Moseki, N. Xanthopoulos, R. Vasquez, J.M. Hans, V.H. Jan, K.R. Thampi, J. Catal. 202 (2001) 229.
[25] N. Kiratzis, P. Holtappels, C.E. Hatchwell, M. Mogensen, J.T.S. Irvine, Fuel Cells 1 (2001) 211.
[26] H.S. Roh, W.S. Dong, K.W. Jun, S.E. Park, Chem. Lett. 88 (2001).
[27] E. Ramirez, A. Atkinson, D. Chadwick, Appl. Catal. B 36 (2002) 193.
[28] M. Ozawa, M. Kimura, A. Isogai, J. Alloys Compd. 193 (1993) 73.
[29] G. Balducci, J. Kaspar, P. Fornasiero, M. Graziani, M.S. Islam, J. Phys. Chem. B 102 (1998) 557.
[30] G. Vlaic, P. Fornasiero, S. Geremia, J. Kaspar, M. Graziani, J. Catal. 168 (1997) 386.
[31] G.R. Rao, J. Kaspar, S. Meriani, R. Dimonte, M. Graziani, Catal. Lett. 24 (1994) 107.
[32] P. Fornasiero, R. Dimonte, G.R. Rao, J. Kaspar, S. Meriani, A. Trovarelli, M. Graziani, J. Catal. 151 (1995) 168.
[33] M. Haneda, K. Miki, N. Kakuta, A. Ueno, S. Tani, S. Matsura, M. Sato, Nihon Kagaku Kaishi (1990) 820.
[34] T. Ohata, Rare Earths 17 (1990) 37.
[35] J.G. Nunan, W.B. Williamson, H.J. Robota, SAE Paper 960768, 1996.
[36] S. Otsuka-Yao, H. Morikawa, N. Izu, K. Okuda, J. Jpn. Inst. Met. 59 (1995) 1237.
[37] M.H. Yao, T.E. Hoost, R.J. Baird, F.W. Kunz, J. Catal. 166 (1997) 67.
[38] D. Kim, J. Am. Ceram. Soc. 72 (1989) 1415.
[39] A.L. Dicks, K.D. Pointon, A. Siddle, J. Power Sources 86 (2000) 523.
[40] P.A. Webb, C. Orr, Analytical Methods in Fine Particle Technology, Micromeritics Instrument Corporation, USA, 1997.
[41] K.D. Pointon, Review of Work on Internal Reforming in the Solid Oxide Fuel Cell, ETSU Report F/01/00121/REP, 1997.
[42] N. Laosiripojana, Reaction engineering of indirect internal steam reforming of methane for application in solid oxide fuel cells, PhD Thesis, University of London, UK, 2003.
[43] E. Ramírez-Cabrera, A. Atkinson, D. Chadwick, Appl. Catal. B 47 (2004) 127.
[44] Y. Lwin, W.R.W. Daud, A.B. Mohamad, Z. Yaakob, Int. J. Hydrogen Energy 25 (1) (2000) 47.
[45] J.N. Amor, Appl. Catal. A 176 (1999) 159.
[46] E. Ramírez-Cabrera, N. Laosiripojana, A. Atkinson, D. Chadwick, Catal. Today 78 (2003) 433.

N. Laosiripojana, W. Sutthisripok and S. Assabumrungrat

"Synthesis gas production from dry reforming of methane over CeO_2 doped Ni/Al_2O_3: Influence of the doping ceria on the resistance toward carbon formation"

Chemical Engineering Journal, 112 (2005) 13-22

(IF-2004 = 1.38)

ELSEVIER

Chemical Engineering Journal 112 (2005) 13–22

Chemical Engineering Journal

www.elsevier.com/locate/cej

Synthesis gas production from dry reforming of methane over CeO_2 doped Ni/Al_2O_3: Influence of the doping ceria on the resistance toward carbon formation

N. Laosiripojana [a,*], W. Sutthisripok [b], S. Assabumrungrat [c]

[a] *The Joint Graduate School of Energy and Environment, King Mongkut's University of Technology Thonburi, Bangkok 10140, Thailand*
[b] *Department of Mining and Materials Engineering, Faculty of Engineering, Prince of Songkla University, Songkhla, Thailand*
[c] *Center of Excellence on Catalysis and Catalytic Reaction Engineering, Department of Chemical Engineering, Faculty of Engineering, Chulalongkorn University, Bangkok 10330, Thailand*

Received 17 January 2005; received in revised form 4 June 2005; accepted 9 June 2005

Abstract

Doping of CeO_2 as an additive promoter on Ni/Al_2O_3 was found to improve dry reforming activity for H_2 and CO productions at solid oxide fuel cell (SOFC) operating temperature (800–900 °C). The catalyst provides significantly higher reforming reactivity and resistance toward carbon deposition compared to conventional Ni/Al_2O_3. These enhancements are mainly due to the influence of the redox property of ceria. During dry reforming process, in addition to the reactions on Ni surface, the gas–solid reactions between the gaseous components presented in the system (CH_4, CO_2, CO, H_2O, and H_2) and the lattice oxygen (O_x) on ceria surface also take place. The reactions of adsorbed methane and carbon monoxide (produced during dry reforming process) with the lattice oxygen (O_x) on ceria surface ($CH_4 + O_x \rightarrow CO + H_2 + O_{x-1}$ and $CO + O_x \Leftrightarrow CO_2 + O_{x-1}$) can prevent the formation of carbon species on Ni surface from methane decomposition reaction and Boudard reaction.

In particular, CeO_2 doped Ni/Al_2O_3 with 8% ceria content showed the best reforming activity among those with the ceria content between 0 and 14%. The amount of carbon formation decreased with increasing Ce content. However, Ni was oxidized when more than 10% of ceria was doped. According to the post-XPS measurement, a small formation of Ce_2O_3 was observed after exposure in dry methane reforming conditions with low inlet CH_4/CO_2 ratio (1.0/0.3). The intrinsic reaction kinetics of 8% CeO_2 doped Ni/Al_2O_3 was studied by varying inlet CH_4 and CO_2 concentrations, and by adding H_2 and CO to the system at different temperatures. The dry reforming rate increased with increasing methane partial pressure and the operating temperature. The reaction orders in methane were always closed to 1.0 in all conditions. Carbon dioxide also presented weak positive impact on the methane conversion, whereas adding of carbon monoxide and hydrogen inhibited the reforming rate.

Keywords: Hydrogen; Synthesis gas; Carbon formation; Dry reforming; CeO_2

1. Introduction

Solid oxide fuel cell (SOFC) with an indirect internal reforming operation (IIR), called IIR-SOFC, is expected to be an important technology for energy generation in the near future due to the high efficiency and its low environmental impact. Regarding this operation, the endothermic reforming reaction takes place at the reformer, which is in close thermal contact with the anode side of fuel cell where the exothermic electrochemical reaction takes place (Fig. 1). IIR gives the advantage on eliminating the requirement for a separate fuel reformer and providing good heat transfer between the reformer and the fuel cell. In addition, the reformer part and the anode side for IIR operation can be operated separately. Therefore, the catalyst for reforming reaction at the reformer part and the material for electrochemical reactions at the anode side of fuel cell can be different

* Corresponding author.
E-mail address: navadol_l@jgsee.kmutt.ac.th (N. Laosiripojana).

1385-8947/$ – see front matter © 2005 Elsevier B.V. All rights reserved.
doi:10.1016/j.cej.2005.06.003

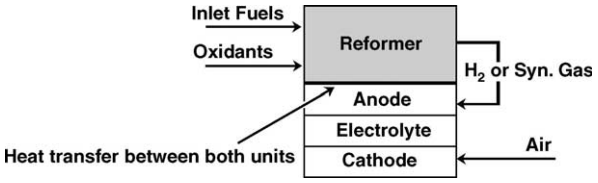

Fig. 1. Diagram of IIR-SOFC operation.

and optimized individually. This operation is expected to simplify the overall system design, making SOFC more attractive and efficient for producing electrical power [1].

The aim of the reformer unit is to reform and maximize the yield of hydrogen production and supply this component to the anode side of SOFC. Theoretically, hydrogen can be produced from several natural hydrocarbon sources including natural gas, bio-ethanol, coal, biomass, and biogas. Biogas consists mainly of methane and carbon dioxide is expected to be the attractive raw material for hydrogen production in the near future due to its economic availability. Due to the rich CO_2 for biogas, carbon dioxide (or dry) reforming reaction would be one of the most suitable processes to convert biogas to hydrogen or synthesis gas (CO and H_2). Compared to the steam reforming, both steam and dry reforming reactions have similar thermodynamic characteristics except that the carbon formation in the dry reforming is more severe than in the steam reforming due to the lower H/C ratio of this reaction [2]. The attractive feature of the dry reforming reaction is the utilisation of CO_2, which is a greenhouse effect gas. In general, the dry reforming reaction (Eq. (1)) is typically accompanied by the simultaneous occurrence of the reverse water-gas shift reaction (RWGS) (Eq. (2)).

$$CH_4 + CO_2 \Leftrightarrow 2CO + 2H_2 \qquad \Delta H = 247\,\text{kJ/mol} \qquad (1)$$

$$CO_2 + H_2 \Leftrightarrow CO + H_2O \qquad \Delta H = 41.1\,\text{kJ/mol} \qquad (2)$$

The hydrogen to carbon monoxide production ratio (H_2/CO ratio) from the dry reforming reaction is always less than 1. Vannice and Bradford [3] presented the apparent activation energies for the consumption of methane and carbon dioxide, as well as the production of carbon monoxide, hydrogen, and water in order to investigate the influence of the RWGS reaction. They observed that the apparent activation energy for hydrogen formation is greater than that for the formation of carbon monoxide, in which supported the influence of the reverse water-gas shift reaction on the reaction mechanism. Sodesawa et al. [4] studied the dry reforming reaction at a stoichiometric feed ratio over several catalysts. They found that the activities of most catalysts deactivated rapidly due to the carbon deposition. Topor et al. [5] suggested that the use of excess carbon dioxide could avoid carbon formation. Chubb et al. [6,7] studied the carbon dioxide reforming using an excess of carbon dioxide with carbon dioxide to methane ratios of 3:1 and 5:1 over Ni/Al_2O_3. They reported that the rate of disintegration is smaller for the higher one. Rostrup-Nielsen and Bak Hansen [8] investigated the activity toward dry reforming over several metals. Their order of reactivity for this reaction was Ru > Rh > Ni ∼ Ir > Pt > Pd, in which similar to their proposed order for steam reforming. They also observed that the replacing of steam with carbon dioxide gave similar activation energies, which indicated a similar rate-determining step in these two reactions. In addition, low levels or no carbon formation was detected from dry reforming over Rh metal at low temperature and CO_2 content [9]. Erdöhelyi et al. [10,11] studied the influence of the catalyst support on the dry reforming of rhodium-based catalyst, and reported that the support had no effect on the activity of Rh. In contrast, Nakamura et al. [12] and Zhang et al. [13] observed that the initial turnover frequency (specific activity) of Rh crystallities was significantly affected by their supports. Zhang et al. [13] also reported that the deactivation of Rh crystallities was strongly dependent on their supports.

In this present study, it is aimed at the development of an alternative catalyst for dry methane reforming reaction, which provided high stability, and activity toward this reaction at such a high temperature (800–900 °C) for later application in IIR-SOFC. According to the economical point of view, Ni/Al_2O_3 was selected as a based catalyst rather than the precious metals. Cerium oxide (CeO_2) was chosen as an additive promoter. This material (called ceria) is an important material for a variety of catalytic reactions involving oxidation of hydrocarbons (e.g. automobile exhaust catalysts). It contains a high concentration of highly mobile oxygen vacancies, which act as local sources or sinks for oxygen involved in reactions taking place on its surface. Nowadays, a potential application of ceria is in solid oxide fuel cells application as a reforming catalyst for in-stack (called indirect internal) reforming of methane, since it is high resistant toward carbon deposition compared to Ni [14]. Recently, the successful test of ceria for the methane steam reforming reaction has been reported [15–17]. Due to the high resistance toward carbon formation, ceria should be a good additive promoter for dry reforming process.

Recently, the use of ceria-based materials as the support and promoter for the catalytic reforming reaction has been reported by several researchers. As the support, it has been reported to be promising support among α-Al_2O_3 [18], γ-Al_2O_3, and γ-Al_2O_3 with alkali metal oxide and rare earth metal oxide [19] and $CaAl_2O_4$ [18–21], while the selected metals were Ni, Pt, or Pd [22–31]. As the promoter, ceria was also reported to be a good promoter for the dry methane reforming at intermediate temperature [32]. Wang and Lu [32] prepared CeO_2 doped Ni/Al_2O_3 by adding CeO_2 on γ-Al_2O_3 powder before impregnated Ni on CeO_2–Al_2O_3 support and tested the dry methane reforming reactivity at 500–800 °C. They found that the doping of CeO_2 significantly improved the resistance of catalyst toward the carbon deposition.

In this work, various amounts of cerium oxide were firstly doped on the surface of Ni/Al_2O_3 in order to determine the suitable doping ratio. The reactivity toward dry reforming and the resistance toward carbon formation over CeO_2 doped Ni/Al_2O_3 was studied and compared to conventional

Ni/Al_2O_3 at the temperature range of 800–900 °C. In addition, the intrinsic kinetics of the dry methane reforming reaction over this catalyst was also studied by varying inlet CH_4, CO_2, and by adding CO and H_2 at different temperatures. The reaction orders in each component and the possible rate isotherm with the fitting parameters were determined. These kinetic informations are important in order to determine the behavior of the catalyst toward this reaction for the large scale or industrial application. By fitting the rate isotherm and parameters in the modeling, the behavior of the whole reformer and the IIR-SOFC system can be predicted.

2. Experimental

2.1. Catalyst preparations

Ni/Al_2O_3 (5 wt.% Ni) was prepared by impregnating α-Al_2O_3 (from Aldrich) with $NiCl_3$ solution at room temperature. This solution was stirred by magnetic stirring (100 rpm) for 6 h, dried overnight in an oven at 110 °C, and calcined in air at 900 °C for 6 h. The catalyst powder was then reduced with 10% H_2/Ar at 700 °C for 6 h. CeO_2 doped Ni/Al_2O_3 was prepared by impregnate different concentration of cerium nitrate ($Ce(NO_3)_3{\cdot}6H_2O$ (99.0%), Fluka) on Ni/Al_2O_3 powder. Similarly, this solution was stirred by magnetic stirring (100 rpm) for 6 h before filtered and washed with deionised water and ethanol to prevent an agglomeration. The sample was dried and calcined in air at 1000 °C for 6 h. It was reduced with 10% H_2/Ar at 700 °C for 6 h before use.

2.2. Apparatus and procedures

In order to investigate the dry reforming and its associated reactions, an experimental reactor system was constructed. The feed gases including the components of interest such as CH_4, CO_2, H_2, or CO were introduced to the reaction section, in which an 8-mm internal diameter and 40-cm length quartz reactor was mounted vertically inside a furnace. The catalyst (50 mg) was loaded in the quartz reactor, which was packed with a small amount of quartz wool to prevent the catalyst from moving. In order to observe the intrinsic reaction kinetics, the methane conversions from dry reforming were always kept below 20% in all experiments.

In the present work, the desired space velocity and suitable catalyst particle size were achieved from several preliminary tests, which were carried out to avoid any limitations by intraparticle diffusion in the experiments. Regarding to these testing, the total flow rate was varied between 20 and 200 $cm^3\ min^{-1}$ under a constant residence time of 5×10^{-4} g min cm^{-3}. When the total flow rate was below 60 $cm^3\ min^{-1}$, the reforming rate increased with increasing the gas flow rate, suggesting that the mass transfer between the bulk gas and the catalyst particles is the rate-determining step. The reforming rate was almost constant in the range where the gas flow rate was higher than 80 $cm^3\ min^{-1}$, indicating that the mass transfer effect is unimportant in this flow rate range. Fig. 2 shows the effect of the total gas flow rate on the reforming rate over 8% CeO_2 doped Ni/Al_2O_3 at different temperatures. The reactions on different average sizes (from 100 to 500 μm) of catalysts were also carried out. It was observed that there were no significant changes in the methane conversion for the catalyst with the particle size between 100 and 200 μm, which indicated that the intraparticle diffusion limitation was negligible in this range of operating conditions. Consequently, the weight of catalyst loading was 50 mg, while the total gas flow was kept constant at 100 $cm^3\ min^{-1}$. The catalyst particle size diameter was between 100 and 200 μm in all experiments.

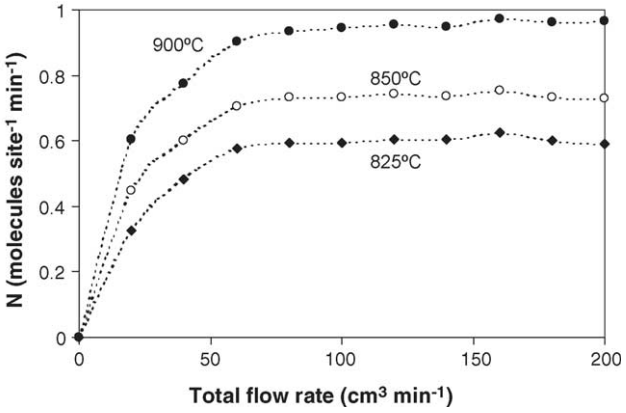

Fig. 2. Effect of the total gas flow rate on the turnover frequencies (*N*) for dry reforming over 8% CeO_2 doped Ni/Al_2O_3 at different temperatures (4 kPa CH_4 and 12 kPa CO_2).

A type-K thermocouple was placed into the annular space between the reactor and the furnace. This thermocouple was mounted on the tubular reactor in close contact with the catalyst bed to minimize the temperature difference between the catalyst bed and the thermocouple. Another type-K thermocouple was inserted in the middle of the quartz tube in order to re-check the possible temperature gradient. The record showed that the maximum temperature fluctuation during the reaction was always ±0.75 °C or less from the temperature specified for the reaction.

After the reactions, the exit gas mixture was transferred via trace-heated lines to the analysis section, which consists of a Porapak Q column Shimadzu 14B gas chromatograph (GC) and a mass spectrometer (MS). The gas chromatography was applied in order to investigate the steady state condition experiments, whereas the mass spectrometer in which the sampling of the exit gas was done by a quartz capillary and differential pumping was used for the transient and carbon formation experiments. In order to study the formation of carbon species on catalyst surface, temperature-programmed oxidation (TPO) was applied by introducing 10% oxygen in helium into the system, after purged with helium. The operating temperature increased from room temperature to 1000 °C by the rate of 10 °C/min. The calibrations of CO and CO_2 productions were performed by injecting a known amount of

these calibration gases from a loop, in an injection valve in the bypass line. The response factors were obtained by dividing the number of moles for each component over the respective areas under peaks. In addition to the TPO method, the amount of carbon deposition was confirmed by the calculation of carbon balance in the system. The amount of carbon deposited on the surface of catalyst would theoretically be equal to the difference between the inlet carbon containing components (CH_4 and CO_2) and the outlet carbon containing components (CO, CO_2, and CH_4). The amount of carbon deposited per gram of catalyst is given by the following equation:

$$C_{\text{deposition}} = \frac{\text{mole}_{\text{carbon (in)}} - \text{mole}_{\text{carbon (out)}}}{m_{\text{catalyst}}} \quad (3)$$

3. Results and discussion

3.1. Catalyst characterizations

After reduction, the catalysts were characterized with several physicochemical methods. The weights content of Ni and Ce loadings were determined by X-ray fluorescence (XRF) analysis. The reducibility and dispersion percentages of nickel were measured from temperature-programmed reduction (TPR) with 5% H_2 in Ar and temperature-programmed desorption (TPD), respectively. The catalyst specific surface areas were obtained from BET measurement. All physicochemical properties of the synthesized catalysts are presented in Table 1. The catalyst specific surface areas slightly increased by the doping of Ce.

3.2. Selection of suitable Ce doping content

After reduction, various Ce contents (from 2 to 14%) doped on Ni/Al_2O_3 were studied in dry reforming at 900 °C. The feed was CH_4/CO_2 in helium with the CH_4/CO_2 ratio of 1.0/0.3. Fig. 3 presents the steady state turnover frequencies (N) for CeO_2 doped Ni/Al_2O_3 with different CeO_2 contents. The turnover frequencies were calculated from the methane conversion following the below equation by assuming that all surface sites accessible by nitrogen adsorption (area per molecule 16.2×10^{-20} m^2 [14]) were active.

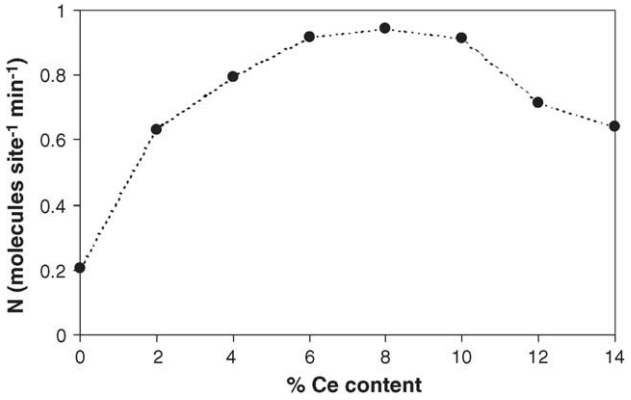

Fig. 3. Effect of Ce doping content on the turnover frequencies (N) for dry reforming (900 °C, 4 kPa CH_4, and 12 kPa CO_2).

$$N = \frac{rN_A A_{N_2}}{m_c S} \quad (4)$$

where r is the reaction rate (moles CH_4 per unit time), N_A the Avagadro's number, A_{N_2} the area occupied by an adsorbed nitrogen molecule (16.2×10^{-20} m^2), m_c the weight of catalyst used (50 mg), and S is the specific surface area of the catalyst. The figure indicates that 8% CeO_2 doping on Ni/Al_2O_3 presents the highest turnover frequencies.

The post-reaction temperature-programmed oxidation experiments were then carried out after a helium purge by introducing of 10% oxygen in helium in order to determine the degree of carbon deposition on the surface of each sample. Table 2 presents the important physicochemical properties of the spent catalysts after exposure in dry reforming conditions for 10 h. According to TPO, the amount of carbon formation decreased with increasing Ce content. No carbon species was observed when the Ce doping content was higher than 8%. The decreasing in the reactivity when more than 10% CeO_2 was doped could be due to the oxidized of Ni, as the reducibility of Ni reduced after exposure in dry reforming for 10 h, regarding to the TPR experiments.

It should also be noted that, at steady state, the main products from this reaction were H_2 and CO with H_2/CO always less than 1, indicating a contribution of the reverse water-

Table 1
Physicochemical properties of the catalysts after reduction at 700 °C

Catalyst	Ni load[a] (wt.%)	Ce load[a] (wt.%)	BET surface area ($m^2\ g^{-1}$)	Ni-reducibility[b] (Ni%)	Ni-dispersion[c] (Ni%)
Ni/Al_2O_3	4.91	0.0	40.2	92.1	4.87
2% Ce-Ni/Al_2O_3	4.84	1.87	40.8	93.5	4.54
4% Ce-Ni/Al_2O_3	4.93	4.02	42.7	91.4	5.12
6% Ce-Ni/Al_2O_3	5.01	5.94	46.5	90.6	4.54
8% Ce-Ni/Al_2O_3	4.96	8.03	49.1	91.1	4.65
10% Ce-Ni/Al_2O_3	4.88	9.86	49.8	89.9	4.77
12% Ce-Ni/Al_2O_3	4.93	12.1	50.4	90.3	4.64
14% Ce-Ni/Al_2O_3	4.92	13.9	50.9	91.0	4.20

[a] Measured from X-ray fluorescence analysis.
[b] Measured from temperature-programmed reduction (TPR) with 5% hydrogen.
[c] Measured from temperature-programmed desorption (TPD) of hydrogen after TPR measurement.

Table 2
Methane conversions, H_2/CO production ratio, and physicochemical properties of the catalysts after exposure in dry reforming (4 kPa CH_4 and 12 kPa CO_2) at 900 °C

Catalyst	CH_4 conversions (%) at steady state	H_2/CO ratio	Ni and Ce load[a] (wt.%)	Carbon formation[b] (monolayers)	BET surface ($m^2\ g^{-1}$)	Ni reducibility[c] (Ni%)	Ni dispersion[d] (Ni%)
Ni/Al_2O_3	3.32	0.89	4.89/0.0	3.48	40.0	92.1	4.84
2% Ce-Ni[e]	9.43	0.88	4.86/1.87	3.01	40.8	93.2	4.48
4% Ce-Ni	12.2	0.84	4.96/4.00	1.62	42.0	91.0	5.07
6% Ce-Ni	14.7	0.81	4.97/5.98	0.43	43.9	90.0	4.52
8% Ce-Ni	15.3	0.80	4.98/8.01	∼0	44.4	90.4	4.60
10% Ce-Ni	14.9	0.77	4.83/9.93	∼0	44.7	87.3	4.71
12% Ce-Ni	11.8	0.75	4.87/11.9	∼0	45.1	70.1	4.55
14% Ce-Ni	10.7	0.71	4.94/14.0	∼0	45.6	67.6	4.14

[a] Measured from X-ray fluorescence analysis.
[b] Calculated using CO and CO_2 yields from temperature-programmed oxidation (TPO) with 10% oxygen.
[c] Nickel reducibility (measured from temperature-programmed reduction (TPR) with 5% hydrogen).
[d] Nickel dispersion (measured from temperature-programmed desorption (TPD) after TPR).
[e] CeO_2 dopedNi/Al_2O_3.

gas shift reaction. Small amount of steam was also observed from the reaction. The H_2/CO ratio decreased with increasing Ce doping content indicated the high reactivity toward the reverse water-gas shift reaction of ceria (Table 2). The reactivities toward the reverse water-gas shift reaction for CeO_2 doped Ni/Al_2O_3 (with several Ce contents) and Ni/Al_2O_3 were tested in order to ensure the above explanation by using TPRx in CO_2/H_2/He gas mixture (5 kPa CO_2 and 10 kPa H_2). Fig. 4 shows the activities of all catalysts toward this reaction. Clearly, the activity toward the RWGS reaction over CeO_2 doped Ni/Al_2O_3 with high Ce content was significantly higher than that over Ni/Al_2O_3 at the same operating conditions.

3.3. Reactivity toward dry reforming

Ni/Al_2O_3 and 8% CeO_2 doped Ni/Al_2O_3 were further studied in dry reforming at 900 °C. The feed was CH_4/CO_2 in helium with different CH_4/CO_2 ratios of 1.0/0.3, 1.0/1.0, and 1.0/3.0. The reforming rate was measured as a function of time in order to indicate the stability and the deactivation rate.

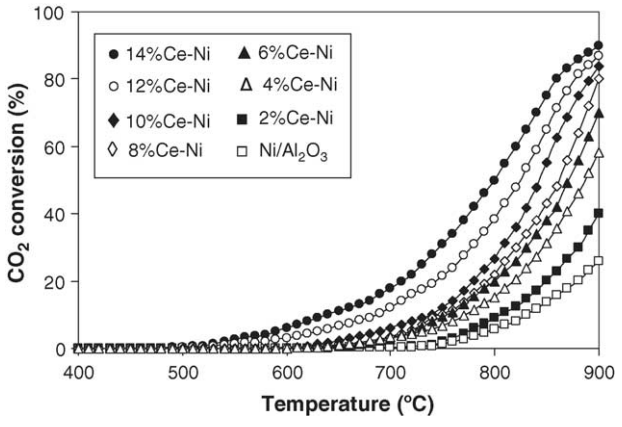

Fig. 4. The activities of Ni/Al_2O_3 and CeO_2 doped Ni/Al_2O_3 (with different Ce contents) toward the reverse water-gas shift reaction using TPRx in CO_2/H_2/He gas mixture (5 kPa CO_2 and 10 kPa H_2).

The variations in turnover frequencies (N) with time at 900 °C for different catalysts and different inlet CH_4/CO_2 ratio are shown in Fig. 5. The significant deactivations were detected for Ni/Al_2O_3 catalyst in all conditions especially at high inlet CH_4/CO_2 ratio, whereas considerable lower deactivations were detected for 8% CeO_2 doped Ni/Al_2O_3. At steady state, the dry reforming over 8% CeO_2 doped Ni/Al_2O_3 with inlet CH_4/CO_2 of 1.0/3.0 showed the best activity. Catalyst stabilities expressed as deactivation percentages are given in Table 3.

The characterization of these spent catalysts by X-ray diffraction (XRD) and X-ray photoelectron spectroscopy (XPS) were then carried out to determine the formation or the changing of chemical states in the spent catalysts, compared to the fresh one after reduction. X-ray diffraction was performed using X-ray defractometer with Cu Kα radiation (λ = 1.54060 Å) and operating parameters of 40 kV and 40 mA. Diffraction patterns were acquired by a step-scanning technique, using a step size ($\Delta 2\theta$) of 0.020°. The XPS spectra were acquired on spectrometer with a hemispherical electron analyser detector, operated in a constant threshold pass energy mode (50 eV), and using a non-monochromatic Al

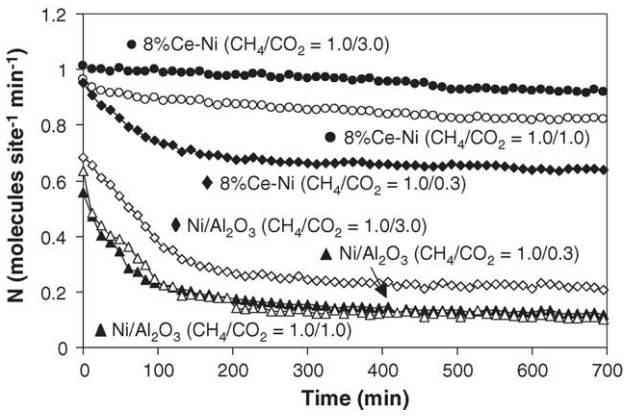

Fig. 5. Dry reforming of methane at 900 °C for several catalysts and various inlet CH_4/CO_2 ratios.

Table 3
Methane conversions, stabilities, and physicochemical properties of the catalysts after exposure in dry reforming conditions at 900 °C for 12 h

Catalyst	CH_4/CO_2 ratio	CH_4 conversions (%) at steady state	Deactivation (%)	Carbon formation[a] (monolayers)	BET after reaction ($m^2\ g^{-1}$)	Ni reducibility[b] (Ni%)
Ni/Al_2O_3	1.0/0.3	1.64	84.2	4.26	40.0	91.0
	1.0/1.0	2.01	78.4	3.97	39.5	93.2
	1.0/3.0	3.32	69.9	3.48	40.0	92.1
8% Ce-Ni[c]	1.0/0.3	10.6	33.1	0.85	44.0	90.0
	1.0/1.0	13.6	14.8	0.34	44.5	89.3
	1.0/3.0	15.3	9.08	~0	44.4	90.4

[a] Calculated using CO and CO_2 yields from temperature-programmed oxidation (TPO) with 10% oxygen.
[b] Nickel reducibility (measured from temperature-programmed reduction (TPR) with 5% hydrogen).
[c] CeO_2 doped Ni/Al_2O_3.

Kα (1.4866 eV) radiation source, which operated at 12 kV and 20 mA. Fig. 6 presents the XRD patterns of the spent and fresh Ni/Al_2O_3 and CeO_2 doped Ni/Al_2O_3. From the XRD results, Ni and $NiAl_2O_4$ reflectance were found in both Ni/Al_2O_3 and CeO_2 doped Ni/Al_2O_3. It is clearly seen that the intensities of $NiAl_2O_4$ peaks for CeO_2 doped Ni/Al_2O_3 were lower than that for Ni/Al_2O_3. This implies that the interaction between NiO and Al_2O_3 was prevented by the doping of CeO_2. A significant carbon peak was observed for the spent Ni/Al_2O_3, indicated the high formation of carbon species on the catalyst surface, whereas a smaller peak of carbon was detect for the spent CeO_2 doped Ni/Al_2O_3.

Table 4 presents the Ce^{3+}/Ce^{4+} ratio for CeO_2 doped Ni/Al_2O_3 before and after exposure in dry methane reforming conditions, determined from XPS. It is seen that no Ce^{3+} (Ce_2O_3) formation was observed for the fresh CeO_2 doped Ni/Al_2O_3 after reduction. Regarding the spent CeO_2 doped Ni/Al_2O_3, no Ce^{3+} formation was detect after exposure in dry methane reforming with the inlet CH_4/CO_2 ratios of 1.0/3.0 and 1.0/1.0, however, a small formation of Ce_2O_3 was observed over CeO_2 doped Ni/Al_2O_3 catalyst after exposure in dry methane reforming with the inlet CH_4/CO_2 ratio of 1.0/0.3. This Ce_2O_3 formation is obviously due to the remaining non-oxidation CeO_2, which will be explained at the end of this section.

Table 4
Ce^{3+}/Ce^{4+} ratio observed from the XPS measurement over CeO_2 doped Ni/Al_2O_3 after reduction and after exposure in dry methane reforming conditions

	Ce^{3+}/Ce^{4+} ratio
After reduction	0
After exposure in dry methane reforming; with CH_4/CO_2 of	
1.0/3.0	0
1.0/1.0	0
1.0/0.3	0.21

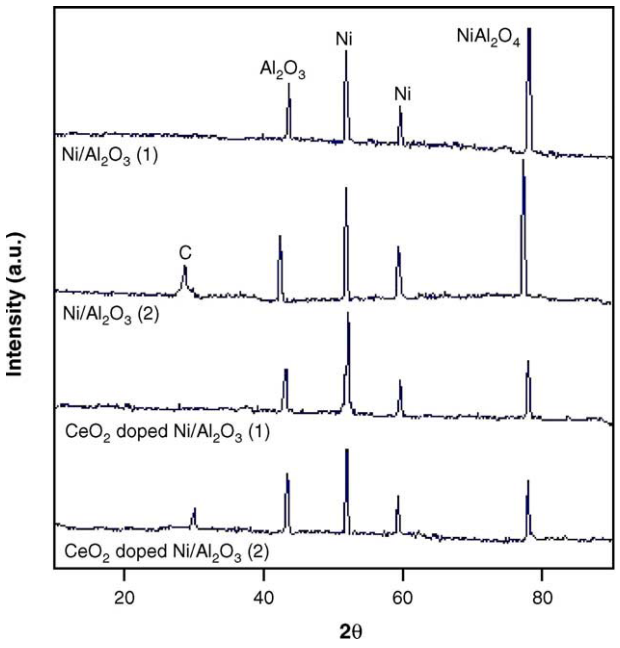

Fig. 6. XRD patterns of the catalysts after reduction (1) and after exposure in dry methane reforming at 900 °C with the inlet CH_4/CO_2 of 1.0/1.0 (2).

The post-reaction temperature-programmed oxidation experiments were then carried out after a helium purge by introducing of 10% oxygen in helium in order to determine whether the observed deactivation is due to the carbon formation. From the TPO results shown in Fig. 7, the huge peaks of carbon dioxide and carbon monoxide were observed for Ni/Al_2O_3 at 600 °C, while smaller peaks of both components were detected for 8% CeO_2 doped Ni/Al_2O_3. The amount of carbon formations on the surface of these catalysts with

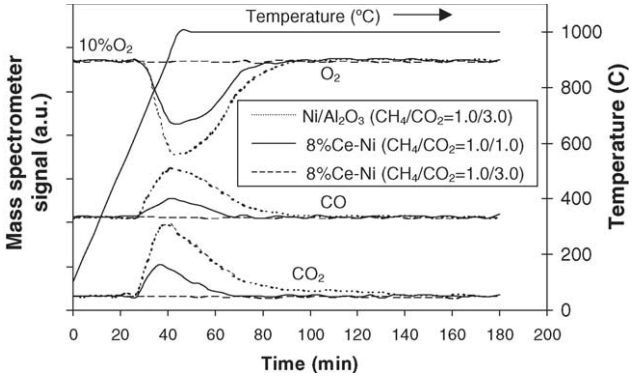

Fig. 7. Temperature-programmed oxidation (TPO) of Ni/Al_2O_3 and 8% CeO_2 doped Ni/Al_2O_3 (10 kPa O_2) after exposure in dry reforming conditions for 10 h.

different inlet CH_4/CO_2 ratios were determined by measuring the CO and CO_2 yields from the TPO results (using Microcal Origin Software). Using a value of 0.026 nm^2 for the area occupied by a carbon atom in a surface monolayer of the basal plane in graphite [17], the quantities of carbon deposited over Ni/Al_2O_3 were observed to be approximately 4.26, 3.97, and 3.48 monolayers, while those over 8% CeO_2 doped Ni/Al_2O_3 were 0.85, 0.34, and ~0 monolayers for the inlet CH_4/CO_2 ratios of 1.0/0.3, 1.0/1.0, and 1.0/3.0, respectively. The total amounts of carbon deposited were ensured by the calculation of carbon balance in the system. Regarding to the calculation for the inlet CH_4/CO_2 ratios of 1.0/0.3, 1.0/1.0, and 1.0/3.0, the moles of carbon deposited per gram of 8% CeO_2 doped Ni/Al_2O_3 were 1.34, 0.49, and ~0 mmol g^{-1}. By the same assumption for the area occupied by a carbon atom [17], these values are equal to 0.87, 0.32, and 0 monolayers, respectively, which is in good agreement with the values observed from the TPO method described above. The results clearly indicated the strong resistance toward carbon formation for 8% CeO_2 doped Ni/Al_2O_3 compared to Ni/Al_2O_3. The BET measurements, as presented in Table 3, indicated that deactivations of 8% CeO_2 doped Ni/Al_2O_3 are also due to the slight sintering of CeO_2. Several researchers also reported the high thermal sintering rate of ceria-based materials at high operating temperature [15,16].

The improvement of dry reforming reactivity and resistance toward carbon formation for CeO_2 doped Ni/Al_2O_3 could be mainly due to the redox property of ceria. During the dry reforming, in addition to the reactions on Ni surface, the solid–gas reaction between CeO_2 and CH_4 also produces synthesis gas with a H_2/CO ratio of two, while the reduced ceria, CeO_{2-x}, can react with CO_2 to produce CO [33–35]. This solid–gas mechanism involves the reactions between methane and/or an intermediate surface hydrocarbon species with the lattice oxygen (O_x) at CeO_2 surface, as illustrated schematically below [36].

$$CH_4 + 2S \Leftrightarrow CH_3{-}S + H{-}S \quad (5)$$

$$CH_3{-}S + S \Leftrightarrow CH_2{-}S + H{-}S \quad (6)$$

$$CH_2{-}S + S \Leftrightarrow CH{-}S + H{-}S \quad (7)$$

$$CH{-}S + S \Leftrightarrow C{-}S + H{-}S \quad (8)$$

$$C{-}S + O_x \Leftrightarrow CO + O_{x-1} + S \quad (9)$$

$$2H{-}S \Leftrightarrow H_2 + 2S \quad (10)$$

During the dry reforming, methane is adsorbed on either a unique site (S) or the lattice oxygen (O_x), whereas CO_2 can react with the reduced site of ceria, O_{x-1}. The steady state reforming rate is mainly due to the continuous supply of the oxygen source by CO_2 (Eq. (11)). Therefore, the Ce_2O_3 formation observed by XPS measurement in Table 4 over spent CeO_2 doped Ni/Al_2O_3 after exposure in dry methane reforming with high inlet CH_4/CO_2 ratio is due to the insufficient supply of inlet CO_2.

$$CO_2 + O_{x-1} \Leftrightarrow O_x + CO \quad (11)$$

Regarding the possible carbon formation during the reforming processes, the following reactions are the most probable reactions that could lead to carbon formation:

$$2CO \Leftrightarrow CO_2 + C \quad (12)$$

$$CH_4 \Leftrightarrow 2H_2 + C \quad (13)$$

$$CO + H_2 \Leftrightarrow H_2O + C \quad (14)$$

$$CO_2 + 2H_2 \Leftrightarrow 2H_2O + C \quad (15)$$

At low temperature, reactions (14) and (15) are favorable, while reaction (12) is thermodynamically unflavored [37]. The Boudard reaction (Eq. (12)) and the decomposition of methane (Eq. (13)) are the major pathways for carbon formation at such a high temperature as they show the largest change in Gibbs energy [38]. According to the range of temperature in this study, 800–900 °C, carbon formation would be formed via the decomposition of methane and Boudard reactions. By doping CeO_2 as the promoter, both reactions (Eqs. (12) and (13)) could be inhibited by the gas–solid reactions between methane and carbon monoxide with the lattice oxygen (O_x) at CeO_2 surface forming hydrogen and carbon dioxide, which is thermodynamically unflavored to form carbon species.

3.4. Effects of temperature and inlet components

The inlet methane partial pressure was varied from 1 to 4 kPa, while inlet carbon dioxide partial pressure was kept constant at 12 kPa. The operating temperature range was 825–900 °C. Fig. 8 illustrates the influence of the inlet methane partial pressure on the turnover frequencies (N) for dry reforming over 8% CeO_2 doped Ni/Al_2O_3 at different operating temperatures. The activities of catalyst increased with increasing inlet methane partial pressure as well as operating temperature. Fig. 9 shows an Arrhenius-type plot

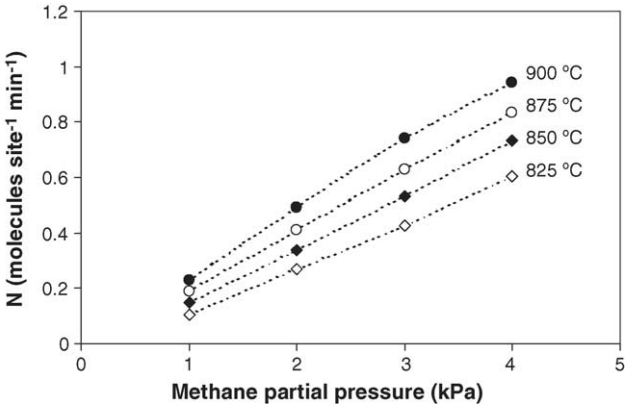

Fig. 8. Effect of methane partial pressure on the turnover frequencies (N) for dry reforming over 8% CeO_2 doped Ni/Al_2O_3 at different temperatures (12 kPa inlet CO_2).

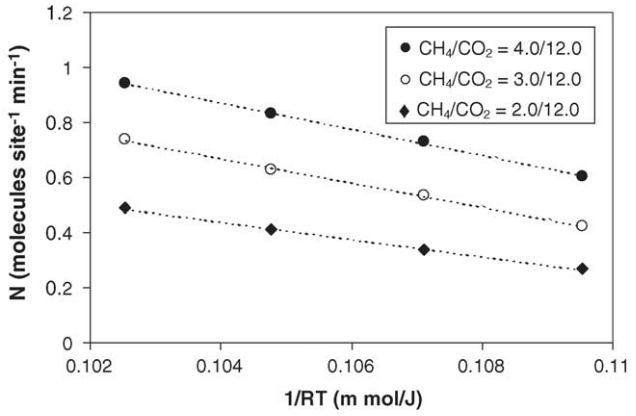

Fig. 9. Arrhenius plot of turnover frequencies (N) for dry reforming of methane over 8% CeO_2 doped Ni/Al_2O_3 with different inlet methane/carbon dioxide ratio.

for dry reforming over CeO_2 doped Ni/Al_2O_3 with various methane/carbon dioxide ratios over the temperature range 825–900 °C. The corresponding activation energy observed for this catalyst is 178 ± 9 kJ/mol, slightly depending on the gas composition.

The reaction order in methane (n) for CeO_2 doped Ni/Al_2O_3 was observed to be 0.96–1.04, and seemed to be essentially independent of the operating temperature and other inlet compositions in the range of conditions studied. These values n were obtained experimentally by plotting $\ln(-r_{CH_4})$ versus $\ln(P_{CH_4})$ according to the equation below.

$$\ln(-r_{CH_4}) = \ln(k) + n\ \ln(P_{CH_4}) \quad (16)$$

where $-r_{CH_4}$ is the dry reforming rate (mol kg_{cat}^{-1} h^{-1}), while P_{CH_4} the methane partial pressure. k is the apparent reaction rate constant and n is the reaction order in methane. The reaction orders in other components (CO_2, H_2, and CO) were achieved using the same approach by varying the inlet partial pressure of the component of interest and keeping other inlet component partial pressures constant.

In order to investigate the influence of CO_2 on the dry reforming rate, several inlet carbon dioxide partial pressures, from 9 to 12 kPa, were introduced to the feed with constant methane partial pressure (3 kPa). Carbon dioxide presented slight positive effect on the dry reforming rate as shown in Fig. 10. The reaction order in carbon dioxide was observed to be a positive value between 0.44 and 0.54, and seemed to be independent of the operating temperature for the range of conditions studied. At 900 °C, the proportion of H_2/CO in the products reduced from 0.80 to 0.67 as the CO_2/CH_4 ratio was increased from 3.0 to 12.0 (Fig. 11). This is as expected from an increasing contribution from the reverse water-gas shift (RWGS) reaction.

The dry reforming in the presences of carbon monoxide and hydrogen were then investigated by adding either carbon monoxide or hydrogen to the feed gas at several operating temperatures. The results show that the reforming rates are also dependent on both carbon monoxide and hydrogen

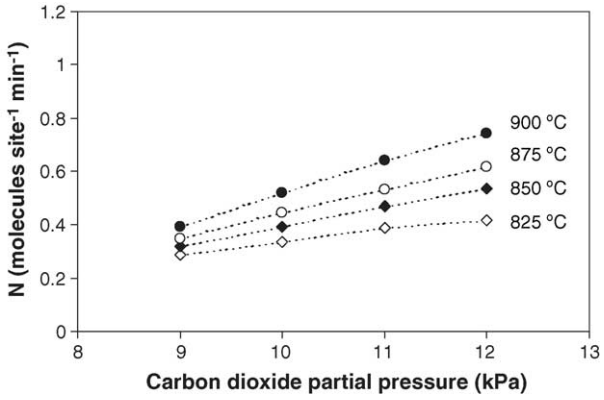

Fig. 10. Effect of carbon dioxide partial pressure on the turnover frequencies (N) for dry reforming over 8% CeO_2 doped Ni/Al_2O_3 at different temperatures (3 kPa CH_4).

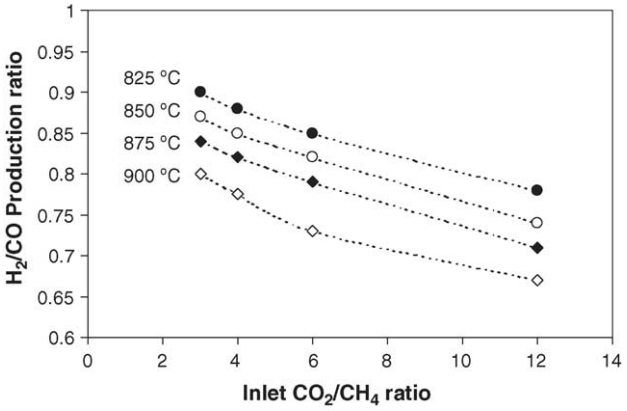

Fig. 11. Influence of inlet carbon dioxide/methane ratio on H_2/CO production ratio from dry reforming of methane over 8% CeO_2 doped Ni/Al_2O_3 at different temperatures (12 kPa CO_2).

concentrations. Unlike CH_4 and CO_2, both components inhibited the dry reforming rate as shown in Figs. 12 and 13. The reaction order in carbon monoxide was in the range of −0.42 to −0.37, while the reaction order in hydrogen was between −0.55 and −0.45 in the range of conditions studied.

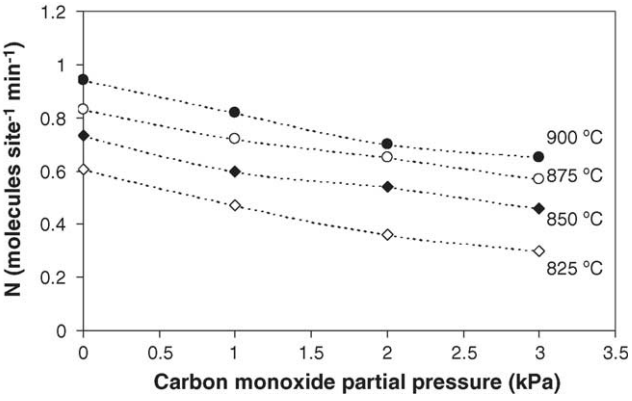

Fig. 12. Effect of carbon monoxide partial pressure on the turnover frequencies (N) for dry reforming of methane over 8% CeO_2 doped Ni/Al_2O_3 at different temperatures (4 kPa CH_4 and 12 kPa CO_2).

Table 5
Reaction orders for the components of interest (CH_4, CO_2, CO, and H_2) from dry reforming over 8% CeO_2 doped Ni/Al_2O_3 at different operating conditions

Components of interest	Temperature (°C)	Other inlet compositions	Reaction order for components of interest
Methane (1–4 kPa)	825	12 kPa CO_2	1.00
	850	12 kPa CO_2	0.97
	900	12 kPa CO_2	0.98
	850	15 kPa CO_2	1.01
	850	17 kPa CO_2	0.99
	825–900	12 kPa CO_2/1 kPa H_2	1.01 ± 0.03
	825–900	12 kPa CO_2/3 kPa H_2	0.98 ± 0.01
	825–900	12 kPa CO_2/1 kPa CO	0.99 ± 0.03
Carbon dioxide (9–12 kPa)	825	3 kPa CH_4	0.44
	850	3 kPa CH_4	0.54
	900	3 kPa CH_4	0.50
	850	3 kPa CH_4/3 kPa H_2	0.48
Hydrogen (1–3 kPa)	825–900	3 kPa CH_4/12 kPa CO_2	-0.49 ± 0.04
	825–850	1 kPa CH_4/12 kPa CO_2	-0.48 ± 0.03
	825–850	3 kPa CH_4/15 kPa CO_2	-0.52 ± 0.03
Carbon monoxide (1–3 kPa)	825–900	3 kPa CH_4/12 kPa CO_2	-0.40 ± 0.01
	825–850	3 kPa CH_4/15 kPa CO_2	-0.38 ± 0.01
	825–850	3 kPa CH_4/17 kPa CO_2	-0.40 ± 0.02

Table 5 presents the summary of observed reaction orders in each component (CH_4, CO_2, CO, and H_2) for CeO_2 doped Ni/Al_2O_3 at different inlet conditions.

Regarding to the above experiments, the experimental data can be fitted well to a simple relative rate coefficient, in which captures the essential features.

$$-r_{CH_4} = \frac{k(T)(P_{CH_4})^n(P_{CO_2})^m}{1 + K_1(T)P_{CO}^a + K_2(T)P_{H_2}^b} \quad (17)$$

where P_i is the partial pressure of chemical component i. The positive effects of methane and carbon dioxide on the dry reforming rate were a consequence of the presence of the $k(T)(P_{CH_4})^n(P_{CO_2})^m$ term, whereas negative effects of carbon monoxide and hydrogen were a consequence of the $K_1(T)P_{CO}^a$ and $K_2(T)P_{H_2}^b$ terms in the denominator. According to the fitting, when n, m, a, and b were taken as 1.0, 0.5, 0.4, and 0.5, a good fit to the data was observed in the range of conditions studied. $k(T)$ increased from 649.0 mol kg^{-1} h^{-1} atm$^{-1.5}$ at 825 °C to 954.3 mol kg^{-1} h^{-1} atm$^{-1.15}$ at 900 °C, while $K_1(T)$ and $K_2(T)$, also temperature dependent parameters, were in the range of 1.68–4.43 atm$^{-0.4}$ and 0.93–3.94 atm$^{-0.5}$, respectively. It should be noted that the apparent activation energy for this reaction, which were achieved by the Arrhenius plots, was approximately 150 kJ/mol.

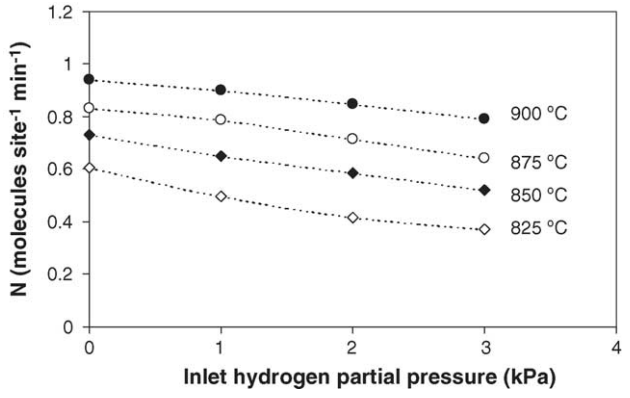

Fig. 13. Effect of hydrogen partial pressure on the turnover frequencies (N) for dry reforming of methane over 8% CeO_2 doped Ni/Al_2O_3 at different temperatures (4 kPa CH_4 and 12 kPa CO_2).

4. Conclusion

8% CeO_2 doped Ni/Al_2O_3 is a good candidate catalyst for the dry reforming of methane due to the high resistance toward the deactivation from carbon formation. During dry reforming process, the gas–solid reaction on ceria surface takes place simultaneously with the reactions on the surface of Ni, in which reduces the degree of carbon deposition on catalyst surface from methane decomposition and Boudard reactions. However, it should also be noted that the doping of too high ceria content results in the oxidation of Ni, which could reduce the reforming reactivity.

The intrinsic kinetic reaction of 8% CeO_2 doped Ni/Al_2O_3 was studied in the conditions where the intraparticle diffusion limitation was negligible. The dry reforming rate increased with increasing methane and carbon dioxide partial pressures as well as the operating temperature. In contrast, the methane conversion was inhibited when hydrogen and carbon monoxide were added to the system during dry reforming process. It can be concluded from the present work that CeO_2 doped Ni/Al_2O_3 seems to be a promise catalyst for the indirect internal reforming solid oxide fuel cells (IIR-SOFC) operation.

Acknowledgement

The financial support from The Thailand Research Fund (TRF) throughout this project is gratefully acknowledged.

References

[1] P. Aguiar, D. Chadwick, L. Kershenbaum, Chem. Eng. Sci. 57 (2002) 1665.
[2] J.H. Edwards, A.M. Maitra, Fuel Process. Technol. 42 (1995) 269.
[3] M.A. Vannice, M.C.J. Bradford, Appl. Catal. A: Gen. 142 (1) (1996) 97–122.
[4] T. Sodesawa, A. Dobashi, F. Nozaki, React. Kinet. Catal. Lett. 12 (1979) 107.
[5] L. Topor, L. Bejan, E. Ivana, N. Georgescu, Rev. Chim. Bucharest 30 (1979) 539.
[6] T.A. Chubb, Sol. Energy 24 (1980) 341.
[7] T.A. Chubb, J.H. McCrary, G.E. McCrary, J.J. Nemecek, D.E. Simmons, Proc. Meet. Am. Sect. Int. Sol. Eng. Soc. 4 (1981) 166.
[8] J.R. Rostrup-Nielsen, J.H. Bak Hansen, J. Catal. 144 (1993) 38.
[9] P. Gronchi, C. Mazzocchia, E. Tempesti, R. Del Rosso, in: G. Centi, et al. (Eds.), Enviromental Catalysis, SCI Publication, Roma, 1995, p. 627.
[10] A. Erdöhelyi, J. Cserényi, F. Solymosi, J. Catal. 141 (1993) 287.
[11] A. Erdöhelyi, J. Cserényi, E. Rapp, F. Solymosi, Appl. Catal. A: Gen. 108 (1994) 205.
[12] J. Nakamura, K. Aikawa, K. Sato, T. Uchijima, Catal. Lett. 25 (1994) 265.
[13] Z.L. Zhang, V.A. Tsipouriari, A.M. Efstathiou, X.E. Verykios, J. Catal. 158 (1996) 51.
[14] E. Ramírez-Cabrera, A. Atkinson, D. Chadwick, Appl. Catal. B 47 (2004) 127–131.
[15] E. Ramírez-Cabrera, N. Laosiripojana, A. Atkinson, D. Chadwick, Catal. Today 78 (2003) 433–438.
[16] N. Laosiripojana, Reaction engineering of indirect internal steam reforming of methane for application in solid oxide fuel cells, Ph.D. Thesis, University of London, England, 2003.
[17] E. Ramirez, A. Atkinson, D. Chadwick, Appl. Catal. B 36 (2002) 193–206.
[18] X. Wang, R.J. Gorte, Appl. Catal. A 224 (2002) 209–218.
[19] H.S. Roh, K.W. Jun, W.S. Dong, J.S. Chang, S.E. Park, Y.I. Joe, J. Mol. Catal. A 181 (2002) 137–142.
[20] Q. Miao, G. Xiong, S. Sheng, W. Cui, L. Xu, X. Guo, Appl. Catal. A 154 (1987) 17–27.
[21] A.A. Lemonidou, M.A. Goula, I.A. Vasalos, Catal. Today 46 (1987) 175–183.
[22] W.S. Dong, H.S. Roh, K.W. Jun, S.E. Park, Y.S. Oh, Appl. Catal. A 226 (2002) 63–72.
[23] M. Mamak, N. Coombs, G. Ozin, Adv. Mater. 12 (2000) 198–202.
[24] M. Mamak, N. Coombs, G. Ozin, J. Am. Chem. Soc. 122 (2000) 8932.
[25] M. Mamak, N. Coombs, G.A. Ozin, Chem. Mater. 13 (2001) 3564.
[26] P. Bera, S. Mitra, S. Sampath, M.S. Hegde, Chem. Commun. (2001) 927.
[27] A. Martinez-Arias, J.M. Coronado, R. Cataluna, J.C. Conesa, J.C. Soria, J. Phys. Chem. B 102 (1998) 4357.
[28] D. Skarmoutsos, F. Tietz, P. Nikolopoulos, Fuel Cells 1 (2001) 243.
[29] T. Takeguchi, S.N. Furukawa, M. Inoue, J. Catal. 202 (2001) 14.
[30] J. Sfeir, P.A. Philippe, P. Moseki, N. Xanthopoulos, R. Vasquez, J.M. Hans, V.H. Jan, K.R. Thampi, J. Catal. 202 (2001) 229.
[31] N. Kiratzis, P. Holtappels, C.E. Hatchwell, M. Mogensen, J.T.S. Irvine, Fuel Cells 1 (2001) 211.
[32] S. Wang, G.Q. Lu, Appl. Catal. B 19 (1998) 267.
[33] K. Otsuka, T. Ushiyama, I. Yamanaka, Chem. Lett. (1993) 1517.
[34] K. Otsuka, M. Hatano, A. Morikawa, J. Catal. 79 (1983) 493.
[35] K. Otsuka, M. Hatano, A. Morikawa, Inorg. Chim. Acta 109 (1985) 193.
[36] N. Laosiripojana, S. Assabumrungrat, Appl. Catal. B 60 (2005) 109–118.
[37] Y. Lwin, W.R.W. Daud, A.B. Mohamad, Z. Yaakob, Int. J. Hydrogen Energy 25 (1) (2000) 47–53.
[38] J.N. Amor, Appl. Catal. A 176 (1999) 159–176.

N. Laosiripojana, W. Sangtongkitcharoen, S. Assabumrungrat

"Catalytic steam reforming ethane and propane over CeO_2-doped Ni/Al_2O_3 at SOFC temperature: Improvement of resistance toward carbon formation by the redox properties of doping CeO_2"

Fuel, 85 (2006), 323-332

(IF-2003 = 1.368)

Available online at www.sciencedirect.com
SCIENCE DIRECT
Fuel 85 (2006) 323–332
FUEL
www.fuelfirst.com

Catalytic steam reforming of ethane and propane over CeO_2-doped Ni/Al_2O_3 at SOFC temperature: Improvement of resistance toward carbon formation by the redox property of doping CeO_2

N. Laosiripojana[a,*], W. Sangtongkitcharoen[b], S. Assabumrungrat[b]

[a]*The Joint Graduate School of Energy and Environment, King Mongkut's University of Technology Thonburi, Bangkok 10140, Thailand*
[b]*Center of Excellence on Catalysis and Catalytic Reaction Engineering, Department of Chemical Engineering, Faculty of Engineering, Chulalongkorn University, Bangkok 10330, Thailand*

Received 21 January 2005; received in revised form 2 June 2005; accepted 28 June 2005
Available online 28 July 2005

Abstract

Ni/Al_2O_3 with the doping of CeO_2 was found to have useful activity to reform ethane and propane with steam under Solid Oxide Fuel Cells (SOFCs) conditions, 700–900 °C. CeO_2-doped Ni/Al_2O_3 with 14% ceria doping content showed the best reforming activity among those with the ceria content between 0 and 20%. The amount of carbon formation decreased with increasing Ce content. However, Ni was easily oxidized when more than 16% of ceria was doped. Compared to conventional Ni/Al_2O_3, 14%CeO_2-doped Ni/Al_2O_3 provides significantly higher reforming reactivity and resistance toward carbon deposition. These enhancements are mainly due to the influence of the redox properties of doped ceria. Regarding the temperature programmed reduction experiments (TPR-1), the redox properties and the oxygen storage capacity (OSC) for the catalysts increased with increasing Ce doping content. In addition, it was also proven in the present work that the redox of these catalysts are reversible, according to the temperature programmed oxidation (TPO) and the second time temperature programmed reduction (TPR-2) results.

During the reforming process, in addition to the reactions on Ni surface, the gas–solid reactions between the gaseous components presented in the system (C_2H_6, C_3H_8, C_2H_4, CH_4, CO_2, CO, H_2O, and H_2) and the lattice oxygen (O_x) on ceria surface also take place. The reactions of adsorbed surface hydrocarbons with the lattice oxygen (O_x) on ceria surface ($C_nH_m + O_x \rightarrow nCO + m/2(H_2) + O_{x-n}$) can prevent the formation of carbon species on Ni surface from hydrocarbons decomposition reaction ($C_nH_m \Leftrightarrow nC + m/2H_2$). Moreover, the formation of carbon via Boudard reaction ($2CO \Leftrightarrow CO_2 + C$) is also reduced by the gas–solid reaction of carbon monoxide (produced from steam reforming) with the lattice oxygen ($CO + O_x \Leftrightarrow CO_2 + O_{x-1}$).

Keywords: Hydrogen; Ethane; Propane; Carbon formation; Steam reforming; CeO_2

1. Introduction

Solid Oxide Fuel Cell (SOFC) is generally operated at high temperature between 700 and 1100 °C [1,2]. Due to its high-operating temperature, fuels such as methane can be in-stack or internal reformed by catalytic steam reforming to produce a H_2/CO rich gas, which is eventually used to generate electrical energy and heat. The operation, called indirect internal reforming (IIR), is expected to simplify the overall system design [3].

Currently, one of the most interesting fuels for SOFC is natural gas consisting mainly of methane. Normally, natural gas also contains significant amounts of higher hydrocarbons such as ethane and propane. When natural gas is reformed internally (IIR) without any pre-treatments, the carbon formation can be easily formed on the catalyst surface due to the decompositions of these hydrocarbons at high temperature. SOFC fueled by natural gas therefore requires a small external pre-reformer unit, where the high hydrocarbon components are reformed readily before introducing to the main part of the system [4]. The pre-reforming unit is normally operated at relatively lower temperature, 300–500 °C, in which the carbon formation is

* Corresponding author.
E-mail address: navadol_l@jgsee.kmutt.ac.th (N. Laosiripojana).

0016-2361/$ - see front matter © 2005 Elsevier Ltd. All rights reserved.
doi:10.1016/j.fuel.2005.06.013

thermodynamically unflavored. The disadvantage of this installation is the extra-requirement of the heat supplied into this unit, which can reduce the fuel cell efficiency [5].

The approach to this problem in this work is developing of an alternative catalyst that is enable to reform high hydrocarbon components with low degree of carbon deposition at SOFC temperature, 700–900 °C. The successful development of this catalyst would help eliminate the requirement of the external pre-reformer, as these high hydrocarbon elements can be simultaneously reformed together with methane at high temperature. In this study, ethane and propane were chosen as the inlet fuels, because they are the main high hydrocarbon components presented in natural gas. According to the economical point of view, Ni/Al_2O_3 was selected as a based catalyst rather than the precious metals such as Pt, Rh and Ru although it is more sensitive to carbon formation. Cerium oxide (CeO_2) was chosen as an additive promoter. This material (called ceria) is an important material for a variety of catalytic reactions involving oxidation of hydrocarbons (e.g. automobile exhaust catalysts). Recently, the use of ceria-based catalysts has shown a rapid increase [6]. A high oxygen mobility [7], high oxygen storage capacity [8–13], strong interaction with the supported metal (strong metal-support interaction) [14] and the modifiable ability [15] render the ceria-based materials very interesting for catalysis and as a support and promoter. It has widely been reported, regarding the above properties, that cerias can promote the action of various metals in the reactions in which hydrogen is involved as a reactant or product [16–20]. According to the catalytic steam reforming reaction, ceria-based materials have been reported by several researchers to be promising supports among α-Al_2O_3 [21], γ-Al_2O_3 and γ-Al_2O_3 with alkali metal oxide and rare earth metal oxide [22], and $CaAl_2O_4$ [21–24]. One of the most promising ceria-based supports for the reforming reactions appeared to be Ce-ZrO_2, where the metal can be Ni, Pt or Pd [25–34].

It has been reported that the gas–solid reaction between CeO_2 and CH_4 produces synthesis gas with a H_2/CO ratio of two according to the following reactions [35,36]. Moreover, the reduced ceria, CeO_{2-x}, can react with CO_2 and steam to produce CO and H_2, respectively [37].

$$CeO_2 + nCH_4 \rightarrow CeO_{2-n} + nCO + 2nH_2 \quad (1)$$

$$CeO_{2-x} + CO_2 \Leftrightarrow CeO_2 + CO \quad (2)$$

$$CeO_{2-x} + H_2O \Leftrightarrow CeO_2 + H_2 \quad (3)$$

Nowadays, a potential application of ceria is in Solid Oxide Fuel Cells (SOFCs) application as a reforming catalyst for in-stack (called indirect internal) reforming of methane, since it is high resistant toward carbon deposition compared to Ni [38]. Recently, the successful tests of ceria for the methane steam reforming reaction have been reported [39,40]. Due to the high resistance toward carbon formation, ceria should be a good additive promoter for the reforming of ethane and propane. In this work, various amounts of ceria were doped on the surface of Ni/Al_2O_3 in order to determine the suitable doping ratio. The reactivity toward steam reforming of ethane and propane, as well as the resistance toward carbon formation of CeO_2-doped Ni/Al_2O_3 were studied and compared to those of conventional Ni/Al_2O_3. The influence of inlet steam content on the product selectivity from this reaction at various temperatures was also determined.

2. Experimental

2.1. Catalyst preparations and characterizations

CeO_2-doped Ni/Al_2O_3 was prepared by impregnating different concentration of cerium nitrate ($Ce(NO_3)_3 \cdot 6H_2O$ (99.0%), Fluka) on Ni/Al_2O_3 powder. Ni/Al_2O_3 (10 wt% Ni) was prepared by impregnating α-Al_2O_3 (from Aldrich) with $NiCl_3$ solution at room temperature. This solution was stirred by magnetic stirring (100 rpm) for 6 h, dried overnight in an oven at 110 °C, and calcined in air at 900 °C for 6 h before use.

After reduction, the catalysts were characterized with several physicochemical methods. The weight contents of Ni and Ce loadings were determined by X-ray fluorescence (XRF) analysis. The reducibility and dispersion percentages of nickel were measured from temperature-programmed reduction (TPR) using 5% H_2 in Ar with the total flow rate of 100 $cm^3\ min^{-1}$ and temperature-programmed desorption (TPD) respectively. The catalyst specific surface areas were obtained from BET measurement. All physicochemical properties of the synthesized catalysts are presented in Table 1.

In addition to the above characterizations, the redox properties and redox reversibilities of the catalysts with different Ce doping contents were determined by the temperature programmed reduction (TPR-1) at high temperature and the temperature programmed oxidation (TPO) following with temperature programmed reduction (TPR-2), respectively. Regarding these experiments, 5% H_2/Ar and 5% O_2/He were used for the TPR and TPO, respectively, while the temperature of the system increased from room temperature to 900 °C and 1000°C, respectively.

2.2. Apparatus and procedures

An experimental reactor system was constructed as shown in Fig. 1. The feed gases including the components of interest (ethane, propane, and steam from the evaporator) and the carrier gas (helium) were introduced to the reaction section, in which a 10-mm diameter quartz reactor was mounted vertically inside a furnace. In the present work, the ethane/propane feed ratio was kept constant at 0.65/0.35, regarding to the approximate ratio of these components presented in natural gas (this information is based on the compositions of natural gas from PTT Company (Thailand)

Table 1
Physicochemical properties of the catalysts after reduction at 700 °C

Catalyst	Ni-load[a] (wt.%)	Ce-load[a] (wt.%)	BET Surface Area ($m^2\ g^{-1}$)	Ni-reducibility[b] (Ni%)	Ni-dispersion[c] (Ni%)
Ni/Al_2O_3	4.91	0.0	40.2	92.1	4.87
$2\%Ce\text{-}Ni/Al_2O_3$	4.84	1.87	40.8	93.5	4.54
$4\%Ce\text{-}Ni/Al_2O_3$	4.93	4.02	42.7	91.4	5.12
$6\%Ce\text{-}Ni/Al_2O_3$	5.01	5.94	46.5	90.6	4.54
$8\%Ce\text{-}Ni/Al_2O_3$	4.96	8.03	49.1	91.1	4.65
$10\%Ce\text{-}Ni/Al_2O_3$	4.88	9.86	49.8	89.9	4.77
$12\%Ce\text{-}Ni/Al_2O_3$	4.93	12.1	50.4	90.3	4.64
$14\%Ce\text{-}Ni/Al_2O_3$	4.92	13.9	50.9	91.0	4.20
$16\%Ce\text{-}Ni/Al_2O_3$	5.00	16.1	51.4	89.7	5.09
$18\%Ce\text{-}Ni/Al_2O_3$	4.94	17.9	51.0	90.1	4.13
$20\%Ce\text{-}Ni/Al_2O_3$	4.98	19.9	52.0	90.3	4.37

[a] Measured from X-ray fluorescence analysis.
[b] Measured from temperature-programmed reduction (TPR) with 5%hydrogen.
[c] Measured from temperature-programmed desorption (TPD) of hydrogen after TPR measurement.

containing 67%CH_4, 8.3%C_2H_6, 4.5%C_3H_8, 2.0%C_4H_{10}, 0.5%C_5H_{12}, and 14.5%CO_2). The catalyst was loaded in the quartz reactor, which was packed with a small amount of quartz wool to prevent the catalyst from moving. The weight of catalyst loading was 50 mg, while a typical range of total gas flow was 20–200 $cm^3\ min^{-1}$ depending on the desired space velocity. A Type-K thermocouple was placed into the annular space between the reactor and the furnace. This thermocouple was mounted on the tubular reactor in close contact with the catalyst bed to minimize the temperature difference between the catalyst bed and the thermocouple. Another Type-K thermocouple was inserted in the middle of the quartz tube in order to re-check the possible temperature gradient. The record showed that the maximum temperature fluctuation during the reaction was always ± 0.75 °C or less from the temperature specified for the reaction. Before the reaction, the catalyst was reduced under 5% H_2 in helium with the flow rate of 100 $cm^3\ min^{-1}$ for 6 h.

During the reactions, the exit gas mixture was transferred via trace-heated lines to the analysis section, which consists of a Porapak Q column Shimadzu 14B gas chromatograph (GC) and a mass spectrometer (MS). The gas chromatography was applied in order to investigate the steady state condition experiments, whereas the mass spectrometer in which the sampling of the exit gas was done by a quartz capillary and differential pumping was used for the transient and carbon formation experiments. In order to study the formation of carbon species on catalyst surface, Temperature programmed Oxidation (TPO) was applied by introducing 10% oxygen in helium into the system, after purged with helium. The operating temperature increased from room temperature to 1000 °C by the rate of 10 °C/min.

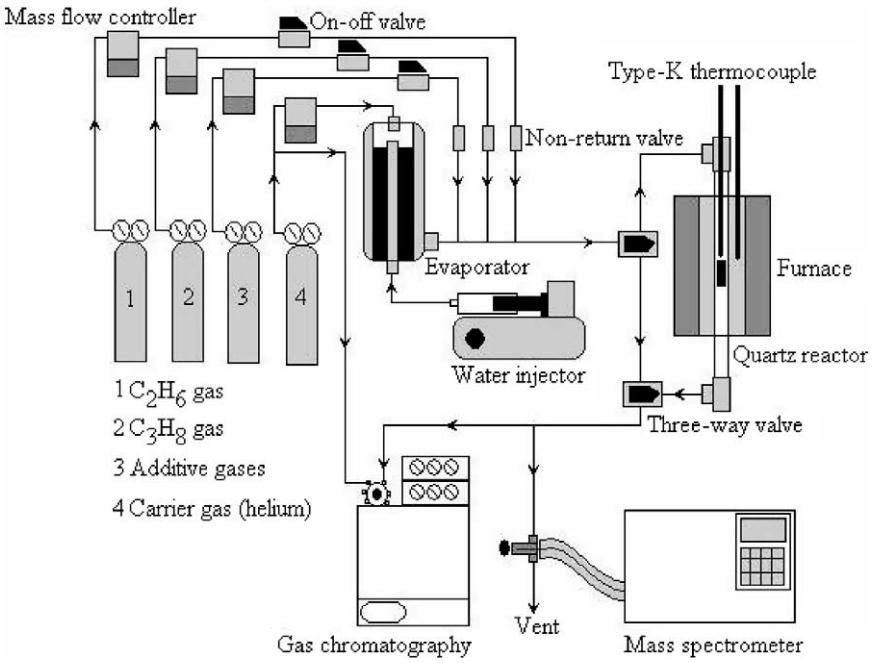

Fig. 1. Schematic diagram of the experimental set-up.

The calibrations of CO and CO_2 productions were performed by injecting a known amount of these calibration gases from a loop, in an injection valve in the bypass line. The response factors were obtained by dividing the number of moles for each component over the respective areas under peaks. The amount of carbon formations on the surface of catalysts were determined by measuring the CO and CO_2 yields from the TPO results (using Microcal Origin Software) assuming a value of 0.026 nm^2 for the area occupied by a carbon atom in a surface monolayer of the basal plane in graphite [38]. In addition to the TPO method, the amount of carbon deposition was confirmed by the calculation of carbon balance in the system. The amount of carbon deposited on the surface of catalyst would theoretically be equal to the difference between the inlet carbon containing components (C_2H_6, and C_3H_8) and the outlet carbon containing components (C_2H_6, C_3H_8, CO, CO_2, CH_4, and C_2H_4). The amount of carbon deposited per gram of catalyst is given by the following equation:

$$C_{\text{deposition}} = \frac{\text{mole}_{\text{carbon(in)}} - \text{mole}_{\text{carbon(out)}}}{m_{\text{catalyst}}} \quad (4)$$

The steam reforming reactivity was defined in terms of the conversions and selectivities. Hydrocarbon conversions (ethane and propane) denoted as $X_{\text{hydrocarbon}}$, and the products selectivity (hydrogen, carbon monoxide, carbon dioxide, methane, and ethylene), denoted as S_{product}, are calculated according to Eqs. (5)–(11):

$$X_{\text{Ethane}} = \frac{100(\%\text{Ethane}_{\text{in}} - \%\text{Ethane}_{\text{out}})}{\%\text{Ethane}_{\text{in}}} \quad (5)$$

$$X_{\text{Propane}} = \frac{100(\%\text{Propane}_{\text{in}} - \%\text{Propane}_{\text{out}})}{\%\text{Propane}_{\text{in}}} \quad (6)$$

$$S_{\text{H}_2} = \frac{100(\%\text{H}_2)}{3(\%\text{Ethane}_{\text{in}} - \%\text{Ethane}_{\text{out}}) + 4(\%\text{Propane}_{\text{in}} - \%\text{Propane}_{\text{out}}) + (\%\text{H}_2\text{O}_{\text{in}} - \%\text{H}_2\text{O}_{\text{out}})} \quad (7)$$

$$S_{\text{CO}} = \frac{100(\%\text{CO})}{2(\%\text{Ethane}_{\text{in}} - \%\text{Ethane}_{\text{out}}) + 3(\%\text{Propane}_{\text{in}} - \%\text{Propane}_{\text{out}})} \quad (8)$$

$$S_{\text{CO}_2} = \frac{100(\%\text{CO}_2)}{2(\%\text{Ethane}_{\text{in}} - \%\text{Ethane}_{\text{out}}) + 3(\%\text{Propane}_{\text{in}} - \%\text{Propane}_{\text{out}})} \quad (9)$$

$$S_{\text{CH}_4} = \frac{100(\%\text{CH}_4)}{2(\%\text{Ethane}_{\text{in}} - \%\text{Ethane}_{\text{out}}) + 3(\%\text{Propane}_{\text{in}} - \%\text{Propane}_{\text{out}})} \quad (10)$$

$$S_{\text{C}_2\text{H}_4} = \frac{100(\%\text{C}_2\text{H}_4)}{(\%\text{Ethane}_{\text{in}} - \%\text{Ethane}_{\text{out}}) + 1.5(\%\text{Propane}_{\text{in}} - \%\text{Propane}_{\text{out}})} \quad (11)$$

3. Results and discussion

3.1. Preliminary tests

The desired space velocity and suitable catalyst particle size were achieved from several preliminary tests, which were carried out to avoid any limitations by intraparticle diffusion in the experiments. The total flow rate was varied between 20 and 200 $cm^3\ min^{-1}$ under a constant residence time of 5×10^{-4} g $min\ cm^{-3}$. When the total flow rate was below 60 $cm^3\ min^{-1}$, the reforming rate increased with increasing the gas flow rate, suggesting that the mass transfer between the bulk gas and the catalyst particles is the rate-determining step. The reforming rate was almost constant in the range where the gas flow rate was higher than 80 $cm^3\ min^{-1}$, indicating that the mass transfer effect is unimportant in this flow rate range. Fig. 2 shows the effect of the total gas flow rate on the reforming rate over 14%CeO_2-doped Ni/Al_2O_3 at different temperatures. The reactions on different average sizes (from 100 to 500 μm) of catalysts were also carried out. It was observed that there were no significant changes in the methane conversion for the catalyst with the particle size between 100 and 200 μm, which indicated that the intraparticle diffusion limitation was negligible in this range. Consequently in this study, the weight of catalyst loading was 50 mg, while the total gas flow was kept constant at 100 $cm^3\ min^{-1}$. The catalyst particle size diameter was between 100 and 200 μm in all experiments.

Before studying the catalyst performance, homogeneous (non-catalytic) steam reforming of ethane and propane was investigated. Inlet $C_2H_6/C_3H_8/H_2O$ in helium with the molar ratio of 0.65/0.35/3.0 was introduced to the system, while the temperature increased from room temperature to 900 °C. From Fig. 3, it was observed that both ethane and propane were converted to methane, ethylene, and hydrogen at

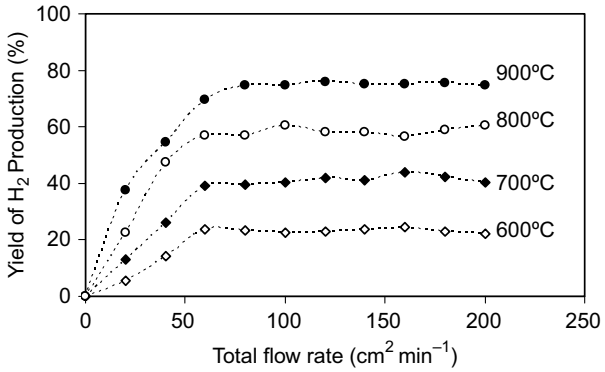

Fig. 2. Effect of the gas flow rate on the yield of H_2 production (%) for steam reforming over 14% CeO_2-doped Ni/Al_2O_3 at different temperatures (2.6 kPa C_2H_6, 1.4 kPa C_3H_8, 12 kPa H_2O).

the temperature above 700 °C. Significant amount of carbons was also detected in the blank reactor after exposure for 10 h. These components were formed via the decomposition of ethane and propane as shown in the equations below [41].

$$C_2H_6 \rightarrow C_2H_4 + H_2 \quad (12)$$

$$C_3H_8 \rightarrow 3/2(C_2H_4) + H_2 \quad (13)$$

$$C_2H_4 \rightarrow 2H_2 + 2C \quad (14)$$

$$C + 2H_2 \rightarrow CH_4 \quad (15)$$

There was no change in steam concentration, and no carbon monoxide and carbon dioxide was produced in the system, indicating that the non-homogenous reforming reaction between steam and hydrocarbon elements took place at this range of conditions studied.

3.2. Investigation of the redox properties and redox reversibility of the catalysts

As described earlier, the oxygen storage capacities and the degree of redox properties for catalysts with different Ce

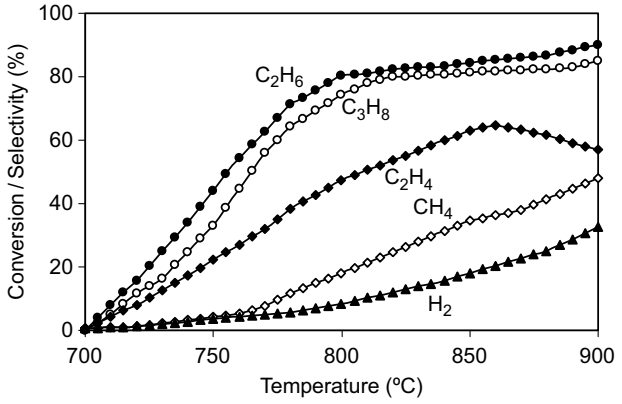

Fig. 3. Homogenous (in the absence of catalyst) reactivity of ethane and propane in the presence of steam (2.6 kPa C_2H_6, 1.4 kPa C_3H_8, and 12 kPa H_2O).

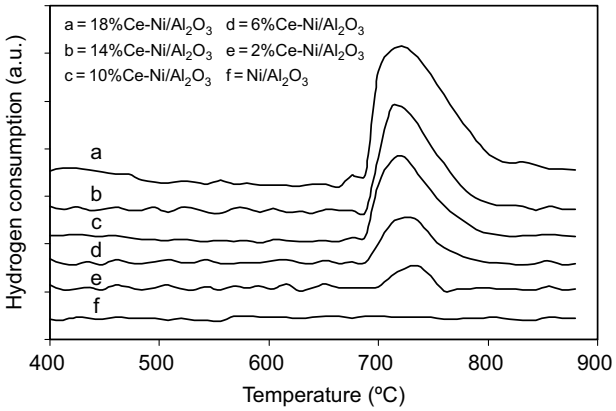

Fig. 4. Temperature Programmed Reduction (TPR-1) of the catalysts with different Ce doping content (0–18% Ce).

doping contents (0–18%) were investigated using temperature programmed reduction (TPR-1), in which performed by heating the reduced catalysts up to 900 °C in 5%H_2 in argon. As shown in Fig. 4, significant amount of hydrogen uptakes were detected from Ni/Al_2O_3 with the doping of CeO_2 at the temperature above 650 °C. The amount of hydrogen uptakes increased with increasing Ce doping content, suggesting the reduction of bulk oxygen ions on ceria surface. In contrast, no hydrogen consumption was observed from the TPR over conventional Ni/Al_2O_3. These results indicated the occurrence of redox properties for Ni/Al_2O_3 with CeO_2 doping at high temperature (650–900 °C), in which increased with increasing Ce content. This redox property provides a great benefit toward the reforming of ethane and propane, which will be presented in Section 3.4.

After purged with helium, the redox reversibility for each catalyst was then determined by applying temperature programmed oxidation (TPO) following with the second time temperature programmed reduction (TPR-2). The TPO was carried out by heating the catalyst up to 1000 °C in 10%O_2 in helium; the amounts of oxygen chemisorbed were then measured, Fig. 5 and Table 2. Regarding the TPR-2 results as shown in Fig. 6 and Table 2, the amount of

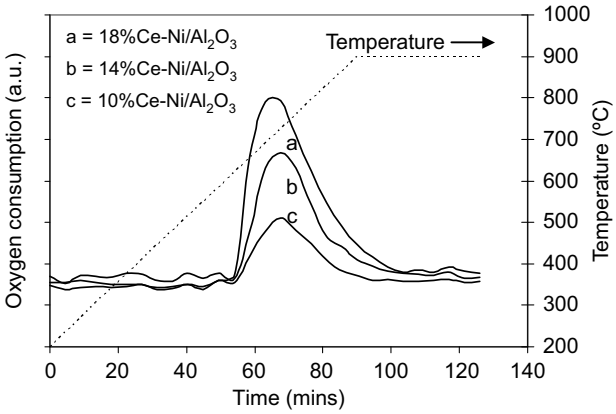

Fig. 5. Temperature Programmed Oxidation (TPO) of CeO_2-doped Ni/Al_2O_3 after TPR-1.

Table 2
Results of TPR(1), TPO, TPR(2) analyses of CeO_2 doped Ni/Al_2O_3 at high temperature

Catalyst	Total H_2 Uptake from TPR(1)[a] ($\mu mol/g_{cat}$)	Total O_2 Uptake from TPO[b] ($\mu mol/g_{cat}$)	Total H_2 Uptake from TPR(2)[c] ($\mu mol/g_{cat}$)
2%Ce-Ni/Al_2O_3	523	271	520
6%Ce-Ni/Al_2O_3	840	402	840
10%Ce-Ni/Al_2O_3	1078	540	1075
14%Ce-Ni/Al_2O_3	1350	691	1350
18%Ce-Ni/Al_2O_3	1505	784	1503

[a] Temperature Programmed Reduction of the reduced catalysts (Relative Standard Deviation = ±3%).
[b] Temperature Programmed Oxidation after TPR (1) (Relative Standard Deviation = ±1%).
[c] Re-Temperature Programmed Reduction after TPO (Relative Standard Deviation = ±2%).

hydrogen uptakes for each catalyst were approximately similar to those from TPR-1, indicated the redox reversibility for these catalysts.

3.3. Selection of suitable Ce doping content for the steam reforming of ethane/propane

After reduction of CeO_2-doped Ni/Al_2O_3, the steam reforming of ethane/propane was performed at 900 °C. The feed was $C_2H_6/C_3H_8/H_2O$ in helium with the molar ratio of 0.65/0.35/3.0. Fig. 7 presents the steady state yield of H_2 production (%) for CeO_2-doped Ni/Al_2O_3 with various CeO_2 contents (0–20%) at 900 °C. It was found that 14% CeO_2 doping on Ni/Al_2O_3 presents the highest hydrogen production yield.

The post-reaction temperature-programmed oxidation (TPO) experiments were then carried out after a helium purge by introducing 10% oxygen in helium in order to determine the degree of carbon deposition on the surface of each sample. Table 3 presents the important physicochemical properties of the spent catalysts after exposure in the steam reforming conditions for 10 h. According to TPO, the amount of carbon formation decreased with increasing Ce content. This is due to the increasing of redox properties by doping more CeO_2, which can inhibit the formation of carbon species on Ni surface. However, as seen from Fig. 7, slight decrease in reforming rate was observed when the Ce doping contents were higher than 14%. This decreasing in reactivity could be due to the possible oxidised of Ni because the reducibility of the catalysts (with 16, 18, and 20% Ce doping) reduced after exposure in the steam reforming for 10 h, according to the TPR experiment. Therefore, 14% CeO_2 doping on Ni/Al_2O_3 is the optimum content, which provides the highest resistance toward carbon deposition and is enable to operate without the oxidised of Ni.

3.4. Reactivity toward steam reforming of ethane/propane

The steam reforming of C_2H_6/C_3H_8 over Ni/Al_2O_3 and 14%CeO_2 doped Ni/Al_2O_3 were studied at 900 °C. After reducing with 5% hydrogen for 6 h, the catalysts were heated up under helium flow to 900 °C. At the isothermal condition, $C_2H_6/C_3H_8/H_2O$ in helium with different $C_2H_6/C_3H_8/H_2O$ molar ratios of 0.65/0.35/1.0, 0.65/0.35/2.0, and 0.65/0.35/3.0 were introduced in order to compare the reforming rates. The variations in hydrogen production yield with time at 900 °C for different catalysts and different inlet $C_2H_6/C_3H_8/H_2O$ ratio are shown in Fig. 8. The significant deactivations were detected for Ni/Al_2O_3 catalyst in all conditions especially at high inlet $C_2H_6/C_3H_8/H_2O$ ratio, whereas considerable lower deactivations were detected for 14%CeO_2 doped Ni/Al_2O_3. Catalyst stabilities expressed as deactivation percentages are given in Table 4.

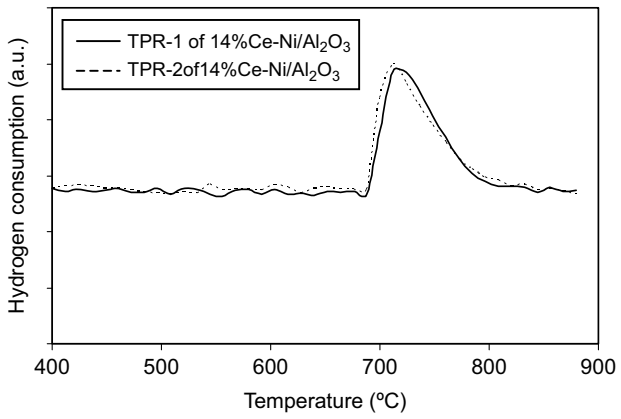

Fig. 6. Second time Temperature Programmed Reduction (TPR-2) of 14% CeO_2-doped Ni/Al_2O_3 compared to that of TPR-1.

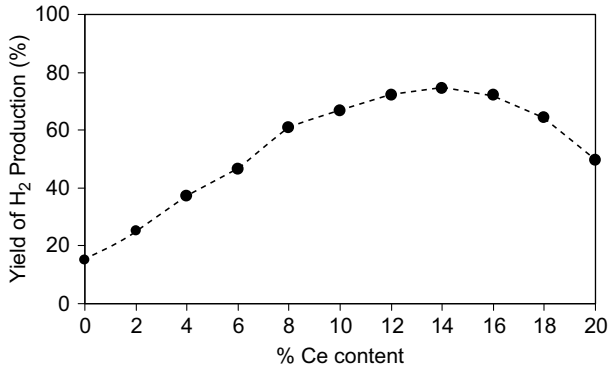

Fig. 7. Effect of Ce doping content on the yield of H_2 production (%) for steam reforming (900 °C, 2.6 kPa C_2H_6, 1.4 kPa C_3H_8, and 12 kPa H_2O).

Table 3
Yield of H_2 production (%), and physicochemical properties of the catalysts after exposure in steam reforming (2.6 kPa C_2H_6, 1.4 kPa C_3H_8, and 12 kPa H_2O) at 900 °C

Catalyst	Yield of H_2 production (%) at steady state	Ni and Ce load[a] (wt.%)	C formation[b] (monolayers)	BET surface ($m^2\ g^{-1}$)	Ni-red.[c] (Ni%)	Ni-disp.[d] (Ni%)
Ni/Al_2O_3	15.2	4.87/0.0	4.85	40.0	92.0	4.80
2%Ce-Ni/Al_2O_3	25.1	4.80/1.84	4.28	40.0	92.6	4.51
4%Ce-Ni/Al_2O_3	36.9	4.91/4.01	4.04	41.4	91.4	5.11
6%Ce-Ni/Al_2O_3	46.2	5.00/5.95	3.21	43.6	90.1	4.49
8%Ce-Ni/Al_2O_3	60.8	4.96/8.00	3.09	45.4	91.9	4.64
10%Ce-Ni/Al_2O_3	66.6	4.87/9.89	2.76	45.2	88.7	4.73
12%Ce-Ni/Al_2O_3	71.8	4.89/12.0	1.98	45.8	90.1	4.59
14%Ce-Ni/Al_2O_3	74.5	4.91/13.9	1.07	45.6	90.4	4.17
16%Ce-Ni/Al_2O_3	72.1	4.98/16.0	1.06	45.5	80.8	4.99
18%Ce-Ni/Al_2O_3	64.3	4.95/17.9	1.02	46.0	71.7	4.10
20%Ce-Ni/Al_2O_3	49.4	4.97/19.9	1.11	46.2	68.5	4.29

[a] Measured from X-ray fluorescence analysis.
[b] Calculated using CO and CO_2 yields from temperature-programmed oxidation (TPO) with 10% oxygen.
[c] Nickel reducibility (measured from temperature-programmed reduction (TPR) with 5%hydrogen).
[d] Nickel dispersion (measured from temperature-programmed desorption (TPD) after TPR).

After operated for 100 h, the steam reforming over 14%CeO_2 doped Ni/Al_2O_3 with inlet $C_2H_6/C_3H_8/H_2O$ of 0.65/0.35/3.0 showed the best activity. The influences of operating temperature and the inlet steam to ethane/propane ratio on the product selectivity were also studied by varying temperature from 700–900 °C and changing the inlet steam to carbon ratio from 1.0/1.0 to 5.0/1.0. As shown in Fig. 9, it was found that, at steady state, the main products from this reaction over 14%CeO_2 doped Ni/Al_2O_3 were H_2, CO, CO_2, and CH_4, with small amount of C_2H_4 depending on the operating temperature. For comparison, the conversions and the product selectivities at equilibrium level were calculated using AspenPlus10.2 simulation program, Fig. 10. Regarding the simulation, the conversions of C_2H_6 and C_3H_8 at equilibrium level are 100% in the range of temperature between 700 and 900 °C. The yields of hydrogen production at equilibrium are slightly higher than those achieved from the experiments, in addition, no C_2H_4 formation was observed at the equilibrium level in this range of temperature due to the complete reforming of this component to CH_4, CO, and CO_2.

Regarding the influence of inlet steam, hydrogen and carbon dioxide selectivity increased with increasing inlet steam concentration, whereas carbon monoxide selectivity decreased, Fig. 11. These are mainly due to the influence of water–gas shift reaction ($CO + H_2O \rightarrow CO_2 + H_2$). Moreover, the appearances of methane and ethylene in the system were found to decrease with increasing steam content, as these components were further reformed to CO, CO_2, and H_2 by the excess steam.

The post-reaction temperature-programmed oxidation (TPO) experiments were carried out after a helium purge by introducing of 10% oxygen in helium in order to determine whether the observed deactivation is due to the carbon formation. From the TPO results shown in Fig. 12, the huge peaks of carbon dioxide and carbon monoxide were observed for Ni/Al_2O_3, while smaller peaks of both components were detected for 14%CeO_2 doped Ni/Al_2O_3. The amount of carbon formations on the surface of these catalysts with different inlet $C_2H_6/C_3H_8/H_2O$ ratios were determined by measuring the CO and CO_2 yields from the TPO results. Using a value of 0.026 nm^2 for the area occupied by a carbon atom in a surface monolayer of the basal plane in graphite [38], the quantities of carbon deposited over Ni/Al_2O_3 were observed to be approximately 5.98, 5.41, and 4.85 monolayers, while those over 14%CeO_2 doped Ni/Al_2O_3 were 2.19, 1.48, and 1.07 monolayers for the inlet $C_2H_6/C_3H_8/H_2O$ ratios of 0.65/0.35/1.0, 0.65/0.35/2.0, and 0.65/0.35/3.0, respectively. The total amounts of carbon deposited were ensured by the calculation of carbon balance in the system. Regarding the calculations, for the inlet $C_2H_6/C_3H_8/H_2O$ ratios of 0.65/0.35/1.0, 0.65/0.35/2.0, and 0.65/0.35/3.0, the moles of carbon deposited per gram of 14%CeO_2 doped Ni/Al_2O_3 were 3.32, 2.33, and 1.68 mmol g^{-1}. By the same assumption for the area

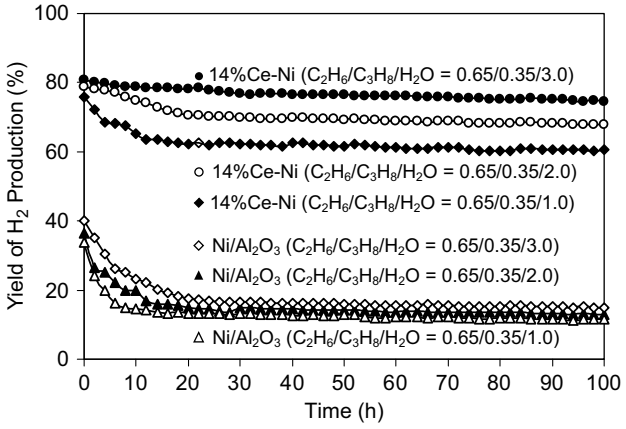

Fig. 8. Steam reforming of ethane/propane at 900 °C for several catalysts and various inlet $C_2H_6/C_3H_8/H_2O$ ratios.

Table 4
Yield of H_2 production (%), deactivation percentages, and physicochemical properties of the catalysts after exposure in steam reforming conditions (various inlet steam/carbon ratio) at 900 °C for 100 h

Catalyst	H_2O/C ratio	Yield of H_2 production (%) at steady state	Deactivation (%)	C formation[a] (monolayers)	BET surface (m^2 g^{-1})	Ni-red.[b] (Ni%)
Ni/Al_2O_3	1.0/1.0	11.5	65.8	5.98	40.0	91.9
	2.0/1.0	12.9	64.6	5.41	39.7	91.8
	3.0/1.0	15.1	62.5	4.85	40.0	92.0
14%Ce-Ni[c]	1.0/1.0	60.2	20.0	2.19	45.4	92.0
	2.0/1.0	67.8	13.6	1.48	45.1	91.8
	3.0/1.0	74.5	7.41	1.07	45.6	90.4

[a] Calculated using CO and CO_2 yields from temperature-programmed oxidation (TPO) with 10% oxygen.
[b] Nickel reducibility (measured from temperature-programmed reduction (TPR) with 5%hydrogen).
[c] CeO_2-doped Ni/Al_2O_3.

occupied by a carbon atom [38], these values are equal to 2.15, 1.51, and 1.09 monolayers, respectively, which are in good agreement with the values observed from the TPO method described above.

The results clearly indicated the strong resistance toward carbon formation for 14%CeO_2 doped Ni/Al_2O_3 compared to Ni/Al_2O_3. The BET measurements, as presented in Table 4, indicated that deactivations of 14%CeO_2 doped Ni/Al_2O_3 are also due to the slight sintering of CeO_2. The improvement of reforming reactivity and resistance toward carbon formation for CeO_2-doped Ni/Al_2O_3 could be mainly due to the redox property of ceria. During the reforming of C_2H_6/C_3H_8, the carbon formation could occur due to several reactions, the following reactions are the most probable reactions that could lead to carbon formation:

$$C_3H_8 \Leftrightarrow 4H_2 + 3C \quad (16)$$

$$C_2H_6 \Leftrightarrow 3H_2 + 2C \quad (17)$$

$$CH_4 \Leftrightarrow 2H_2 + C \quad (18)$$

$$C_2H_4 \Leftrightarrow 2H_2 + 2C \quad (19)$$

$$2CO \Leftrightarrow CO_2 + C \quad (20)$$

$$CO + H_2 \Leftrightarrow H_2O + C \quad (21)$$

$$CO_2 + 2H_2 \Leftrightarrow 2H_2O + C \quad (22)$$

where C is the carbonaceous deposits. At low temperature, Eqs. (21) and (22) are favorable, while Eqs. (16)–(19) are thermodynamically unflavored [42]. The Boudard reaction (Eq. (20)) and the decomposition of hydrocarbons (Eqs. (16)–(19)) are the major pathways for carbon formation at such a high temperature as they show the largest change in Gibbs energy [43]. According to the high temperature in this study, 900 °C, carbon formation would be formed via the decomposition of hydrocarbons and Boudard reactions. With the increase of steam to carbon ratio, the equilibrium of water-gas shift reaction moves forward and produces more CO_2 rather than CO. Therefore, high steam feed can avoid carbon deposition via the Boudouard reaction. However, significant amount of carbon remains detected on the surface of Ni/Al_2O_3 due to the decomposition of ethane, propane, ethylene, and methane (Eqs. (16)–(19)). By doping CeO_2 as the promoter, these reactions could be inhibited by the gas–solid reactions between hydrocarbons

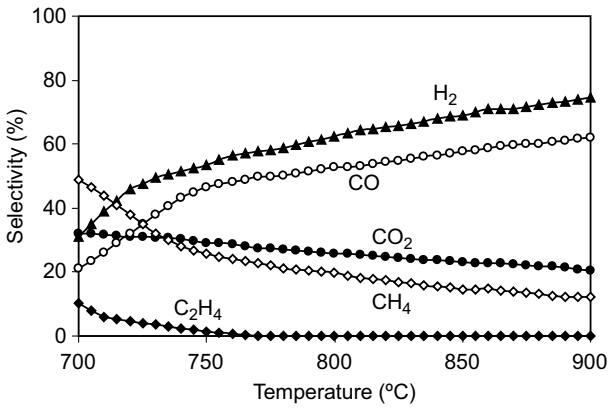

Fig. 9. Effect of reaction temperature on the selectivities of product elements (H_2, CO, CO_2, CH_4, and C_2H_4) from steam reforming over 14%CeO_2-doped Ni/Al_2O_3 (2.6 kPa C_2H_6, 1.4 kPa C_3H_8, and 12 kPa H_2O).

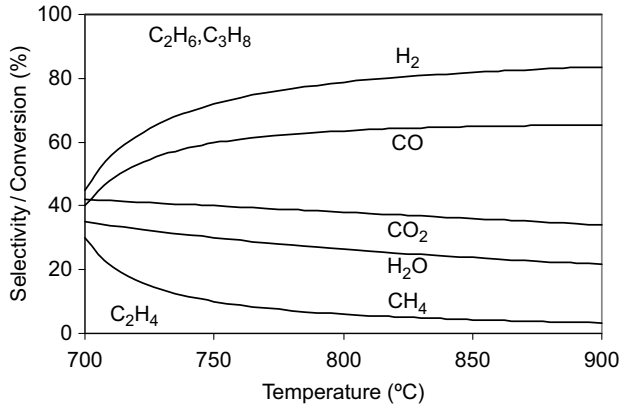

Fig. 10. Conversions of C_2H_6 and C_3H_8, and the selectivities of H_2, CO, CO_2, C_2H_4, and CH_4 at equilibrium level (Inlet conditions of 2.6 kPa C_2H_6, 1.4 kPa C_3H_8, and 12 kPa H_2O).

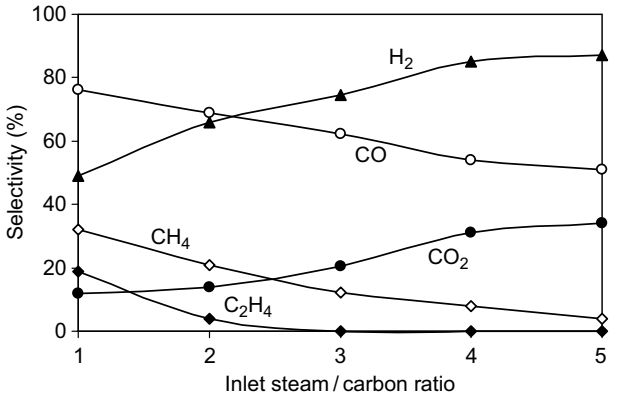

Fig. 11. Effect of inlet steam/carbon molar ratio on the selectivities of product elements (H_2, CO, CO_2, CH_4, and C_2H_4) from steam reforming over 14%CeO_2-doped Ni/Al2O_3 at 900 °C (2.6 kPa C_2H_6, 1.4 kPa C_3H_8, and 12 kPa H_2O).

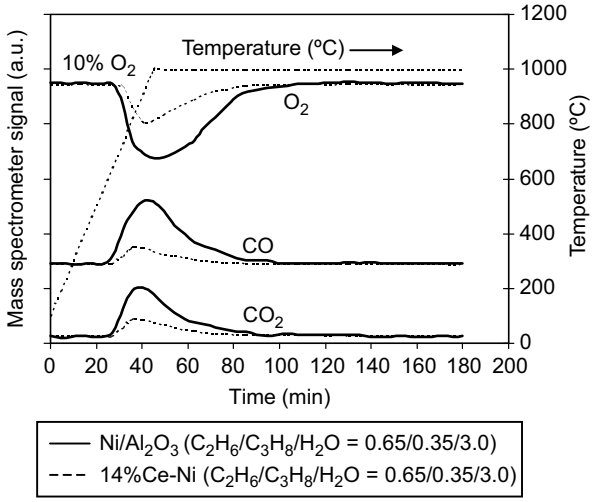

Fig. 12. Temperature Programmed Oxidation (TPO) of Ni/Al_2O_3 and 14%CeO_2-doped Ni/Al_2O_3 (10 kPa O_2) after exposure in steam reforming of ethane/propane (2.6 kPa C_2H_6, 1.4 kPa C_3H_8, and 12 kPa H_2O) for 100 h.

with the lattice oxygen (O_x) at CeO_2 surface forming hydrogen and carbon dioxide, which are thermodynamically unflavored to form carbon species.

Theoretically, the solid–gas reaction between CeO_2 and CH_4 produces synthesis gas, while the reduced ceria, CeO_{2-x}, can react with steam to produce H_2 [35–37]. In the present work, the solid–gas mechanism involves the reactions between hydrocarbons (C_2H_6, C_3H_8, CH_4, and C_2H_4) and/or an intermediate surface hydrocarbon species with the lattice oxygen (O_x) at CeO_2 surface, as illustrated schematically below.

$$C_3H_8 + 3S \Leftrightarrow 2(CH_3-S) + CH_2-S \quad (23)$$

$$C_2H_6 + 2S \Leftrightarrow 2(CH_3-S) \quad (24)$$

$$CH_4 + 2S \Leftrightarrow CH_3-S + H-S \quad (25)$$

$$C_2H_4 + 2S \Leftrightarrow 2(CH_2-S) \quad (26)$$

$$CH_3-S + S \Leftrightarrow CH_2-S + H-S \quad (27)$$

$$CH_2-S + S \Leftrightarrow CH-S + H-S \quad (28)$$

$$CH-S + S \Leftrightarrow C-S + H-S \quad (29)$$

$$C-S + O_x \Leftrightarrow CO + O_{x-1} + S \quad (30)$$

$$2H-S \Leftrightarrow H_2 + 2S \quad (31)$$

where *S* is the catalyst surface site. It can be considered to be a unique site, or the same site as the lattice oxygen (O_x) [40]. During the steam reforming, hydrocarbons are adsorbed on either a unique site (S) or the lattice oxygen (O_x), whereas H_2O can react with the reduced site of ceria, O_{x-1}. The steady state reforming rate is mainly due to the continuous supply of the oxygen source by H_2O.

$$H_2O + O_{x-1} \Leftrightarrow O_x + H_2 \quad (32)$$

It should be noted that the solid–gas reaction on the surface of ceria could also reduce the formation of carbon via Boudouard reaction, as carbon monoxide can adsorb and react with the lattice oxygen (O_x) on the surface of ceria forming carbon dioxide ($CO + O_x \Leftrightarrow O_{x-1} + CO_2$), which is less flavored to form carbon species at high temperature.

4. Conclusion

14%CeO_2-doped Ni/Al_2O_3 is a good candidate catalyst for the reforming of ethane and propane at SOFC temperature (900 °C) due to the high resistance toward the deactivation from carbon formation at high temperature. During reforming process, the gas–solid redox reactions on ceria surface take place simultaneously with the reforming reactions on the surface of Ni, and they reduce the degree of carbon deposition on catalyst surface from hydrocarbons decomposition and Boudard reactions. Regarding the TPR measurement, the redox properties increased with increasing Ce doping content. In addition, this oxygen storage property was proven to be reversible. However, it should also be noted that the doping of too high ceria content on the catalyst results in the oxidation of Ni, which could reduce the reforming reactivity.

In particular, at the temperature above 800 °C and the inlet steam/carbon ratio higher than 3.0, all ethylene formation in which occurs homogenously (non-catalytic) from the thermal cracking of ethane and propane was converted by the steam reforming over this catalyst. By increasing inlet steam content, hydrogen and carbon dioxide selectivities increased, whereas carbon monoxide selectivity decreased. Moreover, the conversions of methane and ethylene were found to increase with increasing steam content in the system.

Acknowledgements

The financial support from The Thailand Research Fund (TRF) throughout this project is gratefully acknowledged.

References

[1] W.L. Lundberg, S.E. Veyo, Conceptual design and performance analysis of a 300 MWel LNG-fuelled pressurised SOFC/Gas turbine power plant, in: Yokohawa, S.C. Singhal (Eds.), Proceeding of the 7th International Symposium Solid Oxide Fuel Cells VII, 2001, 78-87.
[2] Aguiar P, Chadwick D, Kershenbaum L. Chem. Eng. Sci. 2002;57: 1665.
[3] Aguiar P, Lapena-Rey N, Chadwick D, Kershenbaum L. Chemical Engineering Science 2001;56:652.
[4] Peters R, Dahl R, Kluttgen U, Palm C, Stolten D, Power J. Sources 2002;106:238.
[5] N. Laosiripojana, 6th European Solid Oxide Fuel Cell Forum, 28 June - 2 July 2004.
[6] Trovareli A, Leitenburg C, Dolcetti G. Chemtech 1997;32.
[7] Fornasiero P, Balducci G, Monte RD, Kaspar J, Sergo V, Gubitosa G, Ferrero A. M. Graziani. J. Catal. 1996;164:173.
[8] Miki T, Ogawa T, Haneda M, Kakuta N, Ueno A, Tateishi S, Matsuura S. M. Sato, J. Phys. Chem. 1990;94:339.
[9] Padeste C, Cant NW, Trimm L. Catal. Lett. 1993;18:305.
[10] Kacimi S, Barbier Jr. J, Taha R. D. Duperz, Catal. Lett. 1993;22:343.
[11] Zafiris GS, Gorte J. J. Catal. 1993;143:86.
[12] Zafiris GS, Gorte J. J. Catal. 1993;139:561.
[13] Imamura S, Shono M, Okamoto N, Hamada R. S. Ishida, Appl. Catal. A 1996;142:279.
[14] Fan L. K. Fujimoto. J. Catal. 1997;172:238.
[15] Pijolat M, Prin M. M. Soustelle. J. Chem. Soc., Faraday Trans. 1995; 91:3941.
[16] Imamura S, Higashihara T, Saito Y, Aritani H, Kanai H, Matsumura Y. N. Tsuda, Catal. Today 1999;50:369.
[17] Imamura S, Denpo K, Utani K, Matsumura Y. H. Kanai, React. Kinet. Catal. Lett. 1999;67:163.
[18] Imamura S, Denpo K, Kanai K, Yamane H, Saito Y, Utani K. Y. Matsumura, Sekiyu Gakkaishi 2001;44:293.
[19] Imamura S, Yamane H, Kanai H, Shibuta T, Utani K. K. Hamada, J. Jpn. Petrol. Inst. 2002;45:187.
[20] Imamura S, Taniguchi Y, Ikeda Y, Hosokawa S, Kanai H. H. Ando, React. Kinet. Catal. Lett. 2002;76:201.
[21] Roh HS, Jun KW, Dong WS, Chang JS, Park SE, Joe YI. J. Mol. Catal. A 2002;181:137–42.
[22] Miao Q, Xiong G, Sheng S, Cui W, Xu L. Guo. Appl. Catal. A 1987; 154:17–27.
[23] Lemonidou AA, Goula MA, Vasalos IA. Catal. Today 1987;46: 175–83.
[24] Dong WS, Roh HS, Jun KW, Park SE, Oh YS. Appl. Catal. A 2002; 226:63–72.
[25] Mamak M, Coombs N, Ozin G. Adv. Mater. 2000;12:198–202.
[26] Mamak M, Coombs N, Ozin G. J. Am. Chem. Soc. 2000;122:8932.
[27] Mamak M, Coombs N, Ozin GA. Chem. Mater. 2001;13:3564.
[28] Bera P, Mitra S, Sampath S, Hegde MS. Chem. Commun. 2001;927.
[29] Martinez-Arias A, Coronado JM, Cataluna R, Conesa JC, Soria JC. J. Phys. Chem. B 1998;102:4357.
[30] Skarmoutsos D, Tietz F, Nikolopoulos P. Fuel Cells 2001;1:243.
[31] Takeguchi T, Furukawa SN, Inoue M. J. Catal. 2001;202:14.
[32] Sfeir J, Philippe PA, Moseki P, Xanthopoulos N, Vasquez R, Hans JM, Jan VH, Thampi KR. J. Catal. 2001;202:229.
[33] Kiratzis N, Holtappels P, Hatchwell CE, Mogensen M, Irvine JTS. Fuel Cells 2001;1:211.
[34] Roh HS, Dong WS, Jun KW, Park SE. Chem. Lett. 2001;88.
[35] Otsuka K, Ushiyama T. I. Yamanaka, Chemistry Letters 1993;1517.
[36] Otsuka K, Hatano M. A. Morikawa, J. Catalysis 1983;79:493.
[37] Otsuka K, Hatano M. A. Morikawa, Inorganica Chimica Acta 1985; 109:193.
[38] Ramírez-Cabrera E, Atkinson A. D. Chadwick, Applied Catalysis B 2004;47:127–31.
[39] Ramírez-Cabrera E, Laosiripojana N, Atkinson A. D. Chadwick, Catalysis Today 2003;78:433–8.
[40] N. Laosiripojana 2003, Reaction engineering of indirect internal steam reforming of methane for application in solid oxide fuel cells. Ph.D. Thesis, University of London, England.
[41] M.V. Twigg, Catalyst Handbook, 2nd Edition, Wolfe Publishing, London, (1989).
[42] Lwin Y, Daud WRW, Mohamad AB. Z. Yaakob, Int. J. Hydrogen Energy 2000;25(1):47–53.
[43] Amor JN. Appl. Catal. A 1999;176:159–76.

N. Laosiripojana and S. Assabumrungrat

"Hydrogen production from the steam and autothermal reforming of LPG over high surface area ceria at SOFC temperature"

Journal of Power Sources, In Press

(IF-2004 = 2.513)

Available online at www.sciencedirect.com
SCIENCE DIRECT®
Journal of Power Sources xxx (2005) xxx–xxx
JOURNAL OF POWER SOURCES
www.elsevier.com/locate/jpowsour

Hydrogen production from steam and autothermal reforming of LPG over high surface area ceria

N. Laosiripojana [a,*], S. Assabumrungrat [b]

[a] *The Joint Graduate School of Energy and Environment, King Mongkut's University of Technology Thonburi, Bangkok 10140, Thailand*
[b] *Center of Excellence in Catalysis and Catalytic Reaction Engineering, Department of Chemical Engineering, Faculty of Engineering, Chulalongkorn University, Bangkok 10330, Thailand*

Received 22 September 2005; received in revised form 18 October 2005; accepted 18 October 2005

Abstract

Steam and autothermal reforming reactions of LPG (propane/butane) over high surface area CeO_2 (CeO_2 (HSA)) synthesized by a surfactant-assisted approach were studied under solid oxide fuel cell (SOFC) operating conditions. The catalyst provides significantly higher reforming reactivity and excellent resistance toward carbon deposition compared to the conventional Ni/Al_2O_3. These benefits of CeO_2 are due to the redox property of this material. During the reforming process, the gas–solid reactions between the hydrocarbons present in the system (i.e. C_4H_{10}, C_3H_8, C_2H_6, C_2H_4, and CH_4) and the lattice oxygen (O_O^x) take place on the ceria surface. The reactions of these adsorbed surface hydrocarbons with the lattice oxygen ($C_nH_m + O_O^x \rightarrow nCO + m/2(H_2) + V_O^{\bullet\bullet} + 2e'$) can produce synthesis gas (CO and H_2) and also prevent the formation of carbon species from hydrocarbons decomposition reactions ($C_nH_m \Leftrightarrow nC + 2mH_2$). Afterwards, the lattice oxygen (O_O^x) can be regenerated by reaction with the steam present in the system ($H_2O + V_O^{\bullet\bullet} + 2e' \Leftrightarrow O_O^x + H_2$). It should be noted that $V_O^{\bullet\bullet}$ denotes as an oxygen vacancy with an effective charge 2^+.

At 900 °C, the main products from steam reforming over CeO_2 (HSA) were H_2, CO, CO_2, and CH_4 with a small amount of C_2H_4. The addition of oxygen in autothermal reforming was found to reduce the degree of carbon deposition and improve product selectivities by completely eliminating C_2H_4 formation. The major consideration in the autothermal reforming operation is the O_2/LPG (O/C molar ratio) ratio, as the presence of a too high oxygen concentration could oxidize the hydrogen and carbon monoxide produced from the steam reforming. A suitable O/C molar ratio for autothermal reforming of CeO_2 (HSA) was 0.6.

Keywords: LPG; Steam reforming; Autothermal reforming; Ceria; Solid oxide fuel cell

1. Introduction

A fuel cell is an energy conversion device that produces electrical energy with greater conversion efficiency and lower pollutant emissions than combustion processes. Among the various types of fuel cells, the solid oxide fuel cell (SOFC) has attracted considerable interest as it offers the widest range of applications, flexibility in the choice of fuel, and high system efficiency. The waste heat for SOFC can also be utilized in co-generation applications and bottoming cycles to improve the overall system efficiency. Moreover, unlike low-temperature fuel cells, the SOFC anode is not affected by carbon monoxide poisoning. Although, hydrogen is the major fuel for a SOFC, the use of other fuels such as methane, methanol, ethanol, liquefied petroleum gas (LPG), gasoline and other oil derivatives are also possible via internal or in-stack reforming. Since an SOFC is operated at such a high temperature, these hydrocarbons can be internally reformed producing a H_2/CO rich gas, which is eventually used to generate the electrical energy and heat. This operation, called indirect internal reforming (IIR-SOFC), is expected to simplify the overall SOFC system design [1].

Among the above hydrocarbon fuels, liquefied petroleum gas (LPG) is a commercial gas that is easily transported and stored on-site. This gas was proposed to be an attractive fuel for SOFC systems in remote areas where pipeline natural gas is not available [2]. LPG can also be used for auxiliary power units (APU) based on SOFC systems. Typically, the main components of

* Corresponding author. Tel.: +66 2 8729014; fax: +66 2 8726736.
E-mail address: navadol_l@jgsee.kmutt.ac.th (N. Laosiripojana).

0378-7753/$ – see front matter © 2005 Elsevier B.V. All rights reserved.
doi:10.1016/j.jpowsour.2005.10.058

LPG are propane and butane. According to the Australian LPG Association, the composition of LPG in Australia ranges from pure propane to a 40:60 mixture of propane and butane [2]. The steam reforming process has widely been used to produce hydrogen from LPG. The main products from the steam reforming of LPG are hydrogen, carbon monoxide, and carbon dioxide, however, the formation of ethane, ethylene, and methane are usually observed due to the decomposition of LPG and methanation reactions. The major difficulty in reforming LPG is the degradation of the reforming catalyst due to the possible carbon deposition from the decomposition of hydrocarbons, particularly at high temperature. Previously, steam reforming of LPG has been studied by a few researchers [2–8], and most of them have investigated the reforming of LPG over noble metal catalysts (e.g. Rh, Ru, and Pt) on oxide supports. Recupero et al. [8] reported that Pt/CeO_2 provides high reforming reactivity with low carbon formation. Suzuki et al. [3] found that Ru/CeO_2-Al_2O_3 can reform LPG with a low inlet steam requirement at 450 °C. Adding oxygen together with LPG and steam as an autothermal reforming process was reported to provide great benefits in terms of catalyst stability and low coke formation [4,5], however, the yield of hydrogen production could be reduced due to the oxidation of hydrogen by oxygen added. The attractive benefit of this operation is that the exothermic heat from the partial oxidation can directly supply the energy required for the endothermic steam reforming reaction, and so it is considered to be thermally self-sustaining process.

This work is aimed at the development of a catalyst for steam and autothermal reforming of LPG, which provides high stability and activity at a high temperature (700–900 °C) for later application in an IIR-SOFC. Although the precious metals such as Pt, Rh and Ru have been reported by several researchers to provide high activity for the reforming reactions and excellent resistant to carbon formation [9,10], the current prices of these metals are too high for commercial usage, and the availability of some precious metals such as ruthenium was too low to have a major impact on the total reforming catalyst market [11]. In view of these economical considerations, an alternative catalyst was developed and studied instead. Cerium oxide or ceria has been reported to be a catalyst in a wide variety of reactions involving oxidation or partial oxidation of hydrocarbons (e.g. automotive catalysis). A high oxygen mobility (redox property) [12], high oxygen storage capacity [13–18], strong interaction with the supported metal (strong metal–support interaction) [19] and a modifiable capability [20] render this material very interesting for catalysis. It has widely been reported, regarding the above properties, that ceria can promote the action of various metals in the reactions in which hydrogen is involved as a reactant or product [21–25]. According to the catalytic steam reforming reaction, ceria-based materials have been reported by several researchers to be promising supports among α-Al_2O_3 [26], γ-Al_2O_3 and γ-Al_2O_3 with alkali metal oxide and rare earth metal oxide [27], and $CaAl_2O_4$ [26–29]. One of the most promising ceria-based supports for the reforming reactions appeared to be Ce-ZrO_2, where the metal can be Ni, Pt or Pd [30–39]. Recently, a high resistance toward carbon deposition over ceria has been observed [40].

Importantly, CeO_2 has been reported to have reactivity toward methane decomposition at a high temperature (800–1000 °C) [41,42]. It was demonstrated that the gas–solid reaction between CeO_2 and CH_4 produces H_2 and CO, according to Eq. (1). Moreover, the reactions of the reduced ceria (CeO_{2-n}) with carbon dioxide and steam produce more CO and H_2 and regenerate the CeO_2 surface, Eqs. (2) and (3) [43–45]:

$$CH_4 + O_O{}^x = 2H_2 + CO + V_O{}^{\bullet\bullet} + 2e' \quad (1)$$

$$V_O{}^{\bullet\bullet} + 2e' + CO_2 = O_O{}^x + CO \quad (2)$$

$$V_O{}^{\bullet\bullet} + 2e' + H_2O = O_O{}^x + H_2 \quad (3)$$

$V_O{}^{\bullet\bullet}$ denotes an oxygen vacancy with an effective charge 2^+, $O_O{}^x$ is lattice oxygen, e′ is an electron which can either be more or less localized on a cerium ion or delocalized in a conduction band [46].

The major limitation for CeO_2 in high temperature applications is its low specific surface area due to the significant size reduction on thermal sintering [42] and, consequently, the reforming reactivity over CeO_2 was much lower than the conventional metallic catalysts [42]. It was reported that the methane conversion from CeO_2 after exposure in methane steam reforming conditions at 900 °C for 10 h was less than 10%. In addition, the corresponding post-reaction specific surface area for this material after exposure in methane steam reforming conditions was 1.9 $m^2\,g^{-1}$, and the observed size reduction percentage was 23% [42]. Therefore, the use of high surface area ceria (CeO_2 (HSA)) would be a good procedure to improve its catalytic performance at high operating temperatures. Several methods have recently been described for the preparation of a CeO_2 (HSA) solid solution. Among these methods, the surfactant-assisted approach was employed to prepare high surface area CeO_2 with improved textural, structural, and chemical properties [47]. Our previous publication [48] reported the achievement of CeO_2 with a high surface area and good stability after thermal treatment by this preparation method. Regarding the surfactant-assisted method, CeO_2 (HSA) is prepared by reacting a cationic surfactant with a hydrous oxide produced by co-precipitation under basic conditions. At a high pH value, conducting the precipitation of hydrous oxide in the presence of a cationic surfactant allows the cation exchange process between H^+ and the surfactant, resulting in a developed pore structure with an increase in surface area [47]. The achievement of high thermal stability for CeO_2 (HSA) is due to the incorporation of surfactants during preparation, which can reduce the interfacial energy and eventually decrease the surface tension of water contained in the pores. This could reduce the shrinkage and collapse of the catalyst during heating, which consequently helps the catalyst maintain a high surface area after calcination [47].

In the present work, the stability and activity toward steam reforming of LPG over high surface area CeO_2 (CeO_2 (HSA)) was studied and compared to those over the conventional low surface area CeO_2 (CeO_2 (LSA)), and also conventional Ni/Al_2O_3. The resistance towards carbon formation and the influence of the inlet H_2O/LPG molar ratio and temperature on product selectivities over these catalysts were determined. In

Table 1
Specific surface area of CeO_2 (HSA and LSA) after drying and calcinations at different temperatures

Catalyst	BET surface area ($m^2\ g^{-1}$) after drying or calcination at						
	100 °C	200 °C	400 °C	600 °C	800 °C	900 °C	1000 °C
CeO_2 (LSA)[a]	55	49	36	21	15	11	8.5
CeO_2 (HSA)[b]	105	97	69	48	35	29	24

[a] Conventional low surface area CeO_2 prepared by the precipitation method.
[b] Nanocomposite high surface area CeO_2 prepared by the surfactant-assisted approach.

addition, autothermal reforming of LPG was also investigated by adding oxygen at the inlet feed. The improvement in the resistance to carbon deposition by the presence of oxygen and a suitable inlet O_2/LPG molar ratio were determined. It should be noted that the contents of desulpherized LPG used in this work are 60% C_3H_8 and 40% C_4H_{10} (based on the compositions of LPG from PTT Company (Thailand)).

2. Experimental

2.1. Catalyst preparation and characterization

Conventional CeO_2 (CeO_2 (LSA)) was prepared by the precipitation of cerium chloride ($CeCl_3 \cdot 7H_2O$) from Aldrich. The starting solution was prepared by mixing 0.1 M of this metal salt solution with 0.4 M of ammonia in a 2:1 volumetric ratio. This solution was stirred by magnetic stirring (100 rpm) for 3 h, then sealed and placed in a thermostatic bath maintained at 90 °C for 3 days. The precipitate was filtered and washed with deionised water and acetone to remove the free surfactant. It was dried overnight in an oven at 110 °C, and then calcined in air at 1000 °C for 6 h.

High surface area CeO_2 (CeO_2 (HSA)) was prepared by adding an aqueous solution of the appropriate cationic surfactant, 0.1 M cetyltrimethylammonium bromide solution from Aldrich, to a 0.1 M cerium chloride. The molar ratio of ([Ce])/[cetyltrimethylammonium bromide] was kept constant at 0.8. The mixture was stirred and then aqueous ammonia was slowly added with vigorous stirring until the pH was 11.5 [47]. The mixture was continually stirred for 3 h, then sealed and placed in the thermostatic bath maintained at 90 °C for 3 days. After that, the mixture was cooled and the resulting precipitate was filtered and washed repeatedly with water and acetone. The filtered powder was then treated under the same procedures as CeO_2 (LSA). BET measurements of CeO_2 (both LSA and HSA) were carried out at different calcination temperatures in order to determine the loss of specific surface area due to the thermal sintering. As presented in Table 1, after drying, surface areas of 82 and 55 $m^2\ g^{-1}$ were observed for CeO_2 (HSA) and conventional CeO_2, respectively, and as expected, the surface area dramatically decreased at high calcination temperatures. However, the value for CeO_2 (HSA) is still appreciable after calcination at 1000 °C and it is almost three times that of the conventional CeO_2.

The redox properties and redox reversibilities of these synthesized CeO_2 (both LSA and HSA) were then determined by the temperature-programmed reduction (TPR) and temperature-programmed oxidation (TPO). TPR and TPO experiments were conducted in the presence of 5% H_2/Ar and 5% O_2/He, respectively, while the temperature of the system increased from room temperature to 900 °C for both experiments.

For comparison, Ni/Al_2O_3 (5 wt.% Ni) was also prepared by impregnating α-Al_2O_3 (from Aldrich) with $NiCl_3$. After stirring, the solution was dried and calcined at 1000 °C for 6 h. The catalysts were also reduced with 10%H_2/Ar at 500 °C for 6 h before use. After reduction, the catalysts were characterized by several physicochemical methods. The weight content of Ni in Ni/Al_2O_3 was determined by X-ray fluorescence (XRF) analysis. The reducibility and dispersion percentages of nickel were measured from temperature-programmed reduction (TPR) with 5% H_2 in helium and temperature-programmed desorption (TPD), respectively. The catalyst specific surface areas were obtained from BET measurement. All physicochemical properties of the synthesized Ni/Al_2O_3 are presented in Table 2.

2.2. Apparatus and procedures

An experimental reactor system was constructed as shown in Fig. 1. The feed gases including the components of interest (e.g. LPG, steam from the evaporator, and oxygen) and the carrier gas (helium) were introduced to the reaction section, in which a 10 mm diameter quartz reactor was mounted vertically inside a furnace. The reactivities of the catalyst toward steam reforming of LPG were determined by loading the catalyst in this quartz reactor, which was packed with a small amount of quartz wool to prevent the catalyst from moving. The inlet LPG concentration was kept constant at 5 kPa (C_3H_8/C_4H_{10} ratio of 0.6/0.4), while the inlet steam concentrations were varied depending on the inlet H_2O/LPG molar ratio requirement for each experiment (3.0, 4.0, 5.0, 6.0, and 7.0). Regarding the results in our previous publications [48], to avoid any limitations by intraparticle diffusion, the weight of catalyst was always kept constant at 50 mg, while the total gas flow was 100 $cm^3\ min^{-1}$ with a constant residence time of 5×10^{-4} g min cm^{-3} in all experiments. A Type-K

Table 2
Physicochemical properties of synthesized Ni/Al_2O_3 after reduction

Catalyst	Ni-load[a] (wt.%)	BET surface area ($m^2\ g^{-1}$)	Ni-reducibility[b] (Ni%)	Ni-dispersion[c] (Ni%)
Ni/Al_2O_3	4.9	40	92.1	4.87

[a] Measured from X-ray fluorescence analysis.
[b] Measured from temperature-programmed reduction (TPR) with 5% hydrogen.
[c] Measured from temperature-programmed desorption (TPD) of hydrogen after TPR measurement.

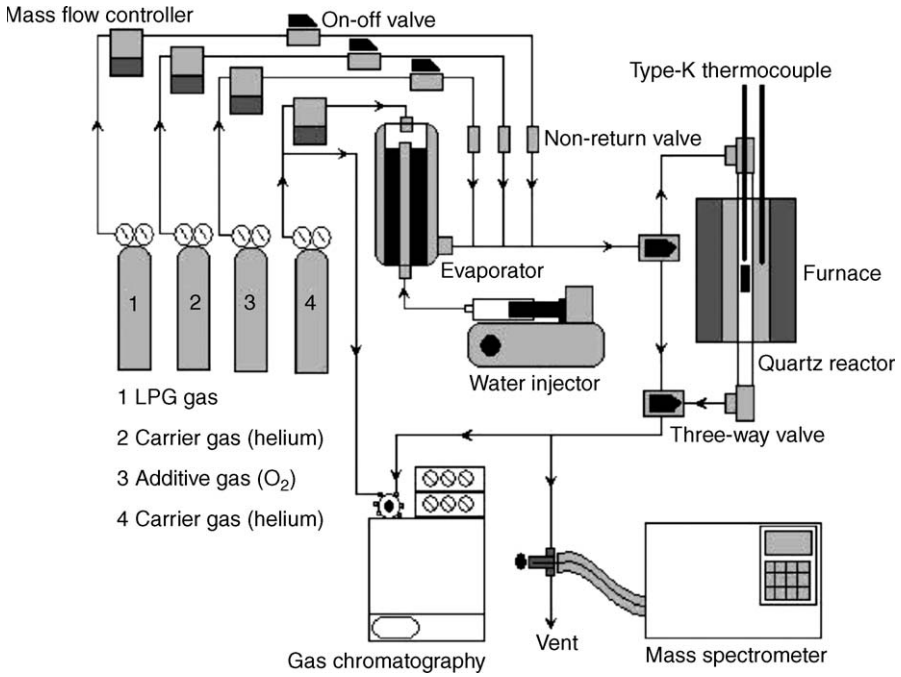

Fig. 1. Schematic diagram of the experimental set-up.

thermocouple was placed in the annular space between the reactor and the furnace. This thermocouple was mounted on the tubular reactor in close contact with the catalyst bed to minimize the temperature difference between the catalyst bed and the thermocouple. Another Type-K thermocouple was inserted in the middle of the quartz tube in order to re-check the possible temperature gradient, especially when O_2 was added along with LPG and H_2O in autothermal reforming. The recorded values showed that the maximum temperature fluctuation during the reaction was always $\pm 0.75\,^{\circ}C$ or less from the temperature specified for the reaction.

After the reactions, the exit gas mixture was transferred via trace-heated lines to the analysis section, which consisted of a Porapak Q column Shimadzu 14B gas chromatograph (GC) and a mass spectrometer (MS). Gas chromatography was used in order to investigate the steady state condition experiments, whereas the mass spectrometer, in which the sampling of the exit gas was done by a quartz capillary and differential pumping, was used in the transient carbon formation experiment. In order to study the formation of carbon species on catalyst surface, temperature-programmed oxidation (TPO) was applied by introducing 5% oxygen in helium into the system, after being purged with helium. The operating temperature was increased from room temperature to 900 °C at a rate of 10 °C min^{-1}. The calibration of CO and CO_2 were performed by injecting a known amount of the gases from a sample loop into an injection valve in the bypass line. The response factors were obtained by dividing the number of moles for each component over the respective areas under peaks. The amount of carbon formed on the surface of catalysts was determined by measuring the CO and CO_2 yields from the TPO results (using Microcal Origin Software) assuming a value of 0.026 nm^2 for the area occupied by a carbon atom in a surface monolayer of the basal plane in graphite [49]. In addition to the TPO method, the amount of carbon deposition was confirmed by the calculation of carbon balance in the system. The amount of carbon deposited on the surface of catalyst would theoretically be equal to the difference between the inlet carbon containing components (C_3H_8 and C_4H_{10}) and the outlet carbon containing components (CO, CO_2, CH_4, C_2H_6, and C_2H_4). The amount of carbon deposited per gram of catalyst is given by the following equation:

$$C_{\text{deposition}} = \frac{\text{mole}_{\text{carbon(in)}} - \text{mole}_{\text{carbon(out)}}}{m_{\text{catalyst}}} \tag{4}$$

The steam reforming reactivity was defined in terms of the conversions and selectivities. Hydrocarbon conversions (propane and butane) denoted as $X_{\text{hydrocarbon}}$, and the products selectivity (hydrogen, carbon monoxide, carbon dioxide, methane, and ethylene), denoted as S_{product}, are calculated according to Eqs. (5)–(12):

$$X_{\text{butane}} = \frac{100(\%\text{butane}_{\text{in}} - \%\text{butane}_{\text{out}})}{\%\text{butane}_{\text{in}}} \tag{5}$$

$$X_{\text{propane}} = \frac{100(\%\text{propane}_{\text{in}} - \%\text{propane}_{\text{out}})}{\%\text{propane}_{\text{in}}} \tag{6}$$

$$S_{H_2} = \frac{100(\%H_2)}{3(\%\text{butane}_{\text{in}} - \%\text{butane}_{\text{out}}) + 4(\%\text{propane}_{\text{in}} - \%\text{propane}_{\text{out}}) + (\%H_2O_{\text{in}} - \%H_2O_{\text{out}})} \tag{7}$$

$$S_{\text{CO}} = \frac{100(\%\text{CO})}{2(\%\text{butane}_{\text{in}} - \%\text{butane}_{\text{out}}) + 3(\%\text{propane}_{\text{in}} - \%\text{propane}_{\text{out}})} \tag{8}$$

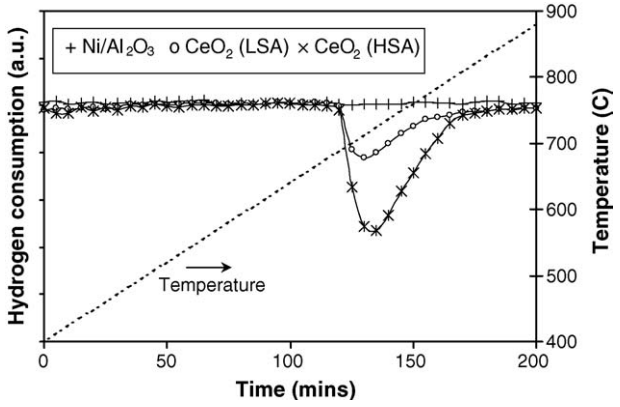

Fig. 2. Temperature-programmed reduction (TPR-1) of fresh catalysts after reduction.

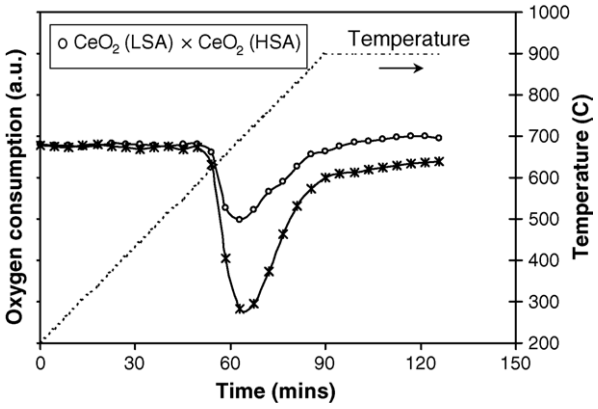

Fig. 3. Temperature-programmed oxidation (TPO) of CeO_2 (HSA and LSA) after TPR-1.

$$S_{CO_2} = \frac{100(\%CO_2)}{2(\%\text{butane}_{in} - \%\text{butane}_{out}) + 3(\%\text{propane}_{in} - \%\text{propane}_{out})} \quad (9)$$

$$S_{CH_4} = \frac{100(\%CH_4)}{2(\%\text{butane}_{in} - \%\text{butane}_{out}) + 3(\%\text{propane}_{in} - \%\text{propane}_{out})} \quad (10)$$

$$S_{C_2H_6} = \frac{100(\%C_2H_6)}{(\%\text{butane}_{in} - \%\text{butane}_{out}) + 1.5(\%\text{propane}_{in} - \%\text{propane}_{out})} \quad (11)$$

$$S_{C_2H_4} = \frac{100(\%C_2H_4)}{(\%\text{butane}_{in} - \%\text{butane}_{out}) + 1.5(\%\text{propane}_{in} - \%\text{propane}_{out})} \quad (12)$$

3. Results

3.1. Redox property and redox reversibility of the synthesized CeO_2

The oxygen storage capacities (OSC) and the redox properties of CeO_2 (both LSA and HSA) were investigated using temperature-programmed reduction (TPR-1) which was performed by heating the reduced catalysts up to 900 °C in 5%H_2 in argon. A test over Ni/Al_2O_3 was also performed for comparison. As shown in Fig. 2, hydrogen uptake was detected from both types of CeO_2 at the temperature above 650 °C. The amount of hydrogen uptake over CeO_2 (HSA) is significantly higher than that over CeO_2 (LSA), suggesting that the OSC and the redox properties strongly depend on the specific surface area of CeO_2. In contrast, no hydrogen consumption was observed from the TPR over Ni/Al_2O_3, indicating the absence of redox properties for this catalyst. The benefit of having a redox property in the reforming of LPG will be presented in Section 4. After being purged with helium, the redox reversibility for each type of CeO_2 was then determined by conducting temperature-programmed oxidation (TPO) following by a second temperature-programmed reduction (TPR-2). The TPO was carried out by heating the catalyst up to 900 °C in 5%O_2 in helium; the amount of oxygen chemisorbed was then measured, as shown in Fig. 3 and Table 3. Regarding the TPR-2 results as shown in Fig. 4 and Table 3, the amount of hydrogen uptake for CeO_2 (both LSA and HSA) were approximately similar to those from TPR-1, indicating the redox reversibility of these synthesized versions of CeO_2.

3.2. Homogenous (non-catalytic) reactions

Before studying the catalyst performance, homogeneous (non-catalytic) steam reforming of LPG was investigated. A

Table 3
Results of TPR(1), TPO, TPR(2) analyses of CeO_2 (both HSA and LSA)

Catalyst	Total H_2 uptake from TPR(1)[a] (μmol g_{cat}^{-1})	Total O_2 uptake from TPO[b] (μmol g_{cat}^{-1})	Total H_2 uptake from TPR(2)[c] (μmol g_{cat}^{-1})
CeO_2 (HSA)	2159	1044	2155
CeO_2 (LSA)	1784	867	1781

[a] Temperature-programmed reduction of the reduced catalysts (relative standard deviation = ±3%).
[b] Temperature-programmed oxidation after TPR(1) (relative standard deviation = ±1%).
[c] Re-temperature-programmed reduction after TPO (relative standard deviation = ±2%).

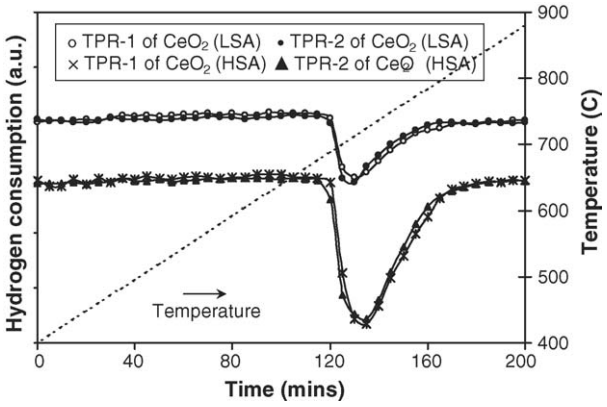

Fig. 4. Second time temperature-programmed reduction (TPR-2) of CeO_2 (HSA and LSA) compared to that of TPR-1.

feed stream consisting a LPG/H_2O at a molar ratio of 1.0/5.0 was introduced into the system, while the temperature increased from ambient to 900 °C. Both propane and butane were converted to methane, ethane, ethylene, and hydrogen at the temperature above 700 °C, as shown in Fig. 5. A significant amount of carbon was also detected in the blank reactor after exposure for 10 h. These components were formed via the decomposition of butane and propane as shown in the equations below.

$$C_4H_{10} \rightarrow C_2H_6 + C_2H_4 \quad (13)$$

$$C_3H_8 \rightarrow 3/2(C_2H_4) + H_2 \quad (14)$$

$$C_2H_6 \rightarrow C_2H_4 + H_2 \quad (15)$$

$$C_2H_4 \Leftrightarrow CH_4 + C \quad (16)$$

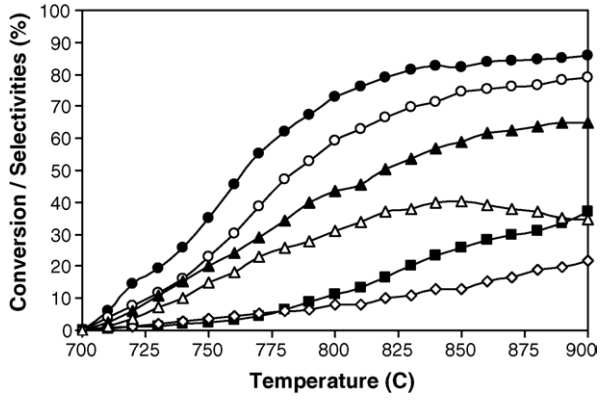

Fig. 5. Homogeneous (in the absence of a catalyst) reactivity of LPG in the presence of steam (with the inlet H_2O/LPG of 5.0) (C_4H_{10} (●), C_3H_8 (◯), C_2H_4 (▲), C_2H_6 (△), CH_4 (■), and H_2 (◇)).

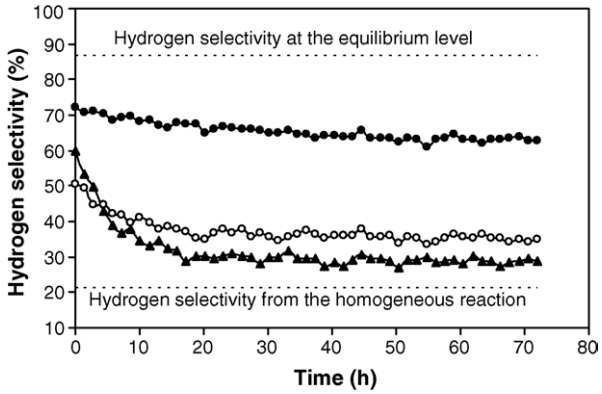

Fig. 6. Hydrogen selectivity from the steam reforming of LPG over CeO_2 (HSA) (●), CeO_2 (LSA) (◯), and Ni/Al_2O_3 (▲) at 900 °C compared to that from the homogeneous reaction and at the equilibrium level.

There was no change in the steam concentration, and no carbon monoxide and carbon dioxide were produced in the system, indicating that the non-homogenous reforming reaction between steam and hydrocarbons did not take place at this range of conditions studied.

3.3. Stability and activity toward the steam reforming of LPG

The synthesized CeO_2 (HSA), CeO_2 (LSA), and Ni/Al_2O_3 were studied in the steam reforming of C_3H_8/C_4H_{10} at 900 °C. The feed was H_2O/LPG in helium with the molar ratio of 5.0 (H_2O/C ratio of 1.45). The reforming rate was measured as a function of time in order to determine the stability and the deactivation rate. The variations in the hydrogen selectivity with time at 900 °C are shown in Fig. 6. Significant deactivation was detected with Ni/Al_2O_3 catalyst, whereas much lower deactivations were observed for CeO_2 (HSA). Catalyst stabilities expressed as deactivation percentages are given in Table 4. It should be noted that, in order to determine whether the observed deactivation is due to the carbon formation, the post-reaction temperature-programmed oxidation (TPO) experiments were carried out.

From the TPO results shown in Fig. 7, a huge amount of carbon deposition was observed on Ni/Al_2O_3, whereas significantly less carbon formation was detected on CeO_2 (LSA) and CeO_2 (HSA) after exposure to the steam reforming conditions for 72 h. The amount of carbon formation (monolayer) on the surface of catalysts was determined by measuring the CO and CO_2 yields (using Microcal Origin Software). Using a value of 0.026 nm^2 for the area occupied by a carbon atom in a surface mono-

Table 4
Physicochemical properties of catalysts after exposure in the steam reforming of LPG at 900 °C for 72 h.

Catalyst	Deactivation (%)	C formation (monolayers)	BET surface (m^2 g^{-1})	Ni-load (wt.%)	Ni-red. (Ni%)	Ni-disp. (Ni%)
CeO_2 (HSA)	12.8	0.51[a] (0.48)[b]	22.0	–	–	–
CeO_2 (LSA)	30.6	0.92 (0.92)	7.1	–	–	–
Ni/Al_2O_3	52.3	4.73 (4.71)	~40.0	4.9	92.1	4.82

[a] Calculated using CO and CO_2 yields from temperature-programmed oxidation (TPO) with 5% oxygen.
[b] Calculated from the balance of carbon in the system.

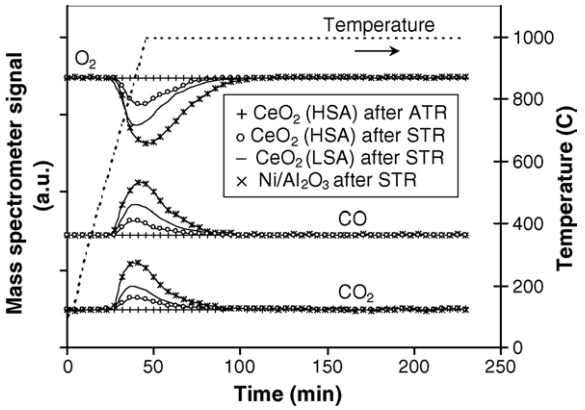

Fig. 7. Temperature-programmed oxidation (TPO) of CeO_2 (HSA), CeO_2 (LSA), and Ni/Al_2O_3 after exposure in the steam reforming (STR) and autothermal reforming (ATR) of LPG (H_2O/LPG of 5.0 for STR and O_2/LPG of 0.6 for ATR) for 72 h.

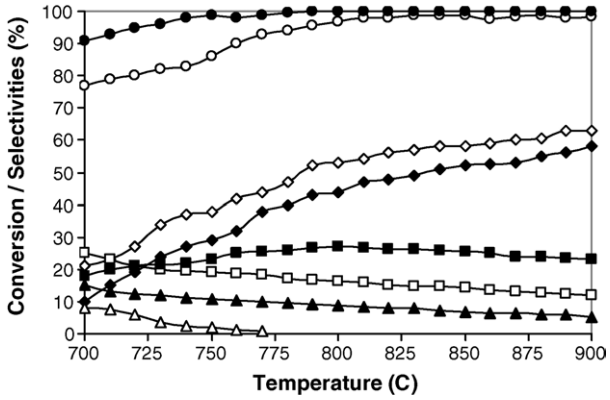

Fig. 8. Effect of reaction temperature on the conversions of C_4H_{10} (●) and C_3H_8 (○), and the selectivities of H_2 (◊), CO (♦), CO_2 (□), CH_4 (■), C_2H_6 (△), and C_2H_4 (▲) from steam reforming over CeO_2 (HSA) (with the inlet H_2O/LPG of 5.0).

layer of the basal plane in graphite [49], the quantities of carbon deposited for each catalyst were observed as in Table 4. The total amounts of carbon deposited were then verified by calculating the carbon balance of the system. Regarding the calculations, the moles of carbon deposited per gram of CeO_2 (HSA), CeO_2 (LSA), and Ni/Al_2O_3 were 0.54, 0.97, and 4.76 mmol g^{-1}. By the same assumption for the area occupied by a carbon atom [49], the values shown in Table 4 are in good agreement with the values observed from the TPO method described above. These results clearly indicate that the deactivation observed on Ni/Al_2O_3 was mainly due to carbon deposition on the surface of catalyst, and CeO_2 especially the high surface area had a significant resistance toward carbon formation as compared to Ni/Al_2O_3. BET measurements were then carried out to observe the percentage decrease in surface area of all catalysts. It should be noted that the BET measurement for Ni/Al_2O_3 was carried out after reducution of the catalyst (after TPO) with hydrogen in order to eliminate all NiO from the TRO experiment, which could affect the catalyst surface area. Results shown in Table 4 suggest that the deactivation of ceria is mainly due to the thermal sintering. However, the surface area reduction percentage of CeO_2 (HSA) is much lower than CeO_2 (LSA), indicating a higher stability toward the thermal sintering.

It should be noted that, the steady-state hydrogen selectivity observed from all catalysts (62.9% for CeO_2 (HSA), 35.0% for CeO_2 (LSA), and 28.6% for Ni/Al_2O_3) was lower than that at equilibrium state, which is approximately 87% (according to the simulation using AspenPlus 10.2), due to the incomplete decomposition of LPG to H_2, CO, and CO_2.

3.4. Effects of temperature and inlet reactants

The influences of operating temperature and the inlet steam content on the conversion of butane and propane, and the product selectivities from the steam reforming of LPG over CeO_2 (HSA) and CeO_2 (LSA) were studied by varying the operating temperature from 700 to 900 °C and changing the inlet H_2O/LPG ratio from 3.0 to 7.0 (H_2O/C ratio from 0.87 to 2.02) as represented in Figs. 8 and 9.

At 900 °C, the main products from the steam reforming reaction over CeO_2 (HSA) were CH_4, H_2 CO, and CO_2. Some formation of C_2H_4 was also observed. Hydrogen and carbon monoxide selectivities increased with increasing temperature, whereas carbon dioxide and ethylene production selectivities decreased. The dependence of methane selectivity on the operating temperature was non-monotonic, the maximum production of methane occurred at approximately 800 °C. Regarding the effect of steam, hydrogen and carbon dioxide selectivities increased with increasing inlet steam concentration, whereas carbon monoxide, methane, and ethylene selectivities decreased. These changes in product selectivities are due to the influence of the exothermic water-gas shift reaction ($CO + H_2O \rightarrow CO_2 + H_2$), whereas the decreased methane and ethylene selectivities could be due to further reforming which would generate more carbon monoxide and hydrogen. Temperature-programmed oxidations of CeO_2 (HSA) after exposure in steam reforming with different inlet H_2O/LPG ratios were then carried out to determine the effect of the inlet steam concentration on the degree of carbon formation. From the TPO results, the amount of carbon deposited slightly decreased with increasing inlet steam concentration, however, a

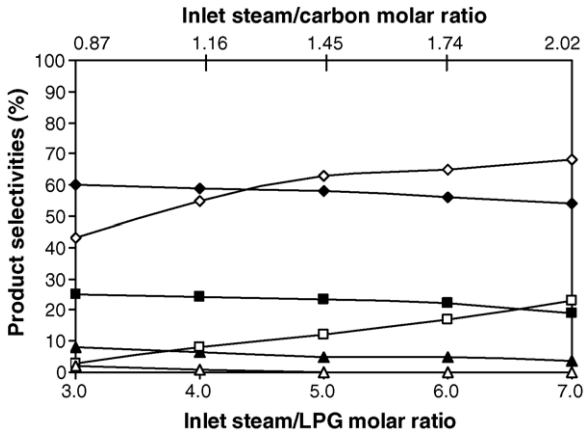

Fig. 9. Effect of inlet steam/LPG molar ratio on the selectivities of H_2 (◊), CO (♦), CO_2 (□), CH_4 (■), C_2H_6 (△), and C_2H_4 (▲) from the steam reforming of LPG over CeO_2 (HSA) at 900 °C.

Table 5
The dependence of hydrogen yield on the H_2O/LPG molar ratio and the amount of carbon formation on CeO_2 (HSA) after exposure in the steam reforming condition for 72 h

H_2O/LPG ratio	Hydrogen selectivity (%) at steady state	Total carbon formation (monolayers)
3.0	43.1	0.82[a] (0.84)[b]
4.0	55.0	0.67 (0.65)
5.0	62.9	0.51 (0.48)
6.0	65.3	0.44 (0.44)
7.0	68.0	0.41 (0.39)

[a] Calculated using CO and CO_2 yields from temperature-programmed oxidation (TPO) with 5% oxygen.
[b] Calculated from the balance of carbon in the system.

significant amount of carbon was detected even at a H_2O/LPG molar ratio of 7.0 (0.39–0.41 monolayers, Table 5).

3.5. Reactivity toward autothermal reforming

In order to reduce the degree of carbon formation and improve the product selectivities, autothermal reforming of LPG over CeO_2 (HSA) was studied by adding oxygen along with LPG and steam. The inlet H_2O/C molar ratio was kept constant at 1.45 (H_2O/LPG molar ratio of 5.0), while the inlet O/C molar ratios were varied at 0.2, 0.4, 0.6, 0.8 and 1.0. It should be noted that, while varying the ratios of H_2O/LPG and O_2/LPG, the overall space velocity was always maintained at a constant value by adjusting the flow rate of carrier gas (helium) to keep the total flow rate constant.

The effect of oxygen concentration on the product selectivities (%) at 900 °C is shown in Fig. 10. The effect of oxygen on the yields of hydrogen and carbon monoxide productions were non-monotonic. Hydrogen selectivity increased with increasing O/C molar ratio until the ratio reached 0.6. The positive effect of oxygen on the hydrogen selectivity in this range is due to the assistance of this component to reform hydrocarbons. However, higher O/C ratios showed a negative effect on the hydrogen selectivity, as too high an oxygen concentration resulted in the oxidation of the hydrogen produced from the steam reforming.

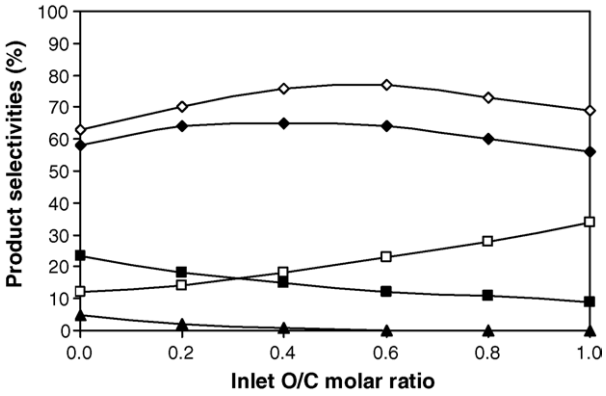

Fig. 10. Effect of inlet oxygen/carbon molar ratio on the selectivities of H_2 (◊), CO (♦), CO_2 (□), CH_4 (■), and C_2H_4 (▲) from the autothermal reforming of LPG over CeO_2 (HSA) at 900 °C.

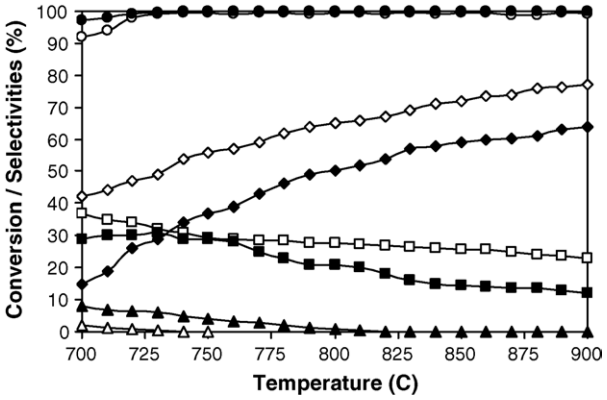

Fig. 11. Effect of reaction temperature on the conversions of C_4H_{10} (●) and C_3H_8 (●), and the selectivities of H_2 (◊), CO (♦), CO_2 (□), CH_4 (■), C_2H_6 (△), and C_2H_4 (▲) from the autothermal reforming over CeO_2 (HSA) (inlet O_2/C molar ratio of 0.6).

Table 6
The dependence of hydrogen yield on the O/C molar ratio and the amount of carbon formation on CeO_2 (HSA) after exposure in the reforming for 72 h

O/C ratio	Hydrogen selectivity (%) at steady state	Total carbon formation (monolayers)
0.0	62.9	0.51[a] (0.48)[b]
0.2	69.8	0.19 (0.21)
0.4	76.1	0.07 (0.06)
0.6	77.0	∼0.0 (∼0.0)
0.8	72.8	∼0.0 (∼0.0)
1.0	69.0	∼0.0 (∼0.0)

[a] Calculated using CO and CO_2 yields from temperature-programmed oxidation (TPO) with 5% oxygen.
[b] Calculated from the balance of carbon in the system.

Fig. 11 presents the product selectivities from the autothermal reforming of LPG (with the O/C molar ratio of 0.6) over CeO_2 (HSA) at different temperatures (700 °C to 900 °C). It was found that the main products from the autothermal reforming are similar to the steam reforming (e.g. H_2, CO, CO_2, and CH_4). Higher H_2, CO, and CO_2 selectivities were observed from autothermal reforming, whereas less CH_4, C_2H_6, and C_2H_4 were found compared to steam reforming under the same operating conditions. At 900 °C, neither C_2H_6 nor C_2H_4 formation was observed from the reaction due to the complete decomposition of these high hydrocarbons by the addition of oxygen. The benefits of the oxygen addition along with LPG and steam are presented in Section 4.

Temperature-programmed oxidation was carried out on the spent catalysts in order to determine the degree of carbon formation on the catalyst surface after exposure to the autothermal reforming reaction. From the TPO results, significantly lower quantities of deposited carbon was observed over CeO_2 (HSA) surface, and no carbon formation was detected when the inlet O/C molar ratio reached 0.6, shown in Fig. 7 and Table 6.

4. Discussion

High surface area ceria (CeO_2 (HSA)), synthesized by a surfactant-assisted approach, provided a high LPG reforming

reactivity and excellent resistance toward carbon deposition compared to conventional Ni/Al_2O_3. Carbon formation during LPG reforming could occur due to the reactions listed below:

$$C_4H_{10} \Leftrightarrow 5H_2 + 4C \quad (17)$$

$$C_3H_8 \Leftrightarrow 4H_2 + 3C \quad (18)$$

$$C_2H_4 \Leftrightarrow 2H_2 + 2C \quad (19)$$

$$CH_4 \Leftrightarrow 2H_2 + C \quad (20)$$

$$2CO \Leftrightarrow CO_2 + C \quad (21)$$

$$CO + H_2 \Leftrightarrow H_2O + C \quad (22)$$

$$CO_2 + 2H_2 \Leftrightarrow 2H_2O + C \quad (23)$$

where C is the carbonaceous deposit. At low temperature, Eqs. (22) and (23) are favorable, while Eqs. (17)–(21) are thermodynamically not favored [50]. The Boudouard reaction (Eq. (21)) and the decomposition of hydrocarbons (Eqs. (17)–(20) are the major pathways for carbon formation at such a high temperature as they show the largest change in Gibbs free energy [51]. Because of the high temperature employed in this study (700–900 °C), carbon formation via the decomposition of hydrocarbons and Boudouard reactions is possible. With the increase in steam to carbon ratio, the equilibrium of the water-gas shift reaction moves forward and produces more CO_2 rather than CO. Therefore, a high steam feed can avoid carbon deposition via the Boudouard reaction. However, a significant amount of carbon still forms due to the decomposition of hydrocarbons.

The high resistance toward carbon deposition on CeO_2, especially on high surface area CeO_2, is mainly due to the high oxygen storage capacity (OSC) of this material. CeO_2 contains a high concentration of highly mobile oxygen vacancies and thus acts as a local source or sink for oxygen on its surface. It has been reported that at high temperature, the lattice oxygen (O_O^x) at the CeO_2 surface can oxidize gaseous hydrocarbons (e.g. methane [42,48,49]). By using CeO_2 (HSA) as the catalyst, the carbon deposition due to the decomposition of hydrocarbons could be inhibited by the gas–solid reactions between the hydrocarbons present in the system (C_4H_{10}, C_3H_8, C_2H_6, C_2H_4, CH_4) and the lattice-oxygen (O_O^x) at the CeO_2 surface (Eq. (24)) forming CO_2 and H_2 from which the formation of carbon is thermodynamically unfavorable at high temperature.

$$C_nH_m + O_O^x \Leftrightarrow nCO + m/2H_2 + V_O^{\bullet\bullet} + 2e' \quad (24)$$

After the reactions, the lattice oxygen (O_O^x) is regenerated by reaction with oxygen containing compounds (e.g. steam) present in the system.

$$H_2O + V_O^{\bullet\bullet} + 2e' \Leftrightarrow O_O^x + H_2 \quad (25)$$

The redox mechanism between the hydrocarbons present in the system and the lattice oxygen (O_O^x) are illustrated below.

$$C_4H_{10} + 4S_{Ce} \Leftrightarrow 2(CH_3{-}S_{Ce}) + 2(CH_2{-}S_{Ce}) \quad (26)$$

$$C_3H_8 + 3S_{Ce} \Leftrightarrow 2(CH_3{-}S_{Ce}) + CH_2{-}S_{Ce} \quad (27)$$

$$C_2H_6 + 2S_{Ce} \Leftrightarrow 2(CH_3{-}S_{Ce}) \quad (28)$$

$$C_2H_4 + 2S_{Ce} \Leftrightarrow 2(CH_2{-}S_{Ce}) \quad (29)$$

$$CH_4 + 2S_{Ce} \Leftrightarrow CH_3{-}S_{Ce} + H{-}S_{Ce} \quad (30)$$

$$CH_3{-}S_{Ce} + S_{Ce} \Leftrightarrow CH_2{-}S_{Ce} + H{-}S_{Ce} \quad (31)$$

$$CH_2{-}S_{Ce} + S_{Ce} \Leftrightarrow CH{-}S_{Ce} + H{-}S_{Ce} \quad (32)$$

$$CH{-}S_{Ce} + S_{Ce} \Leftrightarrow C{-}S_{Ce} + H{-}S_{Ce} \quad (33)$$

$$C{-}S_{Ce} + O_O^x \Leftrightarrow CO + V_O^{\bullet\bullet} + 2e' + S_{Ce} \quad (34)$$

$$2H{-}S_{Ce} \Leftrightarrow H_2 + 2S_{Ce} \quad (35)$$

where S_{Ce} is the CeO_2 surface site and $CH_x{-}S_{Ce}$ is an intermediate surface hydrocarbon species. S_{Ce} can be considered to be a unique site, or the same site as the lattice oxygen (O_O^x). Steele and Floyd [52] reported that the measured value of the oxygen diffusion coefficient for ceria is high and the reaction rate is controlled by a surface reaction rather than by diffusion of oxygen from the bulk of the solid particles to ceria surfaces [52]. During the reaction, hydrocarbons are adsorbed on either a unique site (S_{Ce}) or the lattice oxygen (O_O^x).

Although conventional CeO_2 (CeO_2 (LSA)) has also been reported to provide a high resistance toward carbon formation, the major drawbacks of CeO_2 (LSA) are the low specific surface area and large size reduction due to the thermal sintering, resulting in a significant drop in the redox properties compared to CeO_2 (HSA), as presented in Section 3.1, and consequently low steam reforming reactivity. The corresponding post-reaction specific surface area for CeO_2 (LSA) after exposure in reforming conditions was 7.1 $m^2\,g^{-1}$, and the observed size reduction percentage was 17%, whereas the post-reaction specific surface area for CeO_2 (HSA) was 22 $m^2\,g^{-1}$, and the observed size reduction percentage was 9%. The low redox properties of CeO_2 (LSA) also resulted in a significantly lower resistance toward carbon deposition of this material compared to CeO_2 (HSA). As described earlier, the redox reaction (Eq. (25)) between the lattice oxygen (O_O^x) at the CeO_2 surface and the hydrocarbons present in the system (C_4H_{10}, C_3H_8, C_2H_6, C_2H_4, CH_4) can prevent the formation of carbon by the decomposition of these hydrocarbon components.

It was observed from the study that the addition of oxygen along with LPG and steam in the autothermal reforming reaction reduced the degree of carbon deposition and improved the product selectivities by eliminating the formation of C_2H_6 and C_2H_4. Theoretically, oxygen prevents the formation of high hydrocarbons (i.e. C_2H_6 and C_2H_4) and subsequent carbon deposition from the decomposition reactions (Eqs. (16)–(18)) by oxidizing these hydrocarbons producing the elements that are unfavored to form carbon. The presence of oxygen also helps steam regenerate the lattice oxygen (O_O^x) on the CeO_2 surface ($O_2 + V_O^{\bullet\bullet} + 2e' + S_{Ce} \rightarrow O_O^x$). The major consideration of the autothermal reforming operation is a suitable O_2/LPG ratio. The presence of too high an oxygen concentration could oxidize the hydrogen and carbon monoxide produced from the steam reforming to steam and carbon dioxide.

5. Conclusion

High surface area ceria (CeO_2 (HSA)), synthesized in a surfactant-assisted approach, is a good catalyst for the reforming of LPG (butane and propane) at SOFC temperatures (700–900 °C) due to a high resistance towards the deactivation from carbon formation. During the reforming process, the gas–solid reactions between the hydrocarbons present in the system (i.e. propane, butane, ethane, ethylene, and methane) and the lattice oxygen (O_O^x) take place on the ceria surface, reducing the degree of carbon deposition on the catalyst surface (from hydrocarbons decomposition and Boudouard reactions). At 700–900 °C, the main products from the steam reforming of LPG over CeO_2 (HSA) were H_2, CO, CO_2, and CH_4, whereas a small amount of C_2H_4 was also observed, particularly at low temperatures. By increasing the inlet steam content, hydrogen and carbon dioxide selectivities increased, whereas carbon monoxide selectivity decreased. Moreover, the conversions of methane and ethylene were found to increase with increasing steam content in the system.

The addition of oxygen in autothermal reforming can reduce the degree of carbon deposition and eliminate the formation of higher hydrocarbons (i.e. C_2H_6 and C_2H_4). The major consideration in the autothermal reforming operation is the inlet O_2/LPG molar ratio, as the presence of too high an oxygen concentration could oxidize hydrogen and carbon monoxide, produced from the steam reforming, to steam and carbon dioxide. A suitable O/C molar ratio for autothermal reforming on CeO_2 (HSA) was observed to be 0.6.

Acknowledgement

Financial support from The Thailand Research Fund (TRF) throughout this project is gratefully acknowledged.

References

[1] P. Aguiar, D. Chadwick, L. Kershenbaum, Chem. Eng. Sci. 57 (2002) 1665.
[2] K. Ahmed, J. Gamman, K. Föger, Solid State Ion. 152–153 (2002) 485–492.
[3] T. Suzuki, H.-i. Iwanami, O. Iwamoto, T. Kitahara, Int. J. Hydrogen Energy 26 (9) (2001) 935–940.
[4] A.K. Avci, D.L. Trimm, A.E. Aksoylu, Z.I. Önsan, Catal. Lett. 88 (2003) 17–22.
[5] A.F. Ghenciu, Curr. Opin. Solid State Mater. Sci. 6 (2002) 389–399.
[6] T. Rampe, A. Heinzel, B. Vogel, J. Power Sources 86 (2000) 536–541.
[7] F. Joensen, J.R. Rostrup-Nielsen, J. Power Sources 105 (2002) 195–201.
[8] V. Recupero, L. Pino, A. Vita, F. Cipiti, M. Cordaro, M. Laganà, Int. J. Hydrogen Energy 30 (9) (2005) 963–971.
[9] L.V. Mattos, E. Rodino, D.E. Resasco, F.B. Possos, F.B. Noronha, Fuel Proc. Technol. 83 (2003) 147.
[10] H.S. Roh, K.W. Jun, S.E. Park, Appl. Catal. A 251 (2003) 275.
[11] J.R. Rostrup-Nielsen, J.-H. Bak-Hansen, J. Catal. 144 (1993) 38.
[12] P. Fornasiero, G. Balducci, R.D. Monte, J. Kaspar, V. Sergo, G. Gubitosa, A. Ferrero, M. Graziani, J. Catal. 164 (1996) 173.
[13] T. Miki, T. Ogawa, M. Haneda, N. Kakuta, A. Ueno, S. Tateishi, S. Matsuura, M. Sato, J. Phys. Chem. 94 (1990) 339.
[14] C. Padeste, N.W. Cant, D.L. Trimm, Catal. Lett. 18 (1993) 305.
[15] S. Kacimi, J. Barbier Jr., R. Taha, D. Duperz, Catal. Lett. 22 (1993) 343.
[16] G.S. Zafiris, R.J. Gorte, J. Catal. 143 (1993) 86.
[17] G.S. Zafiris, R.J. Gorte, J. Catal. 139 (1993) 561.
[18] S. Imamura, M. Shono, N. Okamoto, R. Hamada, S. Ishida, Appl. Catal. A 142 (1996) 279.
[19] L. Fan, K. Fujimoto, J. Catal. 172 (1997) 238.
[20] M. Pijolat, M. Prin, M. Soustelle, J. Chem. Soc., Faraday Trans. 91 (1995) 3941.
[21] S. Imamura, T. Higashihara, Y. Saito, H. Aritani, H. Kanai, Y. Matsumura, N. Tsuda, Catal. Today 50 (1999) 369.
[22] S. Imamura, K. Denpo, K. Utani, Y. Matsumura, H. Kanai, React. Kinet. Catal. Lett. 67 (1999) 163.
[23] S. Imamura, K. Denpo, K. Kanai, H. Yamane, Y. Saito, K. Utani, Y. Matsumura, Sekiyu Gakkaishi 44 (2001) 293.
[24] S. Imamura, H. Yamane, H. Kanai, T. Shibuta, K. Utani, K. Hamada, J. Jpn. Petrol. Inst. 45 (2002) 187.
[25] S. Imamura, Y. Taniguchi, Y. Ikeda, S. Hosokawa, H. Kanai, H. Ando, React. Kinet. Catal. Lett. 76 (2002) 201.
[26] H.S. Roh, K.W. Jun, W.S. Dong, J.S. Chang, S.E. Park, Y.I. Joe, J. Mol. Catal. A 181 (2002) 137–142.
[27] Q. Miao, G. Xiong, S. Sheng, W. Cui, L. Xu, X. Guo, Appl. Catal. A 154 (1987) 17–27.
[28] A.A. Lemonidou, M.A. Goula, I.A. Vasalos, Catal. Today 46 (1987) 175–183.
[29] W.S. Dong, H.S. Roh, K.W. Jun, S.E. Park, Y.S. Oh, Appl. Catal. A 226 (2002) 63–72.
[30] M. Mamak, N. Coombs, G. Ozin, Adv. Mater. 12 (2000) 198–202.
[31] M. Mamak, N. Coombs, G. Ozin, J. Am. Chem. Soc. 122 (2000) 8932.
[32] M. Mamak, N. Coombs, G.A. Ozin, Chem. Mater. 13 (2001) 3564.
[33] P. Bera, S. Mitra, S. Sampath, M.S. Hegde, Chem. Commun. (2001) 927.
[34] A. Martinez-Arias, J.M. Coronado, R. Cataluna, J.C. Conesa, J.C. Soria, J. Phys. Chem. B 102 (1998) 4357.
[35] D. Skarmoutsos, F. Tietz, P. Nikolopoulos, Fuel Cells 1 (2001) 243.
[36] T. Takeguchi, S.N. Furukawa, M. Inoue, J. Catal. 202 (2001) 14.
[37] J. Sfeir, P.A. Philippe, P. Moseki, N. Xanthopoulos, R. Vasquez, J.M. Hans, V.H. Jan, K.R. Thampi, J. Catal. 202 (2001) 229.
[38] N. Kiratzis, P. Holtappels, C.E. Hatchwell, M. Mogensen, J.T.S. Irvine, Fuel Cells 1 (2001) 211.
[39] H.S. Roh, W.S. Dong, K.W. Jun, S.E. Park, Chem. Lett. (2001) 88.
[40] E. Ramírez-Cabrera, A. Atkinson, D. Chadwick, Appl. Catal. B 47 (2004) 127–131.
[41] E. Ramírez-Cabrera, N. Laosiripojana, A. Atkinson, D. Chadwick, Catal. Today 78 (2003) 433–438.
[42] N. Laosiripojana, Reaction engineering of indirect internal steam reforming of methane for application in solid oxide fuel cells. Ph.D. Thesis, University of London, England, 2003.
[43] K. Otsuka, T. Ushiyama, I. Yamanaka, Chem. Lett. (1993) 1517.
[44] K. Otsuka, M. Hatano, A. Morikawa, J. Catal. 79 (1983) 493.
[45] K. Otsuka, M. Hatano, A. Morikawa, Inorg. Chim. Acta 109 (1985) 193.
[46] P.J. Gellings, J.M. Henny, Bouwmeester, Solid state aspects of oxidation catalysis, Catal. Today 58 (2000) 1–53.
[47] D. Terribile, A. Trovarelli, J. Llorca, C. de Leitenburg, G. Dolcetti, Catal. Today 43 (1998) 79–88.
[48] N. Laosiripojana, S. Assabumrungrat, Appl. Catal. B: Environ. 60 (2005) 107.
[49] E. Ramirez, A. Atkinson, D. Chadwick, Appl. Catal. B 36 (2002) 193–206.
[50] Y. Lwin, W.R.W. Daud, A.B. Mohamad, Z. Yaakob, Int. J. Hydrogen Energy 25 (1) (2000) 47–53.
[51] J.N. Amor, Appl. Catal. A 176 (1999) 159–176.
[52] B.C.H. Steele, J.M. Floyd, Proc. Br. Ceram. Soc. 19 (1971) 55.

N. Laosiripojana and S. Assabumrungrat

"The effect of specific surface area on the activity of nano-scale ceria catalysts for methanol decomposition with and without steam at SOFC operating temperatures"

Chemical Engineering Science, In Press

(IF-2004 = 1.65)

ARTICLE IN PRESS

ELSEVIER

Chemical Engineering Science ▮▮▮ (▮▮▮▮) ▮▮▮–▮▮▮

Chemical Engineering Science

www.elsevier.com/locate/ces

The effect of specific surface area on the activity of nano-scale ceria catalysts for methanol decomposition with and without steam at SOFC operating temperatures

N. Laosiripojana[a,*], S. Assabumrungrat[b]

[a]*The Joint Graduate School of Energy and Environment, King Mongkut's University of Technology Thonburi, Bangkok 10140, Thailand*

[b]*Center of Excellence on Catalysis and Catalytic Reaction Engineering, Department of Chemical Engineering, Chulalongkorn University, Bangkok 10330, Thailand*

Received 25 August 2005; received in revised form 14 November 2005; accepted 14 November 2005

Abstract

Nano-particulate high surface area CeO_2 was found to have a useful methanol decomposition activity producing H_2, CO, CO_2, and a small amount of CH_4 without the presence of steam being required under solid oxide fuel cell temperatures, 700–1000 °C. The catalyst provides high resistance toward carbon deposition even when no steam is present in the feed. It was observed that the conversion of methanol was close to 100% at 850 °C, and no carbon deposition was detected from the temperature programmed oxidation measurement.

The reactivity toward methanol decomposition for CeO_2 is due to the redox property of this material. During the decomposition process, the gas–solid reactions between the gaseous components, which are homogeneously generated from the methanol decomposition (i.e., CH_4, CO_2, CO, H_2O, and H_2), and the lattice oxygen (O_O^x) on ceria surface take place. The reactions of adsorbed surface hydrocarbons with the lattice oxygen ($C_nH_m + O_O^x \rightarrow nCO + m/2(H_2) + V_{O^{\cdot\cdot}} + 2e'$) can produce synthesis gas (CO and H_2) and also prevent the formation of carbon species from hydrocarbons decomposition reaction ($C_nH_m \Leftrightarrow nC + m/2H_2$). $V_{O^{\cdot\cdot}}$ denotes an oxygen vacancy with an effective charge 2^+. Moreover, the formation of carbon via Boudouard reaction ($2CO \Leftrightarrow CO_2 + C$) is also reduced by the gas–solid reaction of carbon monoxide with the lattice oxygen ($CO + O_O^x \Leftrightarrow CO_2 + V_{O^{\cdot\cdot}} + 2e'$).

At steady state, the rate of methanol decomposition over high surface area CeO_2 was considerably higher than that over low surface area CeO_2 due to the significantly higher oxygen storage capacity of high surface area CeO_2, which also results in the high resistance toward carbon deposition for this material. In particular, it was observed that the methanol decomposition rate is proportional to the methanol partial pressure but independent of the steam partial pressure at 700–800 °C. The addition of hydrogen to the inlet stream was found to have a significant inhibitory effect on the rate of methanol decomposition.

Keywords: Methanol; Internal reforming; Hydrogen; SOFC; CeO_2

1. Introduction

A fuel cell is an energy conversion unit that produces electrical energy and heat with greater energy efficiency and lower pollutant emission than conventional processes (Minh and Takahashi, 1995). Among the various types of fuel cell, the solid oxide fuel cell (SOFCs) has attracted considerable interest as it offers a wide range of applications, flexibility in the choice of fuel, and high-system efficiency. The waste heat can also be utilized in co-generation applications and bottoming cycles. Moreover, unlike the low-temperature fuel cells, the SOFC anode is not affected by carbon monoxide poisoning.

Hydrogen is the major fuel for SOFCs. Nevertheless, the use of other fuels such as methane, methanol, ethanol, gasoline and other oil derivatives is also possible when operated as an internal or in-stack reforming. As SOFCs are operated at such a high temperature, these hydrocarbons can be internally reformed to produce a H_2/CO rich gas, which is eventually used to generate the electrical energy and heat.

* Corresponding author. Tel.: +66 2 8729014; fax: +66 2 8726736.
E-mail address: navadol_l@jgsee.kmutt.ac.th (N. Laosiripojana).

0009-2509/$ - see front matter © 2005 Published by Elsevier Ltd.
doi:10.1016/j.ces.2005.11.024

This operation, called indirect internal reforming (IIR-SOFC), is expected to simplify the overall system design (Aguiar et al., 2001). Douvartzides et al. (2003), applied a thermodynamic analysis to evaluate the feasibility of different fuels, i.e., methane, methanol, ethanol and gasoline, for SOFCs. The results obtained in terms of electromotive force output and efficiency show that ethanol and methanol are very promising alternatives to hydrogen. Among them, methanol is favourable due to its ready availability, high-specific energy and storage transportation convenience (Emonts et al., 1998; Ledjeff-Hey et al., 1998).

Several researchers have studied the catalytic decomposition of methanol with steam (Lwin et al., 2000; Brown, 2001; Maggio et al., 1998). The well known reactions involved in this process can be represented by the decomposition-shift mechanism

$$CH_3OH = 2H_2 + CO \quad \text{(methanol decomposition)}, \tag{1}$$

$$CO + H_2O = H_2 + CO_2 \quad \text{(water gas shift reaction)}, \tag{2}$$

$$CO + 3H_2 = CH_4 + H_2O \quad \text{(methanation)}. \tag{3}$$

Firstly, methanol can be directly converted to hydrogen and carbon monoxide by the decomposition process (Eq. (1)). In the presence of steam, the water–gas shift reaction (Eq. (2)) takes place to produce carbon dioxide and more hydrogen. Methane can be formed by the methanation reaction (Eq. (3)). It should be noted that the formations of higher molecular weight compounds such as formaldehyde, methyl formate and formic acid were found to be negligible (Lwin et al., 2000).

A major concern of the methanol decomposition is catalyst deactivation by carbon formation which, consequently, leads to the loss of system performance and poor durability (Dicks, 1996). The following are the most probable carbon formation reactions:

$$2CO = CO_2 + C, \tag{4}$$

$$CH_4 = 2H_2 + C, \tag{5}$$

$$CO + H_2 = H_2O + C, \tag{6}$$

$$CO_2 + 2H_2 = 2H_2O + C. \tag{7}$$

At low temperature, reactions (6)–(7) are favourable while reaction (5) is thermodynamically unfavoured. The Boudouard reaction (Eq. (4)) and the decomposition of methane (Eq. (5)) are the major pathways for carbon formation at high temperature as they show the largest change in Gibbs energy (Amor, 1999). Regarding the IIR-SOFC operation, the reforming temperatures are in the range of 700–1000 °C (Aguiar et al., 2001). The potential formation of carbon species on the surface of catalyst therefore arises from the decomposition and Boudouard reactions.

In order to maximize hydrogen production from the decomposition of methanol and to reduce the amount of carbon deposition, selection of catalyst is an important issue as it has been evident that the degree of carbon formation strongly depends on the type of catalyst used (Rostrup-Nielsen and Bak-Hansen, 1993). It is well established that cerium oxide is a useful catalyst for a wide variety of reactions involving the oxidation or partial oxidation of hydrocarbons (e.g. automotive catalysis). This material contains a high concentration of highly mobile oxygen vacancies and thus acts as a local source or sink for oxygen involved in reactions taking place on the ceria surface. There is now increasing interest in using ceria in more severe reducing conditions, such as in methane reforming at the anodes of SOFC, where the possibility of deactivation through carbon deposition is much higher (Marina et al., 1998). The excellent resistance toward carbon formation from methane cracking reaction over CeO_2 under SOFC conditions was reported (Laosiripojana, 2003). Recently, the successful use of ceria as a key constituent of the anode for a SOFC operated directly with 'dry' methane has also been presented. Furthermore, successful developments of the direct internal reforming (DIR-SOFC), in which the hydrocarbons can be reformed internally at the anode side of SOFC, using copper–ceria-based anodes (i.e., Cu–CeO_2, and Cu–CeO_2-YSZ) fueled by several hydrocarbon and oxyhydrocarbon compounds (i.e., C_4H_{10} and CH_3OH) were also reported (Kim et al., 2005; Jung et al., 2005; Costa-Nunes et al., 2005; Gorte et al., 2004; An et al., 2004; Brett et al., 2005). It was demonstrated that the addition of ceria at the anode can provide a stable operation and reasonable performance with a wide variety of hydrocarbon fuels (Jung et al., 2005; Costa-Nunes et al., 2005).

The gas–solid reaction between CeO_2 and CH_4 produces synthesis gas with a H_2/CO ratio of two, according to the following reaction (Otsuka et al., 1983):

$$CH_4 + O_O^x = 2H_2 + CO + V_{O^{\cdot\cdot}} + 2e'. \tag{8}$$

$V_{O^{\cdot\cdot}}$ denotes an oxygen vacancy with an effective charge 2^+, e' is an electron which can either be more or less localized on a cerium ion or delocalized in a conduction band. Moreover, it was also demonstrated that the reactions of the reduced ceria with CO_2 and steam produced CO and H_2, respectively, and regenerated the CeO_2 surface (Otsuka et al., 1985; Gellings and Bouwmeester, 2000)

$$V_{O^{\cdot\cdot}} + 2e' + CO_2 = O_O^x + CO, \tag{9}$$

$$V_{O^{\cdot\cdot}} + 2e' + H_2O = O_O^x + H_2. \tag{10}$$

The major limitation for the application of ceria to high temperature applications is its low specific surface area due to the significant size reduction by thermal sintering (Laosiripojana, 2003). It was reported that the corresponding post-reaction specific surface area for CeO_2 after exposure in methane steam reforming conditions at 900 °C for 10 h was 1.9 $m^2\,g^{-1}$, and the observed size reduction percentage was 23% (Laosiripojana, 2003). Therefore, the use of nano-particulate high surface area ceria would be a promising procedure to improve its catalytic performance at high operating temperatures.

The present work is focused on the study of hydrogen production from methanol decomposition at SOFC operating temperature of 700–1000 °C. The decomposition of methanol with and without steam presence over nano-particulate high surface area CeO_2 (CeO_2 (HSA)), synthesized by Nanophase Technologies Corporation, was investigated. The reactivity toward this reaction and the resistance toward carbon formation of this

material were compared to CeO_2 prepared by a precipitation method (CeO_2 (LSA)). At steady state, the influences of temperature and inlet components on the product selectivities were determined.

2. Experimental

2.1. Catalyst preparation and characterization

Nano-particulate high surface area CeO_2 powder (CeO_2 (HSA)) (NanoArc Cerium Oxide SGH grade with the average particle size of 11 nm) was supplied by Nanophase Technologies Corporation, USA. This material is prepared by the patent-pending NanoArc^{TM} Synthesis (NAS) process, using arc energy to produce nanoparticles. The nanomaterials produced by the NAS process consist of discrete, fully-dense particles of defined crystallinity. This method has been used to produce particles with average sizes ranging from 7 to 45 nm (http://www.nanophase.com). CeO_2 (HSA) was dried in an oven and calcined in air at 1000 °C for 6 h in order to minimize sintering at the maximum reaction temperature used in subsequent experiments (Ramírez-Cabrera et al., 2002). For comparison, a synthesized CeO_2 (CeO_2 (LSA)) was also prepared by precipitation of cerium chloride ($CeCl_3 \cdot 7H_2O$) from Aldrich. The starting solution was prepared by mixing 0.1 M of this metal salt solution with 0.4 M of ammonia at a 2:1 volumetric ratio. The mixture was stirred by a magnetic stirrer (100 rpm) and then aqueous ammonia was slowly added with the constant rate of 0.165 $cm^3\ min^{-1}$ until the pH was 11.5. We found that the rate of ammonia doping has a significant impact on the particle size and specific surface area of the synthesized CeO_2. This solution was stirred for 3 h, then sealed and placed in a thermostatic bath maintained at 90 °C for three days. The precipitate was filtered and washed with deionized water and acetone to remove the free surfactant. It was dried overnight in an oven at 110 °C, and then calcined in air at 1000 °C for 6 h. BET measurements of CeO_2 were carried out before and after the calcinations in order to determine the specific surface area. As presented in Table 1, after drying in the oven, surface areas of 82 and 55 $m^2\ g^{-1}$ were observed for CeO_2 (HSA) and CeO_2 (LSA), respectively, and as expected, the surface area dramatically decreased at high calcination temperatures. However, the value for CeO_2 (HSA) is still appreciable after calcination at 1000 °C and it is almost 3 times of that for the CeO_2 (LSA). The average mean particle sizes of CeO_2 (HSA) and CeO_2 (LSA) after calcination at 1000 °C were 60–90 and 135–160 nm, respectively.

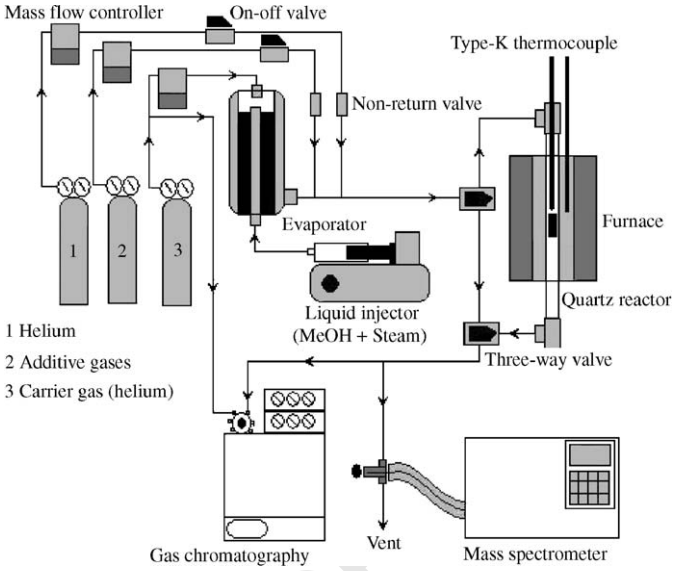

Fig. 1. Schematic diagram of the experimental set-up.

The redox properties and redox reversibilities of CeO_2 (HSA) and CeO_2 (LSA) were compared by the temperature programmed reduction (TPR-1) at high temperature and the temperature programmed oxidation (TPO) following with the second time temperature programmed reduction (TPR-2), respectively. In these experiments, 5% hydrogen and 10% oxygen in helium were used for the TPR and TPO, respectively, while the temperature of the system increased from room temperature to 900 °C by the rate of 8 °C/ min for both experiments.

2.2. Apparatus and procedures

An experimental reactor system was constructed as shown in Fig. 1. The feed gases including the components of interest (methanol and steam from the evaporator) and the carrier gas (helium) were introduced to the reaction section, in which 10-mm diameter quartz reactor was mounted vertically inside a furnace. The inlet methanol concentration was 5% (5 kPa), while the inlet steam concentrations were varied depending on the inlet H_2O/CH_3OH molar ratio requirement for each experiment (0, 1, and 3). The total gas pressure was always kept constant at 101.3 kPa. The catalyst (50 mg) was loaded in the quartz reactor, which was packed with a small amount of quartz wool to prevent the catalyst from moving. A Type-K thermocouple was placed into the annular space between the reactor and the furnace. This thermocouple was mounted on the tubular

Table 1
Specific surface area of the catalysts after drying and calcinations at different temperatures

Catalyst	BET surface area ($m^2\ g^{-1}$) after drying and calcination at						
	100 °C	200 °C	400 °C	600 °C	800 °C	900 °C	1000 °C
CeO_2 (LSA)	55	49	36	21	15	11	8.1
CeO_2 (HSA)	82	79	68	56	43	35	24

reactor in close contact with the catalyst bed to minimize the temperature difference between the catalyst bed and the thermocouple. Another Type-K thermocouple was inserted in the middle of the quartz tube in order to re-check the possible temperature gradient. The record showed that the maximum temperature fluctuation during the reaction was always ±0.75 °C or less from the temperature specified for the reaction.

After the reactions, the exit gas mixture was transferred via trace-heated lines to the analysis section, which consists of a Porapak Q column Shimadzu 14B gas chromatograph (GC) and a mass spectrometer (MS). The gas chromatography was applied in order to investigate the steady state condition experiments, whereas the mass spectrometer in which the sampling of the exit gas was done by a quartz capillary and differential pumping was used for the transient carbon formation experiment. In the present work, the outlet of the GC column was directly connected to a thermal conductivity detector (TCD) and a frame ionization detector (FID). In order to satisfactorily separate CH_3OH, CH_4, CO, CO_2, and H_2, the temperature setting inside the GC column was programmed varying with time. In the first 3 min, the column temperature was constant at 60 °C, it was then increased steadily by the rate of 15 °C/ min until 120 °C. Finally, the temperature was decreased to 60 °C. The analytical method applied is an internal standardization in which the peak area is related to the molar concentration through the response factor (RF)

$$\mathrm{RF} = \frac{\text{concentration (ppm)}}{\text{peak area}}. \tag{11}$$

In order to study the formation of carbon species on catalyst surface, TPO was applied by introducing 10% oxygen in helium into the system, after purging with helium. The operating temperature increased from room temperature to 1000 °C by a rate of 20 °C/min. The calibrations of CO and CO_2 productions were performed by injecting a known amount of these calibration gases from a loop, in an injection valve in the bypass line. The response factors were obtained by dividing the number of moles for each component over the respective areas under peaks. The amount of carbon formation on the surface of catalysts were determined by measuring the CO and CO_2 yields from the TPO results (using Microcal Origin Software) assuming a value of 0.026 nm^2 for the area occupied by a carbon atom in a surface monolayer of the basal plane in graphite (Ramírez-Cabrera et al., 2004). In addition to the TPO method, the amount of carbon deposition was confirmed by the calculation of carbon balance in the system. The amount of carbon deposited on the surface of catalyst would theoretically be equal to the difference between the inlet carbon containing components (CH_3OH) and the outlet carbon containing components (CO, CO_2, and CH_4). The amount of carbon deposited per gram of catalyst is given by the following equation:

$$C_{\text{deposition}} = \frac{\text{mole}_{\text{carbon(in)}} - \text{mole}_{\text{carbon(out)}}}{m_{\text{catalyst}}}. \tag{12}$$

2.3. Kinetic parameters formulae

The rate of methanol decomposition was defined in term of the turnover frequencies (N) which is calculated from the following equation. It was assumed that all surface sites accessible by nitrogen adsorption were active

$$N = \frac{r N_A A_{N_2}}{m_c S}, \tag{13}$$

where r is the reaction rate (moles of CH_3OH per unit time), N_A is the Avagadro's number, A_{N_2} is the area occupied by an adsorbed nitrogen molecule (16.2×10^{-20} m^2 $molecule^{-1}$ (Ramírez-Cabrera et al., 2004)), m_c is the mass of catalyst (50 mg), and S is the specific surface area of the catalyst.

Methanol conversions denoted as X_{Methanol}, and the product selectivities (hydrogen, carbon monoxide, carbon dioxide, and methane), denoted as S_{Product}, are calculated according to

$$X_{\text{Method}} = \frac{100(\text{Methanol}_{\text{in}} - \text{Methanol}_{\text{out}})}{\text{Methanol}_{\text{in}}}, \tag{14}$$

$$S_{\text{Product}} = \frac{100(\text{Mole of a specific product})}{(\text{Total moles of all products})}. \tag{15}$$

3. Results

3.1. Preliminary tests

In order to avoid any limitations by intraparticle diffusion, we checked the impact of the total flow rate at the minimum (700 °C) and maximum operating temperature (1000 °C) before the formal investigations. The total flow rate was changed between 20 and 200 cm^3 min^{-1} under the same residence time of 5×10^{-4} g min cm^{-3}. From Fig. 2, when the total flow rate was below 60 cm^3 min^{-1}, the methanol conversion and the hydrogen selectivity increased with increasing the gas flow rate, suggesting that the mass transfer between the bulk gas and the catalyst particles is the rate-determining step. The steady state

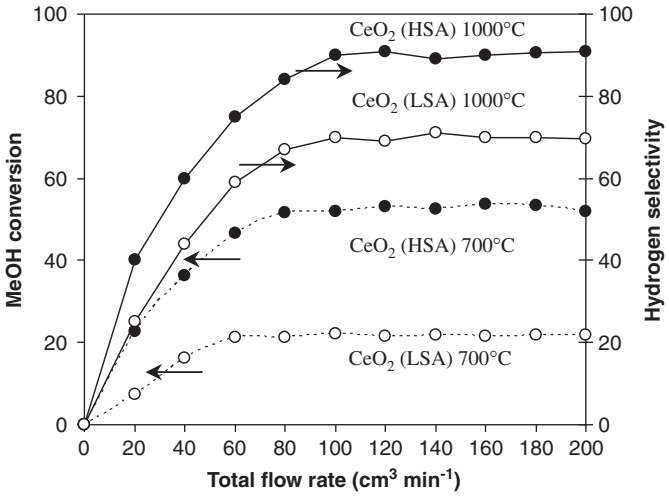

Fig. 2. Effect of the total gas flow rate on the methanol conversion over CeO_2 (LSA) and CeO_2 (HSA) at 700 °C (1 kPa MeOH, and 3 kPa H_2O).

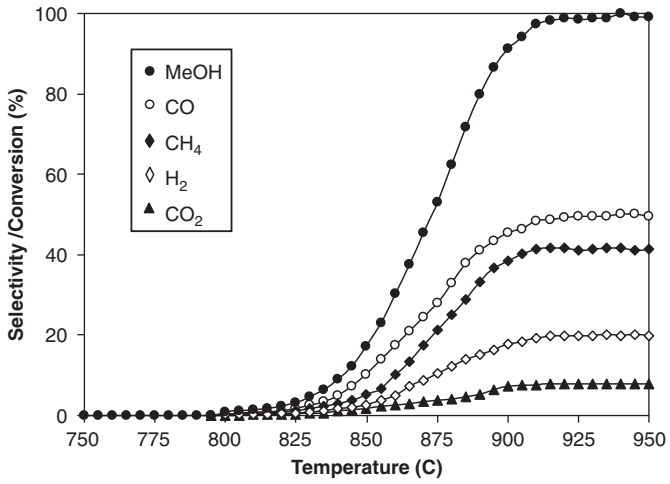

Fig. 3. Homogeneous (in the absence of catalyst) reactivity of methanol decomposition (1 kPa MeOH, and 3 kPa H_2O).

reforming rate was almost constant in the range where the gas flow rate was higher than 80 $cm^3\,min^{-1}$, indicating that the mass transfer effect is unimportant in this flow rate range. Consequently, the mass of catalyst loading was 50 mg, while the total gas flow was kept constant at 100 $cm^3\,min^{-1}$ in all experiments.

3.2. Homogeneous (non catalytic) reaction

Before studying the catalyst performance, homogeneous (non-catalytic) decomposition of methanol was investigated. Inlet H_2O/CH_3OH in helium with the molar ratio of 3 was introduced to the system, while the temperature increased from room temperature to 950 °C. From Fig. 3, it was observed that methanol was converted to methane, carbon monoxide, carbon dioxide, and hydrogen at the temperature above 800 °C. These components were formed via the decomposition of methanol, water–gas shift and methanation reactions.

3.3. Redox properties and redox reversibility of CeO_2

The oxygen storage capacities (OSC) and the degree of redox properties for fresh CeO_2 (both LSA and HSA) after calcinations were investigated using TPR-1, which was performed by heating the reduced catalysts up to 900 °C in 5% H_2 in helium. As shown in Fig. 4, hydrogen uptakes are detected from both CeO_2 at the temperature above 650 °C. The amount of hydrogen uptake over CeO_2 (HSA) is significantly higher than that over CeO_2 (LSA), suggesting that the OSC and the redox properties depend on the specific surface area of CeO_2. The benefit of the redox property on the reforming of methanol will be later presented in Section 3.4 and the discussion section. After purged with helium, the redox reversibilities for both CeO_2were then determined by applying TPO followed by TPR-2. The TPO was carried out by heating the catalyst up to 900 °C in 10% O_2 in helium; the amounts of oxygen chemisorbed were then measured, Fig. 5 and Table 2. Regarding the TPR-2 results as

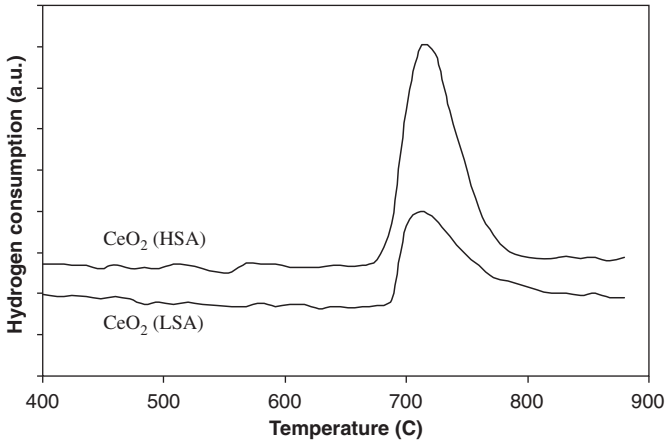

Fig. 4. TPR-1 of fresh ceria after reduction.

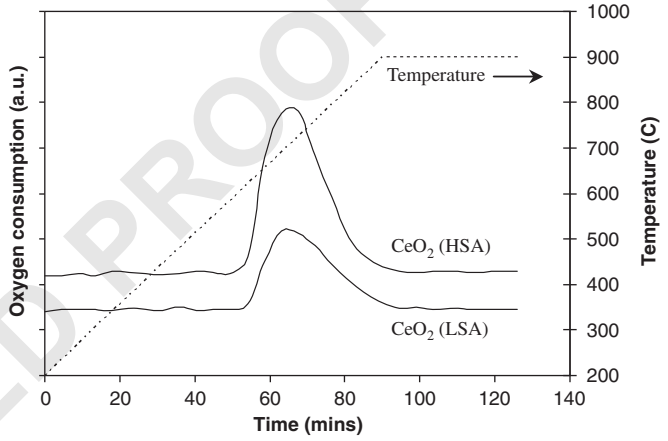

Fig. 5. TPO of CeO_2 (HSA, LSA) after TPR-1.

shown in Fig. 6 and Table 2, the amount of hydrogen uptakes for CeO_2 (both LSA and HSA) were approximately similar to those from TPR-1, indicating the redox reversibility for the synthesized CeO_2.

3.4. Reactivity toward methanol decomposition

The decomposition of methanol with and without steam over CeO_2 (HSA) and CeO_2 (LSA) were studied at 900 °C. The feed was H_2O/CH_3OH in helium with the molar ratios of 0, 1, and 3. The variations in hydrogen selectivities (%) with time at 900 °C for different catalysts and different inlet H_2O/CH_3OH ratio are shown in Fig. 7. After being operated for 100 h, the hydrogen selectivities for CeO_2 (HSA) were significantly higher than those for CeO_2 (LSA) in all conditions. However, the deactivations were also observed in all catalysts. Catalyst stabilities expressed as deactivation percentages are given in Table 3.

The post-reaction TPO experiments were carried out after a helium purge by introduction of 10% oxygen in helium in order to determine whether the observed deactivation is due to the carbon formation. From the TPO results shown in Fig. 8, small peaks of carbon dioxide and carbon monoxide were observed

Table 2
Results of TPR-1, TPO, TPR-2 analyses of CeO_2

Catalyst	Total H_2 uptake from TPR(1)[a] ($\mu mol/g_{cat}$)	Total O_2 uptake from TPO[b] ($\mu mol/g_{cat}$)	Total H_2 uptake from TPR(2)[c] ($\mu mol/g_{cat}$)
CeO_2 (LSA)	1784	867	1781
CeO_2 (HSA)	2076	989	2070

[a]Temperature Programmed Reduction of the reduced catalysts (Relative Standard Deviation = ±3%).
[b]Temperature Programmed Oxidation after TPR (1) (Relative Standard Deviation = ±1%).
[c]Re-Temperature Programmed Reduction after TPO (Relative Standard Deviation = ±2%).

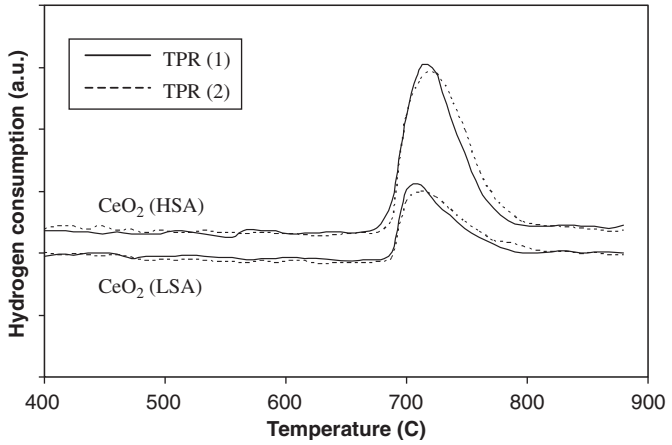

Fig. 6. TPR-2 of CeO_2 (HSA and LSA) compared to that of TPR-1.

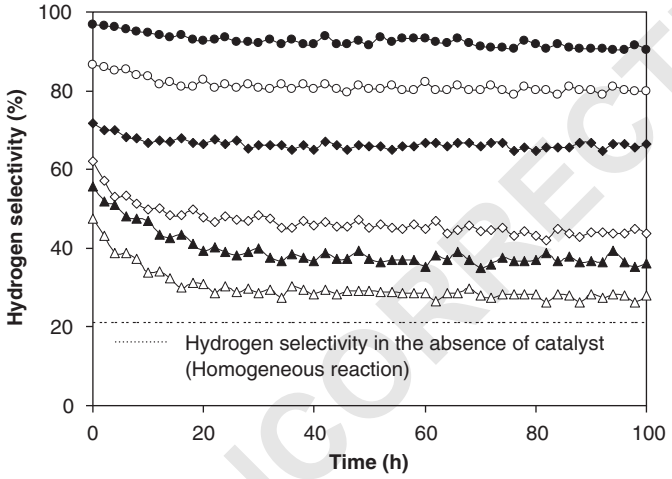

Fig. 7. Hydrogen selectivities from methanol decomposition at 900 °C for CeO_2 (HSA) with H_2O/CH_3OH of 3 (●), CeO_2 (HSA) with H_2O/CH_3OH of 1 (○), CeO_2 (HSA) with H_2O/CH_3OH of 0 (♦), CeO_2 (LSA) with H_2O/CH_3OH of 3 (◇), CeO_2 (LSA) with H_2O/CH_3OH of 1 (▲), and CeO_2 (LSA) with H_2O/CH_3OH of 0 (△).

for CeO_2 (LSA), whereas no peak of either carbon dioxide or carbon monoxide was detected for CeO_2 (HSA). The amount of carbon formations on the surface of CeO_2 (LSA) with different inlet H_2O/CH_3OH ratios were determined by measuring the CO and CO_2 yields from the TPO results. Using a value of 0.026 nm^2 for the area occupied by a carbon atom in a surface monolayer of the basal plane in graphite (Ramírez-Cabrera et al., 2004), the quantities of carbon deposited over this catalyst were observed to be approximately 0.35, 0.17, and 0.06 monolayer for the inlet H_2O/CH_3OH ratios of 0, 1, and 3, respectively. The total amounts of carbon deposited were ensured by the calculation of carbon balance in the system. Regarding the calculation, for the inlet H_2O/CH_3OH ratios of 0, 1, and 3, the moles of carbon deposited per gram of CeO_2 (LSA) were 0.39, 0.21, and 0.07 mmol g^{-1}. By the same assumption for the area occupied by a carbon atom (Ramírez-Cabrera et al., 2004), these values are equal to 0.33, 0.18, and 0.06 monolayer, respectively, which are in good agreement with the values observed from the TPO method described above. The TPO results clearly indicated the excellent resistance toward carbon formation for CeO_2 (HSA).

The BET measurement, as presented in Table 3, suggested that the deactivations of ceria are also due to the thermal sintering. Regarding the BET results, the surface area reduction percentage of CeO_2 (HSA) is lower than that of CeO_2 (LSA), indicating its better stability toward the thermal sintering.

3.5. Effects of temperature and inlet reactants

At steady state, the main products from this reaction over CeO_2 (HSA) were H_2, CO, and CO_2, with small amount of CH_4 depending on the operating conditions. The influences of operating temperature and the inlet steam content on the product selectivities and methanol conversion were studied by varying temperature from 700 to 1000 °C and changing the inlet steam to methanol ratio from 0.0 to 3.0.

As seen from Fig. 9, hydrogen and carbon monoxide selectivities increased with increasing temperature, whereas carbon dioxide and methane production selectivities decreased. Regarding the effect of steam, the conversion of methanol and the methane selectivity seem to be independent of the inlet steam content. However, hydrogen and carbon dioxide selectivities increased with increasing inlet steam concentration, whereas carbon monoxide selectivity decreased. Table 4 presents the comparison of product selectivities from methanol steam reforming at 900 °C between CeO_2 (HSA), and CeO_2 (LSA). It should be noted that the product selectivities from the homogeneous reaction (Fig. 6) and the product selectivities at equilibrium level, which were calculated by AspenPlus10.2 simulation program, are also shown in the table for comparison. Clearly, hydrogen and carbon monoxide selectivities from this reaction over CeO_2

Table 3
Deactivation percentages, steady state hydrogen selectivities, specific surface area, and amount of carbon deposition on the surface of catalysts after exposure in methanol decomposition conditions (various inlet H_2O/CH_3OH ratios) at 900 °C for 100 h

Catalyst	H_2O/CH_3OH ratio	Deactivation (%)	Hydrogen selectivity (%) at steady state	C formation[a] (monolayers)	BET surface ($m^2\ g^{-1}$)
CeO_2 (LSA)	0	40.9	28.0	0.35	6.0
	1	34.9	36.2	0.17	6.0
	3	29.7	43.6	0.06	6.1
CeO_2 (HSA)	0	7.4	66.5	~ 0	22.0
	1	7.6	80.0	~ 0	22.2
	3	6.5	90.4	~ 0	22.1

[a]Calculated using CO and CO_2 yields from temperature-programmed oxidation (TPO) with 10% oxygen.

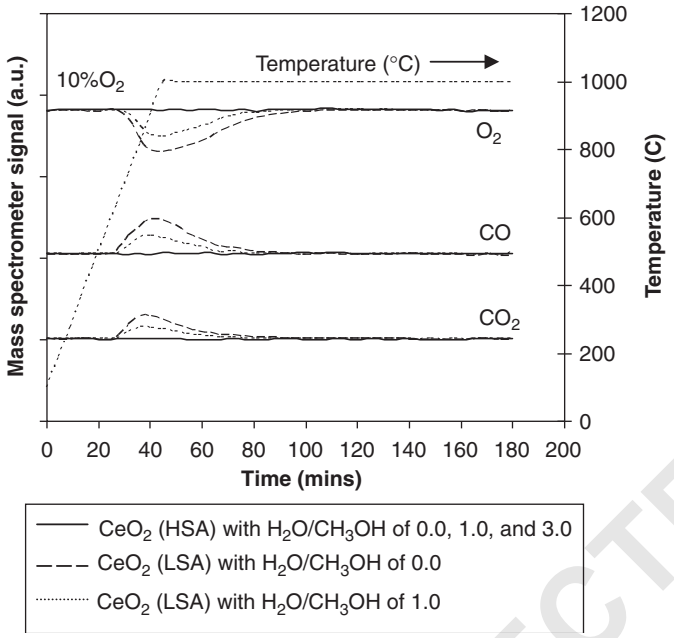

Fig. 8. TPO of CeO_2 (LSA) and CeO_2 (HSA) (10 kPa O_2) after exposure in methanol decomposition reaction at various inlet H_2O/CH_3OH ratios for 100 h.

(HSA) are higher and closer to their equilibrium levels than those over CeO_2 (LSA) in all conditions.

Without inlet steam, the effect of methanol concentration on the rate of decomposition at different temperatures was also studied by varying inlet methanol partial pressure from 1.0 to 4.0 kPa. The operating temperature range was between 700 and 800 °C in order to prevent the influence of homogeneous (non-catalytic) reaction. Fig. 10 presents the Arrhenius plots of the turnover frequencies at various inlet methanol concentrations. The results show that the decomposition rate is proportional to the methanol concentration and the temperature. The reaction order in methanol for CeO_2 (HSA) was observed to be between 0.37 and 0.68, independent of the steam partial pressure, for the range of conditions studied. These values were obtained experimentally by plotting $\ln(N)$ versus $\ln P_{CH_3OH}$ (where P_{CH_3OH} is the partial pressure of methanol; kPa). The reaction orders in other components (H_2O, and H_2) were achieved using the same approach by varying the inlet partial pressure of the component of interest while keeping the other inlet component partial pressures constant. Regarding the independence of inlet steam partial pressure on the rate of methanol decomposition, the reaction order in steam is therefore 0.

According to the post-reaction TPO, no carbon formation was observed on the surface of catalysts. In addition, the oxygen balance calculation was carried out during the stability testing to confirm the role of CeO_2. It was found from the calculation that the mole of oxygen (from methanol) fed into the system is almost similar to that in the products (CO, and CO_2) in all testing times, which indicates the unchanged state of CeO_2 (to Ce_2O_3) during the experiments. Furthermore, the TPO result for CeO_2 (HSA) in Fig. 8 also proves the unchanged state of spent CeO_2, as no oxygen uptakes were detected from the TPO of CeO_2 (HSA) after exposure in methanol decomposition conditions.

The influence of hydrogen on the rate of methanol decomposition was also investigated by adding various concentrations of hydrogen (1–3 kPa) in the feed. As shown in Fig. 11, the methanol conversion was significantly inhibited by the presence of hydrogen in the feed. The reaction order in hydrogen was between −0.29 and −0.17 in the range of conditions studied.

4. Discussion

CeO_2 (HSA) has a high reactivity for methanol decomposition and an excellent resistance toward carbon deposition without steam having to be present in the gas. This high resistance toward carbon deposition has been reported by several investigators (Laosiripojana, 2003; Ramírez-Cabrera et al., 2003, 2004; Laosiripojana and Assabumrungrat, 2005) and is mainly due to the high oxygen storage capacity of this material. CeO_2 contains a high concentration of highly mobile oxygen vacancies and thus acts as a local source or sink for oxygen on its surface. It has been reported that at high temperature the lattice oxygen (O_O^x) at the CeO_2 surface can oxidize gaseous hydrocarbons (methane, Ramírez-Cabrera et al., 2003, 2004; ethane and propane, Laosiripojana and Assabumrungrat, 2005) and also carbon monoxide (Laosiripojana, 2003).

In the decomposition of methanol at high temperature the presence of steam is normally required as it minimizes the carbon deposition on the catalyst surface, which is due to

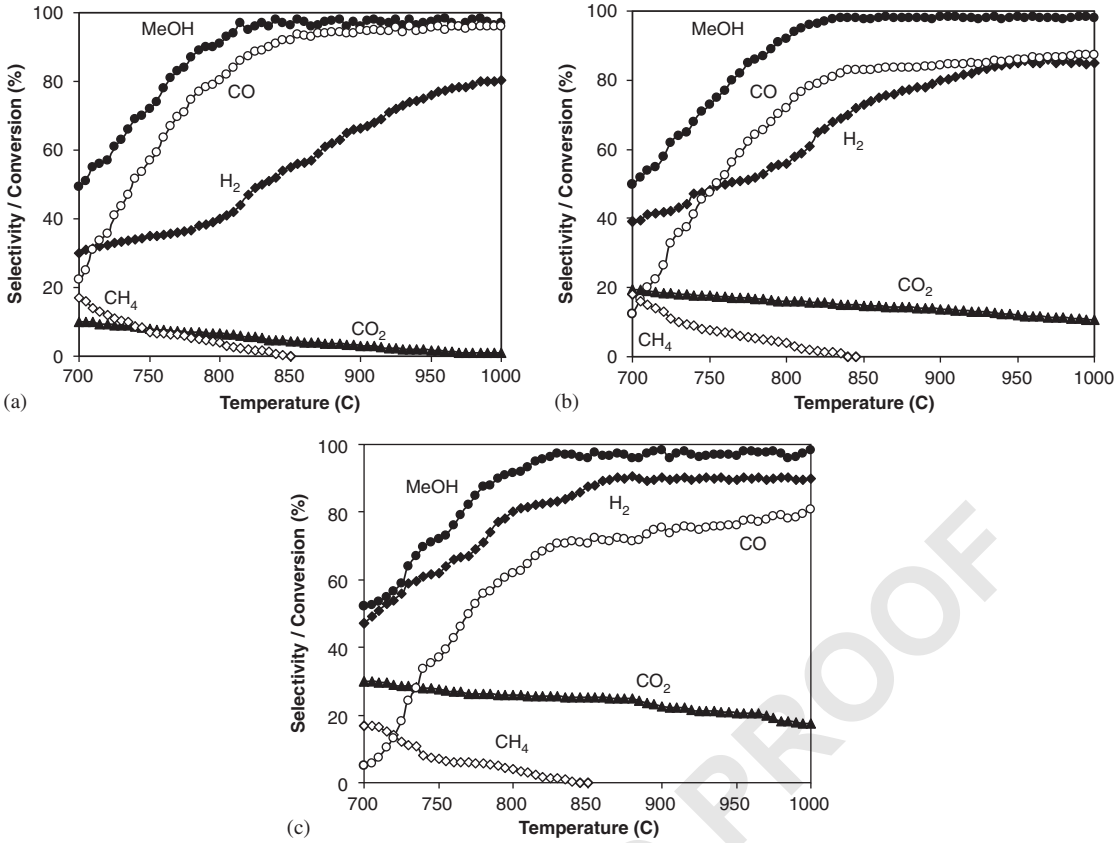

Fig. 9. Effects of reaction temperature and inlet H_2O/CH_3OH ratio on methanol conversion and product selectivities (H_2, CO, CO_2, and CH_4) from methanol decomposition over CeO_2 (HSA): (a) inlet H_2O/CH_3OH ratio of 0; (b) inlet H_2O/CH_3OH ratio of 1; (c) inlet H_2O/CH_3OH ratio of 3.

Table 4
Methanol conversion and product selectivities from the decomposition of methanol at various inlet H_2O/CH_3OH molar ratios (at isothermal condition, 900 °C)

Catalyst	H_2O/CH_3OH	Conversion and product selectivities at 900 °C				
	ratio	CH_3OH	H_2	CO	CO_2	CH_4
CeO_2 (LSA)	0	93.1	22.4	58.6	4.2	30.3
	1	94.2	27.1	55.0	11.0	28.2
	3	93.8	33.2	52.9	18.1	22.8
CeO_2 (HSA)	0	98.1	66.5	92.0	6.1	0
	1	98.2	80.0	84.4	13.7	0
	3	98.1	90.4	75.5	22.6	0
Homogeneous[a]	0	92.1	13.5	49.9	0	41.2
	1	92.4	17.4	49.1	3.4	39.9
	3	92.9	20.8	48.1	5.6	39.2
Equilibrium[b]	0	100	71.1	93.4	6.6	0
	1	100	89.4	85.2	14.8	0
	3	100	95.0	76.1	23.9	0

[a]Homogeneous (non-catalytic) reaction.
[b]Calculated by AspenPlus 10.2 simulation program.

reactions (4) and (5) mentioned in Section 1. By using CeO_2 as the catalyst, the carbon deposition from these reactions could be inhibited by the gas–solid reactions between CO and CH_4 formed with the lattice-oxygen (O_O^x) at the CeO_2 surface forming CO_2 and hydrogen from which the formation of carbon is thermodynamically unfavourable at high temperature. The reactions taken place can be summarized as follows:

$$C_nH_m + O_O^x = nCO + m/2H_2 + V_{O^{\cdot\cdot}} + 2e', \quad (16)$$

$$CO + O_O^x = 2CO_2 + V_{O^{\cdot\cdot}} + 2e'. \quad (17)$$

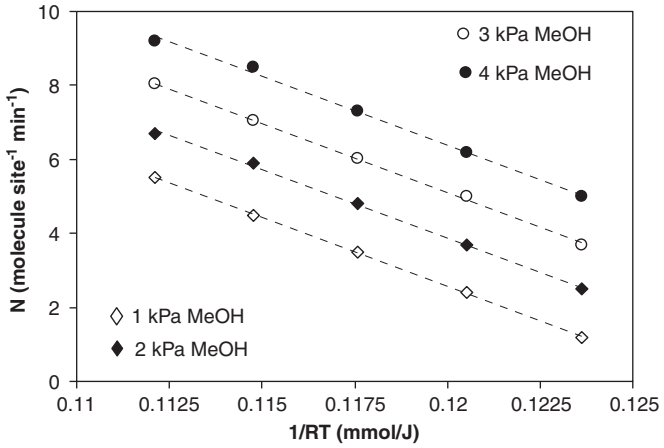

Fig. 10. Arrhenius plot of turnover frequencies (N) for methanol decomposition without steam over CeO_2 (HSA) with different inlet methanol partial pressures (1–4 kPa) at 700–800 °C.

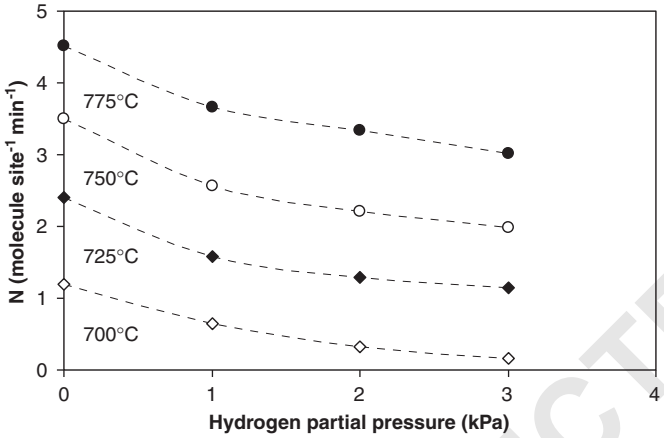

Fig. 11. Effect of hydrogen partial pressure on the turnover frequencies (N) for methanol decomposition over CeO_2 (HSA) at different temperatures (1 kPa MeOH and 3 kPa H_2O).

The lattice oxygen (O_O^x) is regenerated by reactions with oxygen containing compounds (methanol, steam) present in the system. The strong linear dependence of the methanol decomposition rate on methanol partial pressure and its independence of the steam partial pressure indicate that the lattice oxygen (O_O^x) is replenished by a sufficiently rapid reaction of the partially reduced CeO_2 with the oxygen containing molecules in the system, whereas the inhibitory effect of hydrogen could be due to the reverse of the methanol decomposition. According to the studies on the effect of temperature, hydrogen and carbon monoxide selectivities increased with increasing temperature, whereas carbon dioxide and methane production selectivities decreased. The changes of hydrogen, carbon monoxide, and carbon dioxide selectivities are mainly due to the influence of the mildly exothermic water–gas shift reaction ($CO + H_2O \rightarrow CO_2 + H_2$), whereas the decrease in methane production selectivity could be due to the further reforming to carbon monoxide and hydrogen.

Although the CeO_2 (LSA) can decompose methanol producing synthesis gas (CO and H_2), the major weaknesses of CeO_2 (LSA) are its nature, low specific surface area and its high size reduction due to the thermal sintering, which resulted in its low OSC as presented in Section 3.3. The low OSC for CeO_2 (LSA) results in its lower redox property (Eqs. (16) and (17)) and consequently caused the low reforming reactivity (almost three times lower than CeO_2 (HSA)) and low product selectivities (i.e., H_2 and CO). The comparative reforming reactivities between CeO_2 (HSA) and CeO_2 (LSA) are in good agreement with the results from the characterizations (i.e., BET and TPR)—the specific surface area of CeO_2 (HSA) and the amount of hydrogen uptakes from the temperature programmed reduction (TPR-1 and TPR-2) were significantly higher than those over the CeO_2 (LSA). By the same reason, the higher resistance toward carbon deposition for CeO_2 (HSA) compared to CeO_2 (LSA) is mainly due to the higher lattice oxygen (O_O^x) on its surface, which promotes the gas–solid reactions (Eqs. (16) and (17)) and consequently prevents the formation of carbon species via the methane decomposition and Boudouard reactions.

Due to the good performance of CeO_2 (HSA) in terms of high resistance toward carbon deposition and good product selectivities (producing only H_2, CO, and CO_2) at high temperature, this catalyst would be a good candidate to be applied as the internal or in-stack reforming catalyst for IIR-SOFC. Also, this material could be a promising option for application in the anode of SOFC (DIR-SOFC) compared to the CeO_2 (LSA), as it presents higher resistance toward carbon deposition and lower sintering rate. Importantly, without the presence of steam being required to reform methanol, the consideration of water management in SOFC system is negligible. Regarding the above benefits, the use of CeO_2 (HSA) is expected to simplify the overall SOFC system design (i.e., DIR and IIR), making SOFCs more attractive to be used commercially.

5. Conclusion

Nano-particulate high surface area CeO_2 (CeO_2 (HSA)) has a useful methanol decomposition activity at SOFC temperatures producing H_2, CO, CO_2, and small amount of CH_4 without the presence of steam being required. The conversion of methanol from the decomposition process over this catalyst was close to 100% at 850 °C, and no carbon deposition was observed on the surface of CeO_2 according to the TPO results. Hydrogen selectivities up to 90% can be produced. Regarding the influences of inlet components on the rate of methanol decomposition, the decomposition rate over CeO_2 (HSA) is proportional to the methanol partial pressure and independent of the steam partial pressure at 700–800 °C. Hydrogen was found to have a significant inhibitory effect on the rate of methanol decomposition.

Due to the good performance of CeO_2 (HSA) toward methanol decomposition in terms of high resistance toward carbon deposition and good product selectivities at SOFC temperature, this catalyst is a good candidate to be applied as the internal or in-stack reforming catalyst for solid oxide fuel cell application (IIR-SOFC).

Acknowledgements

The financial support from The Thailand Research Fund (TRF) throughout this project is gratefully acknowledged. The first author would like to acknowledge Professor David Chadwick from Department of Chemical Engineering and Chemical Technology, Imperial College London for his valuable suggestion.

References

Aguiar, P., Lapena-Rey, N., Chadwick, D., Kershenbaum, L., 2001. Improving catalyst structures and reactor configurations for autothermal reaction systems: application to solid oxide fuel cells. Chemical Engineering Science 56, 652.

Amor, J.N., 1999. The multiple roles for catalysis in the production of H_2. Applied Catalysis A 176, 159–176.

An, S., Lu, C., Worrell, W.L., Gorte, R.J., Vohs, J.M., 2004. Characterization of Cu–CeO_2 direct hydrocarbon anodes in a solid oxide fuel cell with lanthanum gallate electrolyte. Solid State Ionics 175 (1–4), 135–138.

Brett, D.J.L., Atkinson, A., Cumming, D., Ramírez-Cabrera, E., Rudkin, R., Brandon, N.P., 2005. Methanol as a direct fuel in intermediate temperature (500–600 °C) solid oxide fuel cells with copper based anodes. Chemical Engineering Science 60 (21), 5649–5662.

Brown, L.F., 2001. A comparative study of fuels for on-board hydrogen production for fuel-cell-powered automobiles. International Journal of Hydrogen Energy 26, 381–397.

Costa-Nunes, O., Gorte, R.J., Vohs, J.M., 2005. Comparison of the performance of Cu–CeO_2–YSZ and Ni–YSZ composite SOFC anodes with H_2, CO, and syngas. Journal of Power Sources 141 (2), 241–249.

Dicks, A.L., 1996. Hydrogen generation from natural gas for the fuel cell systems of tomorrow. Journal of Power Sources 61 (1–2), 113–124.

Douvartzides, S.L., Coutelieris, F.A., Demin, K., Tsiakaras, P.E., 2003. Fuel options for solid oxide fuel cells: a thermodynamic analysis. A.I.Ch.E. 49, 248–257.

Emonts, B., Hansen, J.B., Jorgensen, S.L., Hohlein, B., Peters, R., 1998. Compact methanol reformer test for fuel-cell powered light-duty vehicles. Journal of Power Sources 71, 288.

Gellings, P.J., Bouwmeester, H.J.M., 2000. Solid state aspects of oxidation catalysis. Catalysis Today 58, 1–53.

Gorte, R.J., Vohs, J.M., McIntosh, S., 2004. Recent developments on anodes for direct fuel utilization in SOFC. Solid State Ionics 175 (1–4), 1–6.

Jung, S., Lu, C., He, H., Ahn, K., Gorte, R.J., Vohs, J.M., 2005. Influence of composition and Cu impregnation method on the performance of Cu/CeO_2/YSZ SOFC anodes. Journal of Power Sources, in press.

Kim, T., Liu, G., Boaro, M., Lee, S.-I., Vohs, J.M., Gorte, R.J., Al-Madhi, O.H., Dabbousi, B.O., 2005. A study of carbon formation and prevention in hydrocarbon-fueled SOFC. Journal of Power Sources, in press.

Laosiripojana, N., 2003. Reaction engineering of indirect internal steam reforming of methane for application in solid oxide fuel cells. Ph.D. Thesis, University of London, England.

Laosiripojana, N., Assabumrungrat, S., 2005. Catalytic steam reforming of ethane and propane over CeO_2-doped Ni/Al_2O_3 at SOFC temperature: improvement of resistance toward carbon formation by the redox property of doping CeO_2. Fuel, in press.

Ledjeff-Hey, K., Formanski, V., Kalk, T., Roes, J., 1998. Compact hydrogen production systems for solid polymer fuel cells. Journal of Power Sources 71 (1–2), 199–207.

Lwin, Y., Daud, W.R.W., Mohamad, A.B., Yaakob, Z., 2000. Hydrogen production from steam-methanol reforming: thermodynamic analysis. International Journal of Hydrogen Energy 25 (1), 47–53.

Maggio, G., Freni, S., Cavallaro, S., 1998. Light alcohols/methane fuelled molten carbonate fuel cells: a comparative study. Journal of Power Sources 74, 17–23.

Marina, O.A., Bagger, C., Primdahl, S., Mogensen, M., 1998. In: Stevens, P., Bossell, U. (Eds.), Proceedings of Third European SOFC Forum, Oberrohrdorf, Nantes, Switzerland, p. 427.

Minh, N.Q., Takahashi, T., 1995. Science and Technology of Ceramic Fuel Cells. Elsevier, Amsterdam.

Otsuka, K., Hatano, M., Morikawa, A., 1983. Hydrogen from water by reduced cerium oxide. Journal of Catalysis 79, 493.

Otsuka, K., Hatano, M., Morikawa, A., 1985. Decomposition of water by cerium oxide of δ-phase. Inorganica Chimica Acta 109, 193.

Ramírez-Cabrera, E., Atkinson, A., Chadwick, D., 2002. Reactivity of ceria, Gd- and Nb-doped ceria to methane. Applied Catalysis B 36, 193.

Ramírez-Cabrera, E., Laosiripojana, N., Atkinson, A., Chadwick, D., 2003. Methane conversion over Nb-doped ceria. Catalysis Today 78, 433–438.

Ramírez-Cabrera, E., Atkinson, A., Chadwick, D., 2004. Catalytic steam reforming of methane over $Ce_{0.9}Gd_{0.1}O_{2-x}$. Applied Catalysis B 47, 127–131.

Rostrup-Nielsen, J.R., Bak-Hansen, J.-H., 1993. CO_2-reforming of methane over transition metals. Journal of Catalysis 144, 38.

N. Laosiripojana and S. Assabumrungrat

"Catalytic steam reforming of ethanol over high surface area CeO_2: The role of CeO_2 as an internal pre-reforming catalyst"

Applied Catalysis B: Environmental, revised

(IF-2004 = 4.06)

Submitted to Applied Catalysis B: Environmental (Revised)
Type of Contribution: Research Paper

Catalytic steam reforming of ethanol over high surface area CeO_2: The role of CeO_2 as an internal pre-reforming catalyst

N. Laosiripojana[1,*] and S. Assabumrungrat[2]

[1] The Joint Graduate School of Energy and Environment,
King Mongkut's University of Technology Thonburi, Bangkok, 10140, Thailand
[2] Center of Excellence on Catalysis and Catalytic Reaction Engineering,
Department of Chemical Engineering, Faculty of Engineering, Chulalongkorn University, Bangkok, Thailand

[*] Corresponding author (navadol_l@jgsee.kmutt.ac.th)

Abstract

In the present work, it was found that high surface area ceria (CeO_2 (HSA)), synthesized by a surfactant-assisted approach, have useful ethanol steam reforming activity under Solid Oxide Fuel Cells (SOFCs) temperatures. The catalyst provides good reforming reactivity and high resistance toward carbon deposition compared to Ni/Al_2O_3 and conventional low surface area ceria (CeO_2 (LSA)). Although the hydrogen selectivity at steady state from the ethanol steam reforming over CeO_2 (HSA) was lower than Rh/Al_2O_3, the resistance toward carbon deposition of CeO_2 (HSA) was considerably higher. The good reactivity toward the steam reforming of ethanol for CeO_2 (HSA) is due to the high redox property of this material. During the reforming process, the gas-solid reactions between the gaseous hydrocarbon components and the lattice oxygen (O_O^x) on CeO_2 surface take place ($C_nH_m + O_O^x \rightarrow nCO + m/2(H_2) + V_O^{\bullet\bullet} + 2\ e'$) forming synthesis gas and also preventing the formation of carbon species from hydrocarbon decomposition reactions ($C_nH_m \rightarrow nC + m/2H_2$).

At the temperature of 900ºC, the main products from the steam reforming of ethanol over CeO_2 (HSA) (with inlet C_2H_5OH/H_2O molar ratio of 1.0/3.0) were 67.5% H_2, 37.9%CH_4, 50.5%CO, and 11.6%CO_2. In contrast, the formations of C_2H_4 (5.8-15.8%) and C_2H_6 (1.2-8.5%) were also observed from the steam reforming of ethanol

over Ni/Al_2O_3 and CeO_2 (LSA). The combination use of CeO_2 and Ni/Al_2O_3 was studied in an annular ceramic reactor by applying CeO_2 as an internal pre-reforming catalyst. The main purpose of CeO_2 is to convert all ethanol and other high hydrocarbon compounds (e.g. C_2H_4 and C_2H_6) forming CH_4, CO, CO_2, and H_2, while Ni/Al_2O_3 is applied to reform all CH_4 left from the pre-reforming section and maximize the yield of hydrogen production. After operated at 900ºC for 100 h, this combination pattern offers high hydrogen selectivity (87.0-91.4%) and good resistance toward carbon deposition. This successful development eliminates the requirement of expensive noble metal catalysts or the installation of an external pre-reformer in order to reform ethanol internally (IIR-SOFC).

Keywords: Ethanol**,** internal reforming, ceria, redox, solid oxide fuel cell

1. Introduction

Solid Oxide Fuel Cell (SOFC) with an indirect internal reforming operation (IIR), called IIR-SOFC, is expected to be an important technology for energy generation in the near future due to the high efficiency and its lower pollutant emission. Regarding this operation, the endothermic reforming reaction takes place at the reformer, which is in close thermal contact with the anode side of fuel cell where the exothermic electrochemical reaction occurs, Fig. 1 [1]. The aim of the reformer unit is to reform and maximize the yield of hydrogen production, which can be generated from several sources such as natural gas, bio-ethanol, coal, biomass, and biogas, and supply this component to the anode side of SOFC. IIR-SOFC gives the advantage on eliminating the requirement for a separate fuel reformer and providing good heat transfer between the reformer and the fuel cell. In addition, the reformer part and the anode side for IIR operation can be operated separately. Therefore, the catalyst for reforming reaction at the reformer part and the material for electrochemical reactions at the anode side of fuel cell can be different and optimized individually. This operation is expected to simplify the overall SOFC system design, making SOFC more attractive and efficient for producing electrical power [1].

Regarding the current oil crisis and the shortage of fossil fuels, the development of the biomass-based fuels therefore attracts much attention. Among various resources, bio-ethanol is a promising candidate for hydrogen for SOFC, since it is readily produced by renewable resources (e.g., fermentation of biomasses) and has reasonably high

hydrogen content [2,3]. The major difficulty to reform ethanol is the deactivation of the reforming catalyst due to the possible carbon deposition from the ethanol decomposition. It has widely been reported that ethanol can homogenously decompose to several hydrocarbon elements (e.g. acetaldehyde, methane, carbon monoxide, carbon dioxide, ethylene, and ethane) without the requirement of catalyst [4]. The formations of ethylene and ethane are the major problem, as these components act as very strong promoters for carbon formation. When ethanol is reformed internally (IIR-SOFC) without any pre-treatments, the carbon formation can be easily formed on the catalyst surface.

SOFC fueled by high organic compounds (e.g. natural gas, DME, LPG, and bio-ethanol) normally requires a small external preliminary reforming unit (pre-reformer), where these high hydrocarbons are reformed readily forming low hydrocarbon compounds (e.g. methane) before introducing to the main part of the SOFC system [5]. The pre-reforming unit is normally operated at relatively lower temperatures, 300-500ºC, in which the carbon formation problem is less severe, but the disadvantage of this installation is the extra-requirement of the heat supplied into this unit, which can reduce the fuel cell efficiency.

The approach in this work is developing of an alternative catalytic reforming operation that is enabling to reform ethanol with low degree of carbon deposition at SOFC temperatures, 800-1000ºC. The successful development of this operation would help eliminate the requirement of the external pre-reformer. Previously, hydrogen production from the reforming of ethanol has been studied by several researchers [6-27], most of them have investigated the reforming of ethanol over noble metal catalysts (e.g. Rh, Ru, Pt, Pd) on several oxide supports (e.g. Al_2O_3, MgO, SiO_2, TiO_2) [11,13,14,17,24,25,26]. Freni et al. [11, 14, 16, 25] presented that Rh/Al_2O_3 provides the highest reforming reactivity among these noble metal catalysts. Burch and coworkers [19] found that the order of the ethanol steam reforming reactivity of the metals is Rh > Pd > Ni = Pt. In the present work, Ni/Al_2O_3 was selected as a based catalyst rather than these precious metals. Although the precious metals have been reported to be active for the ethanol steam reforming and provide high resistance to the carbon formation than Ni based catalysts [28, 29], the current prices of these metals are very high for commercial uses, and the availability of some precious metals such as ruthenium was too low to have a major impact on the total reforming catalyst market [30]. The main procedure to improve the ethanol steam reforming reactivity in this work is to investigate the use of